Escola de Camins
Escola Tècnica Superior d'Enginyeria de Camins, Canals i Ports
UPC BARCELONATECH

A Design Review of Pile-Supported Wharves Under Seismic Conditions

Treball realitzat per:
Toni Ejarque Caldés

Dirigit per:
Enrique Mirambell Arrizabalaga
Guillermo Calicó Torras

Màster en:
Enginyeria de Camins, Canals i Ports

Barcelona, 21 de juny de 2021

Departament d'Enginyeria Civil i Ambiental

TREBALL FINAL DE MÀSTER

A DESIGN REVIEW OF PILE-SUPPORTED WHARVES UNDER SEISMIC CONDITIONS

Author: Toni Ejarque Caldés.

Tutors: Enrique Mirambell Arrizabalaga, Guillermo Calicó Torras.

ABSTRACT

Keywords: *pile, wharf, seismic design, performance-based design, displacement-based design, substitute structure, non-linear static pushover analysis, soil-pile interaction.*

Seismic design of pile-supported wharves using traditional force-based designs can lead to very uneconomical solutions. The alternative approach of performance-based design allows to rationalize design by allowing certain levels of damage to specific seismic hazards.

Soil-structure interaction, torsional effects due to stiffness irregularities and inelasticity caused by large seismic demands shall be considered in structural analysis. Rapidly, structural models can become large and numerically complex, therefore the need for models that allow engineering production of these structures is apparent.

This thesis reviews the fundamentals of performance-based design, as well as displacement-based design, to identify relevant and useful approaches for seismic design for production purposes. Pertinent structural analyses are applied to a particular wharf case study by SAP2000 software modeling.

Non-linear static pushover analyses are performed to determine structural displacement capacity, which is observed to be related to axial load on critical piles. The substitute structure method is used to obtain purely transverse demand, and results are found to be very sensible to equivalent damping modeling. Expression given by ASCE 61-14 provides consistent results, although in some cases may be conservative, and should be used in design.

The Dynamic Magnification Factor is defined to extrapolate purely transverse results to the simultaneous longitudinal and transversal seismic loading of the wharf, as well as to consider torsional effects. Formulation in ASCE 61-14 better fits particular structures than other expressions found in literature.

Non-linear time-history analyses may be performed using "Super-Pile" approach, which reduces greatly numerical complexity. However, results are strongly variable and should only be used for verification purposes.

CONTENTS

LIST OF FIGURES

LIST OF TABLES

1. INTRODUCTION

Pile-supported wharves are structurally simple: a deck acts as an operational surface for port activities, while vertical piles transmit loads to the soil. The deck, also referred as the superstructure, is usually composed of a slab and coupling beams between piles. These wharves are commonly placed on sloped soil surfaces to avoid the need of retaining structures, for instance concrete retaining walls. Design of piles shall fulfill three main requirements: driving loads under construction, bearing capacity against vertical loads and resistance of lateral loads. Horizontal loading of piles may come from service loads, for instance mooring and berthing of vessels, or due to accidental situations, such as an earthquake. The study of the latter scenario is the central theme of this project.
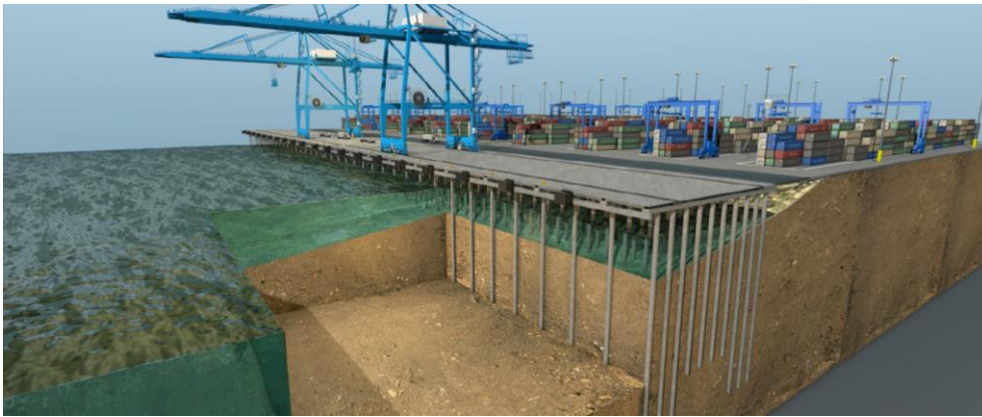
Figure 1.1. Typical pile supported wharf (Ramirez-Henao & Paul Smith-Pardo, 2015).

Structural simplicity does not necessarily imply a straightforward analysis or design. In fact, various aspects make this problem significantly complex. First, soil-structure interaction plays an important role, as piles are partly buried under ground. Secondly, due to the fact of laying on sloped surfaces, the distance from the deck to soil on seaward piles will be larger than on land side, therefore lateral stiffness of piles is not uniform. Consequently, the center of gravity and the center of rigidity of the wharf will frequently be eccentric, which implies a torsional response of the wharf under seismic condition. Third, seismic loading will commonly entail inelastic behavior of the structure, which plays a central role on redistribution of forces and energy dissipation.

Traditional seismic design of structures has been done by means of force-based design. In short, internal forces that result from structural analyses are compared to cross-section resistance. However, this design approach may lead to very uneconomical structures when designing in high intensity seismic zones (International Navigation Association, 2001) especially if stiffness is not uniform along the structure. A different approach to seismic design is performance-based design, which contributes to rationalize the conception of the wharf. In brief, it consists on allowing the structure functionality to be altered for different seismic hazards (Ghobarah, 2001). For instance, the port facility should guarantee its serviceability for low intensity seismic events, while focusing on life protection for large scale earthquakes by avoiding collapse. Structural

functionality is commonly associated to structural damage, which in turn may be defined in terms of strains or rotations of structural elements, among others. Then, each association of a seismic hazard and a damage limitation is referred as a performance level.

ASCE 61-14, Seismic Design of Piers and Wharves (American Society of Civil Engineers, 2014) is the only available standard regarding seismic design of pile supported wharves. Additionally, some design guidelines are available, such as The Port of Long Beach Wharf Design Criteria 2015 (POL-B), developed by the Harbor Department of the City of Long beach, and the Port of Los Angeles Code for Seismic Design 2010 (POL-A), introduced by the City of Los Angeles Harbor Department. Finally, the Permanent International Association for Navigation Congresses, or PIANC (International Navigation Association, 2001), formed a working group (WG34) that focused on seismic affectations on port structures. All these documents are mainly based on performance-based principles, particularly adopting displacement-based design.

Displacement-based design, a particular performance-based design, assumes that damage can be correlated with the horizontal drift of the structure. In this case, for each performance level, a maximum allowable displacement can be assigned, referred as capacity, which is then compared to the actual displacement of the structure under seismic situation, called demand. Concisely, if demand is inferior to capacity, seismic design is verified. Different structural analyses and methods may be used to determine capacity and demand.

A complete 3D design could result in the most realistic approach to structural modeling. For instance, (Su et al., 2017) developed a coupled soil-structure model using three-dimensional finite elements of a pile-supported wharf, and performed time history analyses. Even if results might be of greater accuracy, this approach is impractical for design, as computational complexity is extremely high. Even less complex three-dimensional models, for instance using common structural analysis software, turn out to be very computer demanding for time-history analyses. Therefore, their applicability to practical design is limited.

Simpler approaches to determine the wharf displacement capacity may be done using non-static linear pushover analyses. Its main idea is to track the relationship between an increasing lateral force on the structure and the drift of a representative point, situated at the wharf deck. Due to inelastic behavior of the system, such as yielding of soil or structural elements, the resulting relationship is typically non-linear. This relationship is commonly known as the capacity curve of the structure.

On the other hand, different methods exist to analyze seismic demand of the wharf. By focusing on the peak response of the wharf rather than on its time-step behavior, computer complexity is reduced. The response spectrum analysis, based on a three-dimensional modal analysis of the structure, may be well suited for elastic design, but loses its interest when large inelastic response is expected. Alternatively, a purely transverse analysis of the structure may be followed, which relies on the structural uniformity of the wharf along its longitudinal direction. The substitute structure method is based on this approach, and allows to consider structural non-linearities in the analysis. Although the structural modeling might have reduced substantially, these methods need, however, special care for applying them, as different aspects can influence greatly results.

In any case, some correlation between purely transverse demand and global demand will be needed. The Dynamic Magnification Factor is defined to this purpose (Benzoni & Priestley, 2003). Indeed, it is clear that simultaneous longitudinal and transversal seismic excitation of the wharf, as well as torsional effects, will induce displacement demands along both horizontal directions, while purely transverse analysis will only capture demand along one direction.

Due to uncertainties regarding geotechnical characterization, seismic design is assessed considering different soil conditions. Typically, soil stiffness and strength are multiplied by some safety factors, both for increasing or decreasing their properties, defining upper and lower soil cases. Additionally, another aspect that may influence design of piles is a geotechnical failure such as lateral spreading. The load applied by the soil to the piles is known as kinematic forces, and to be able to implement them into structural models, simplified methodologies are needed.

The research presented in this thesis reviews the most important concepts of seismic design of pile-supported wharves. The document intends to facilitate the comprehension of specific code requirements, such as ASCE 61-14 or POL-B, as well as to contrast their approaches and requirements.

The first objective of this thesis is to provide contextualization and comprehension basis to specific seismic wharf design standards, with emphasis in performance and displacement-based design. Secondly, this study aims to identify and examine relevant structural analysis methods that are most suitable for production purposes. Third, most important aspects influencing seismic design of wharves shall be identified. And fourth, the objective of developing some design guidance to facilitate and clarify engineering practice.

A practical case study which consists on a regular pile-supported wharf is the tool to achieve the purpose of the present thesis. This structure is composed by steel piles and a reinforced concrete super-structure. Although the geotechnical component of the problem is not the main scope of this study, particular soil properties are chosen to develop necessary soil-structure interaction modeling. Seismic hazard is defined using code-specific design spectra. The following models are developed. First, a three-dimensional complete model for performing modal analyses. Second, a non-linear transverse model for purely transverse seismic loading of the structure. Finally, non-linear time history analyses are applied to simplified wharf models using the "Super-Pile" approach, which reduces very significantly numerical complexity.

This document is organized in five main chapters, being the first one the present introduction. Second chapter, state of the art, reviews performance-based and displacement-based approaches. Methods for obtaining displacement capacity and demand are revised, with special emphasis on the substitute structure method. Third chapter, methodology and modeling, describes the case study, as well as all necessary modeling assumptions and procedures to constitute structural models. Fourth chapter, results, performs relevant structural analysis to the case study, notably non-linear static pushover analyses, purely transverse demand analysis and time-history analysis. Finally, last chapter, conclusions, summarizes main findings.

2. STATE OF THE ART

The main objective of this section is to review the design approach provided by ASCE 61-14, POL-A, POL-B and PIANC, and to identify those aspects that may differ between them, be unclear, or which need further consideration. These codes and design guidelines will be complemented with literature in order to contrast information and contribute to the topic. The precise relevant details of the codes will not be reviewed at this stage, but rather be detailed in the section 3.

2.1.   PERFORMANCE-BASED DESIGN

The fundamental idea of performance-based design is assigning to various seismic intensities a certain level of functionality of the structure. For instance, maintaining serviceability of the facility after low intensity earthquakes, and life safety protection for larger magnitude events. A common approach is to correlate functionality to structural damage (Ghobarah, 2001).

PIANC (International Navigation Association, 2001) classifies damage into four categories: serviceable, repairable, near collapse and collapse. The first damage level does not imply any or little structural degradation, and operations on the structure may persist. The repairable damage condition will probably lead to limited inelastic response of the structure, which requires some feasible reparations that may cause short-term loss of serviceability. Next, near collapse damage is characterized by large inelastic behavior, with total loss of serviceability, while being able to resist gravity loads. Long-term repair works or complete substitution of the structure may be needed. However, the structure should guarantee the protection of human lives. Lastly, when the structure loses its integrity completely, it falls into the fourth damage level, collapse.

Subsequently, different seismic hazard levels must be identified and classified in order to be able to assess the performance of the wharf. Naturally, for increasingly demanding ground movements, damage requirements to the structure will become less restrictive. Typically, seismic hazard is classified by its probability of exceedance. PIANC identifies two seismic levels, one for probable earthquakes during the wharf life-span, and the other for rare strong shaking that may imply large demands on the structure. Combining damage and seismic hazard levels leads to defining performance levels.

Figure 2.1. Performance-based design philosophy

The choice of a performance level should be determined regarding the structure importance, in terms of potential human lives loss, contingency after an earthquake, and socioeconomic impact. Usually, the authority having jurisdiction will dictate the minimum requirements of a

type of structure, but the owner may always choose to request supplementary performance properties.

The Seismic Design of Piers and Wharves Standard (American Society of Civil Engineers, 2014) considers three seismic hazard levels and three acceptable damage categories, resulting in three performance levels. Seismic hazards are classified in Operating Level Earthquake (OLE), associated with frequent low intensity earthquakes, Contingency Level Earthquake (CLE), with stronger ground shaking and, finally, Design Earthquake (DE), which is the most severe case considered in design. Life safety protection is always required by ASCE 61-14 under the design earthquake. The three acceptable damage levels according to ASCE 61-14 may be summarized in the following manner:

- Minimal Damage:
  - o The inelastic behavior of the structure is very limited.
  - o Serviceability is guaranteed after an event.
- Controlled and Repairable Damage:
  - o The response of the structure is inelastic with enough ductility.
  - o Damage is located in accessible positions, allowing its reparation.
  - o Serviceability may be interrupted, but for a period of maximum several months.
- Life Safety Protection:
  - o Gravity loads must be supported by the structure after a major seismic event.
  - o Damage must not prevent evacuation of the structure.

With the combination of seismic hazards and performance levels, three design classifications are possible, according to the structure importance: high, moderate and low. For the "high" design classification, seismic hazards to be considered in design with the corresponding damage levels can be found in Table 2.1.

Table 2.1. Seismic hazards and performance levels for ASCE 61 high design classification.

	Probability of exceedance	Damage level
Operating level earthquake (OLE)	20% in 50 years	Minimal Damage
Contingency level earthquake (CLE)	10% in 50 years	Controlled and Repairable Damage
Design earthquake (DE)	Code Specific	Life Safety Protection

Quantifying damage to the structure is a necessary step for applying this philosophy. Indeed, damage could be assessed in multiple manners: strains, stresses, rotations, fissures, etc. In order to determine which magnitude may be most useful to control performance, possible damage to a pile-supported wharf should be reviewed first in a holistic approach.

Three main structural components can be distinguished in a pile-supported wharf: the deck, the substructure (pile foundation) and the dike. Inertial forces on the structure will displace the

deck, bending the piles underneath. A geotechnical failure may also occur, resulting in displacements and stresses in piles deep in ground.
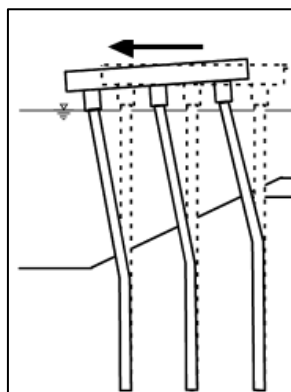
Figure 2.2. Drift of a pile-supported wharf (PIANC).

The horizontal translation of the deck may have multiple consequences, being the bending of the piles the most obvious one. While the buried part of the foundation may experiment no displacement with respect to the soil, the free length of piles will experiment substantial deformations as a consequence of the inertial loading of the deck, and large rotations can concentrate on the pile top, as well as near the dike surface. As a result of this typical deformed shape, bending laws will typically develop with peaks at the deck connection as well as below the mud line. Regarding the deck, one obvious consequence will be large horizontal displacements. However, tilting can also occur, which may be an issue for large ship to shore cranes serviceability. In concordance with the repairability of different elements, inelastic behavior of members should be preferred at the pile-deck connection. Likewise, inelastic behavior in the deck is generally not permitted.

There exists sufficient consensus on the indicators to be used to control damage in pile supported wharves, which are mainly related to the constitutive behavior of structural members. PIANC states that performance levels should be assessed by controlling the amount of inelastic response of piles during the peak seismic response. Nonetheless, it does not give any further details about which would be the limits for each seismic scenario.

On the other hand, ASCE 61-14, POL-A and POL-B propose specific strain limitations for the three seismic scenarios, OLE, CLE and DE, for different structural members. Table 2.2 summarizes strain limitations from ASCE 61-14 on steel pipe pile wharf structures, for the three seismic scenarios. These strain limitations refer to the potential appearance of plastic hinges, where rotation will concentrate. Three different locations are given: top of pile, in ground, or deep in ground. The first position corresponds to the pile-to-deck connection, which typically consists of a concrete plug that is inserted at the top of the steel pile. Note that in this case, there are no steel strain limitations, only concrete and reinforcing steel, since at that point all structural performance is carried by the connection, and not the pile. In ground hinges are those

considered to appear between the mud line and ten times the pile diameter underground. Finally, deep in ground hinges are considered to be deeper than ten times the pile diameter.

Table 2.2. Maximum strains for each seismic hazard level according to ASCE 61-14.

SEISMIC CASE	COMPONENT	TOP OF PILE HINGE	IN GROUND HINGE	DEEP IN GROUND HINGE
OLE	Steel pipe	-	$\varepsilon_s \leq 0.010$	$\varepsilon_s \leq 0.010$
	Concrete	$\varepsilon_c \leq 0.010$	-	-
	Reinforcing steel	$\varepsilon_s \leq 0.015$	-	-
CLE	Steel pipe	-	$\varepsilon_s \leq 0.025^{(a)}$	$\varepsilon_s \leq 0.035$
	Concrete	$\varepsilon_c \leq 0.025$	-	-
	Reinforcing steel	$\varepsilon_s \leq 0,6\varepsilon_{smd}^{(b)} \leq 0,06$	-	-
DE	Steel pipe	-	$\varepsilon_s \leq 0.035^{(a)}$	$\varepsilon_s \leq 0.050$
	Concrete	No limit	-	-
	Reinforcing steel	$\varepsilon_s \leq 0.8\varepsilon_{smd}^{(b)} \leq 0.08$	-	-

(a) If the pile is infilled with concrete, the strain limitation can be taken as 0.035 for CLE and 0.050 for DE.

(b) ε_{smd} is the steel reinforcement strain at peak stress.

Additionally, both ASCE 61-14 and POL-B only allow damage on piles due to bending. On the other hand, piles must be capacity protected for shear. Similarly, the superstructure of the deck must be capacity protected against bending and shear.

2.2.   DISPLACEMENT-BASED DESIGN

Over the last 30 years, displacement-based design has evolved greatly, and has come to be an engineering tool rather than just an approach in research studies. This approach allows to consider inelastic response of the structure directly in the design, having more control about the global behavior of the structure (Ghobarah, 2001). Displacement based-design is a performance-based design. Hence, it will be governed by the intensity of ground shakings and the maximum admissible damage to the structure. Nevertheless, displacement-based design still may use key developments of usual earthquake engineering such as response spectrums. Therefore, it gives engineers new tools to analyze structures in greater detail, but without losing the advantages of working with well stablished tools in international structural codes.

The main idea of displacement-based design, as its name implies, is to control displacements rather than stresses. Therefore, structural check will consist on comparing the demand displacements, which is the response of the structure under a specific seismic scenario, and the structural displacement capacity, which is defined as the maximum displacement that the

structure can provide at a specific level of performance. Being Δ_d the displacement demand and Δ_c the displacement capacity of the structure for a given seismic intensity, equation (1) represents the main idea of displacement-based design.

$$\Delta_d \leq \Delta_c \tag{1}$$

2.2.1. Displacement Capacity Analysis Methods

As stated previously, depending on the seismic level that acts on the structure, different damage to the structure will be allowed. For frequent low intensity events, low damage and mainly elastic response is expected, and therefore serviceability is may be assured, while for severe infrequent earthquakes, more damage is allowed, such that extensive repairs shall be conducted, while guaranteeing live protection.

Two methods are mentioned in ASCE 61-14 to obtain capacity: nonlinear static pushover analysis and nonlinear time-history analysis. The former is based on obtaining gradually the nonlinear relation between a horizontal action on the structure and the displacement of a control point, while updating at each step the structural properties due to inelastic response. On the other hand, nonlinear time-history analysis consists on direct integration of the nonlinear response of the structure under a specific seismic accelerogram, which allows to check at each time step demand versus capacity.

2.2.1.1. *Non-linear static pushover analysis*

The pushover analysis, although it is not based on a rigorous theoretical basis, allows designers to obtain the sequence of nonlinearity in a given structure by applying increasing actions and tracking its response (Leslie et al., 2009).

Structural properties of the wharf will evolve with increasing displacements. Soil non-linearity, as well as plastic hinge formation in structural elements, will contribute to the inelastic behavior. Furthermore, the yielding sequence of different members and soil is not known in advanced, even if it may be estimated.

The main output of this type of analysis is the so-called pushover curve, or capacity curve, which is the relation between the displacement of a representative point of the structure, and the total lateral force applied to the structure, referred also as base shear. The displacement control point is commonly assumed to be the roof displacement for typical building structures, while for a wharf structure it would be the displacement of the deck. Note that a fundamental hypothesis is made, which is assuming a specific displacement field of the deformed structure. This should not be a problem for fundamentally one degree of freedom structures, such as short buildings, or wharves in the transverse direction, as the influence of higher order modes on the real dynamic response of the structure is negligible. Since wharves are three-dimensional eccentric structures, it may not seem apparent pushover analysis applicability. However, due to the fact

that along longitudinal direction of the wharf (parallel to shore), only little variations of soil and structural properties are expected, the structure is usually longitudinally symmetric. Therefore, pure transverse response of the wharf is not eccentric. Additionally, although the wharf is not a single degree of freedom system in the three-dimensional configuration, as usually the first mode is torsional, the transverse mode of the structure is purely translational (Blandon, 2007). As a consequence, if the wharf is regarded as a two-dimensional structure along its transverse axis, the problem is reduced to a single degree of freedom purely translational system. POL-B and ASCE 61 recognize this aspect, and allow capacity to be based on transversal analysis.

Generally speaking, the vertical distribution of the lateral load on the structure is relevant, especially for multiple story buildings, and may influence the results of the pushover curve (Leslie et al., 2009). However, in the case of wharves, most part of the mass is concentrated in the deck level, and therefore choice of load pattern on the structure is limited. Applying a lateral force at the deck level and controlling analysis by displacement of the deck is common practice (Priestley et al., 2007).

Due to dike slope, landward piles will have more flexural rigidity than on the sea side. As the top displacements of piles is linked by the deck, which acts as a horizontal diaphragm providing a monolithic behavior, first plastic hinges will appear on the piles with shortest free length to the deck, defined as the distance between the dike and the deck soffit (deck lowest part). Figure 2.3 represents an example of pushover analysis on a typical wharf section. Note that in the pushover curve, there is an initial elastic phase until the first plastic hinge appears. However, this initial branch may show slight non-linearity due to inelastic behavior of soil springs. It may also be observed that the appearance of in-ground plastic hinges creates mechanisms on piles increase lateral flexibility of the structure. It is clear that the formation of plastic hinges in all piles both in pile top and in-ground is completely unacceptable, even if damage limits are not achieved, as structural stability of the wharf would be compromised. Finally, for each load step on the pushover analysis, strains at each member will be known, with plastic rotation being of especial interest. Therefore, the capacity of the structure for OLE, CLE and DE levels will be the displacement of the deck that causes the most developed plastic hinge to reach maximum permitted strains.
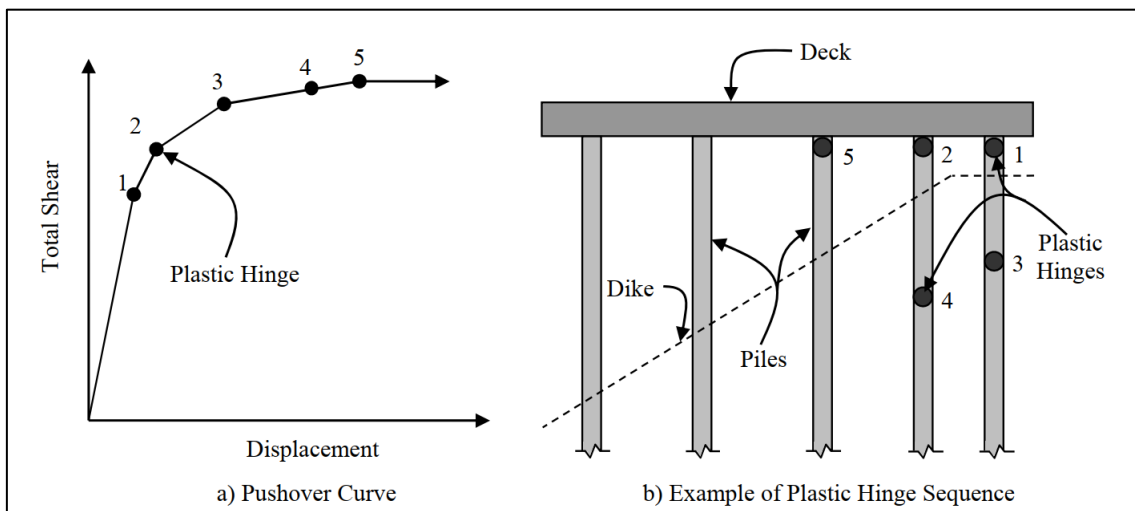
Figure 2.3. Pushover curve and plastic hinge on piles sequence for a typical wharf section (POL-B).

9

2.2.1.2.   *Non-linear time history analysis*

Another indirect approach to assess seismic capacity of the structure is to model directly the inelastic properties of members in a complete model of the wharf, and exciting the system using accelerograms compatible with design spectra. Time-step integration of the structure will provide the response under seismic conditions, and maximum plastic rotations will be checked against maximum strains according to each performance level for each time step. This is an indirect method to assess capacity, as maximum acceptable displacements are not known by this analysis, but rather it is checked explicitly that strains, or rotations, do not exceed allowable limits. As a result, non-linear time history analysis may be considered as both a capacity and a demand method. Section 2.5 presents further details on time-history analysis.

2.2.2.   Displacement Demand Analysis Methods

Two main groups can be distinguished: 2D and 3D methods. Bi-dimensional methods focus on the demand of the structurally regarding only the transverse direction, and then longitudinal demand and torsional effects is considered via the so-called Dynamic Magnification Factor (Benzoni & Priestley, 2003). On the other hand, 3D methods consider simultaneously the effect of transversal and longitudinal seismic excitation. POL-B and ASCE 61-14 have some differences regarding seismic demand, although the main approach is similar.

Two methods are available in the two-dimensional analysis group, the elastic stiffness method and the substitute structure method. The first one is linear, and it is based on the elastic spectral response of a one degree of freedom structure characterized by initial equivalent elastic properties of the wharf. On the other hand, the substitute structure method is non-linear, and considers stiffness degradation and inelastic dissipation based on the capacity curve. Three-dimensional analysis may be performed by a multimodal response spectrum analysis, which is linear, or a non-linear time history analysis. Due to potential high complexity of computer models, the three-dimensional complete model might be simplified using the "Super-Pile" approach (POL-B).
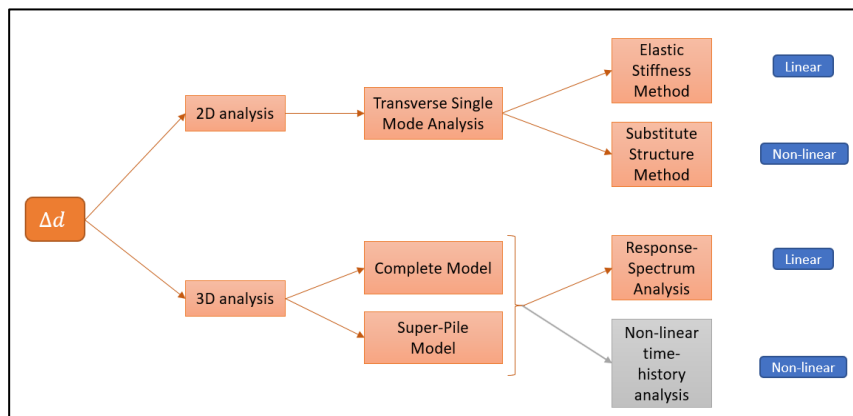
Figure 2.4. Structural analysis methods to obtain seismic demands, according to POL-B.

2.2.2.1.   Response spectrum analysis

Both ASCE 61-14 and POL-B consider response spectrum analysis as a valid demand method, but with some limitations.

The first step to perform this type of analysis is the modal discretization of the structure. According to both ASCE 61-14 and POL-B, a minimum amount of 90% of the participating mass in each principal direction must be captured by all considered modes. Then, modal spectral response will be obtained using, according to POL-B, at an equivalent damping of 5%, unless a higher ratio can be justified. For both longitudinal and transverse directions, modal combination should be done using the Complete Quadratic Combination rule. Finally, combined response of orthogonal directions shall be obtained via an absolute sum, considering 100% and 30% of longitudinal and transverse responses respectively, and vice versa, whichever is larger. Being Δ_{XL} and Δ_{XT} the transversal displacement caused by longitudinal and transverse excitation, respectively, and Δ_{YL} and Δ_{YT}, idem for the longitudinal direction, demand using the response spectrum method will be obtained by equation (2).

$$\Delta_{X1} = \Delta_{XL} + 0.3\Delta_{XT}$$
$$\Delta_{Y1} = \Delta_{YL} + 0.3\Delta_{YT}$$
$$\Delta_{X2} = 0.3\Delta_{XL} + \Delta_{XT}$$
$$\Delta_{Y2} = 0.3\Delta_{YL} + \Delta_{YT}$$
$$\Delta d = max\left(\sqrt{\Delta_{X1}^2 + \Delta_{Y1}^2}; \sqrt{\Delta_{X2}^2 + \Delta_{Y2}^2} \right)$$

(2)

ASCE 61-14 states that effective secant stiffness shall be used instead of initial elastic properties if yielding of piles is expected. However, effective stiffness depends on the displacement demand, which is not known at this step, making this approach quite impractical for design. Furthermore, while this effective stiffness may be relatively simple to obtain in the transverse direction using pushover analysis, performed for evaluating displacement capacity, complexity increases when orthogonal effective properties should be considered, as well as torsional effects. And, finally, as response spectrum considers multiple modes, it is not clear how to obtain effective properties for them. Additionally, POL-B states that response spectrum analysis should not be used if displacement demand to capacity ratio exceeds 85%.

2.2.2.2.   Transverse single mode analysis

The response of a wharf under transversal seismic action behaves essentially as a one degree of freedom system. In fact, transversally, the main period is the translation of the wharf, while higher order modes may correspond to vibration of individual or groups of piles, as well as flexure of the deck. As a consequence, the influence of higher order modes is usually negligible.

Although POL-A and POL-B propose two possible approaches, the elastic stiffness method and substitute structure model, ASCE 61-14 only mentions the latter. Both methods are similar in their philosophy, but the first is linear and based on initial structural properties, while the second is non-linear and considers stiffness degradation and plastic dissipation. In fact, the elastic

stiffness method can be understood as a simpler particular case of the substitute structure method. Section 2.3 reviews more in depth relevant central aspects of this method.

2.3. SUBSTITUTE STRUCTURE METHOD

The substitute structure method (Shibata & Sozen, 1976) extrapolates the original structure, with inelastic properties, to an elastic single degree of freedom structure with effective properties, such that expected maximum seismic displacements for both structures are equal. This substitute structure, in addition to a reduced effective stiffness, has an equivalent elastic damping, that contributes to dissipate more energy, simulating the inelastic behavior of the original structure. Effective properties of the substitute structure will then be used to obtain seismic demand using design response spectra. Note that effective properties depend on displacement demand, as it can be observed in a pushover analysis, and that demand is not known at first stage. Therefore, an iterative approach has to be used, where demand is initially assumed, effective properties are obtained, and spectral demand is obtained. Comparing resulting spectral displacement to assumed demand will indicate if the latter corresponds indeed to the substitute structure.

Although the main idea is simple, there are some key aspects that should be assessed in detail in order to perform an appropriate modeling. First, how to obtain effective stiffness from pushover curve. Then, how to model hysteretic behavior of structural members by an equivalent elastic damping. And finally, how to reduce design spectra, usually defined for a 5% equivalent viscous damping, to the effective damping of the substitute structure. Either in ASCE 61-14, POL-A and POL-B, there is not little guidance on these aspects.

2.3.1. Effective Stiffness

Both ASCE 61-14 and POL-B suggest a bilinearization of the pushover curve according to the equal energy approach. The initial stiffness, noted k_i, should follow the linear part of the pushover curve. No details are given in POL-B, although in ASCE 61-14, this initial elastic branch is defined as the line that passes through the origin and the first yielding of the soil or the structure. The nonlinear part of the pushover curve is modeled by a less steep branch. POL-B states that this second branch should be determined from the estimated displacement demand for CLE, with no further specifications. On the other hand, ASCE 61-14 recommends determining the secondary branch from the point where pushover curve starts to lose strength, or based on the expected displacement demand for DE. On both cases, the second point of the inelastic branch will be on the linear branch, defining the effective yield displacement of the structure. This point is found such that the area at both sides of the intersection of the plastic branch with the pushover curve between these two curves, must be equal. This is required such that dissipated energy of both curves is equal.
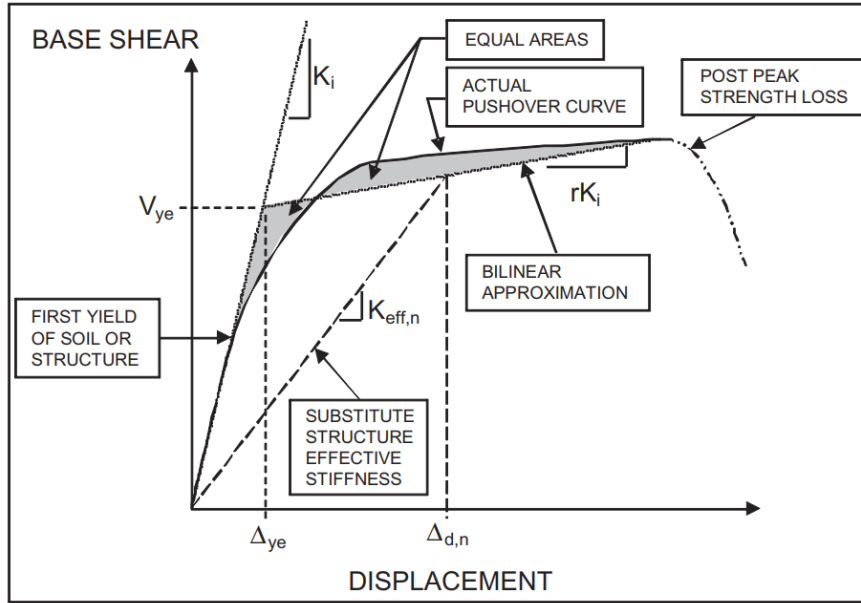
Figure 2.5. Bilinear approximation of the pushover curve to obtain effective properties (ASCE 61-14).

The ductility of the structure is defined as the ratio between displacement demand (Δ_d) and effective yield displacement (Δ_y), and is noted by μ.

$$\mu = \frac{\Delta_d}{\Delta_y} \tag{3}$$

Once the bilinear pushover approximation is obtained, the effective stiffness can easily be computed geometrically, according to equation (4), being the slope of the secondary inelastic branch r times the initial stiffness, k_i, also known as tangent stiffness.

$$k_{eff} = \frac{k_i}{\mu}[r(\mu - 1) + 1] \tag{4}$$

2.3.2. Equivalent Viscous Damping

During strong ground shaking of the ground, the structure will behave inelastically and plastic hinges will dissipate energy. Typically, on seismic design, which analyzes elastically the response of a structure, an elastic damping of 5% is considered. This damping models different factors that are not intrinsically considered in the structural model, such as foundation compliance or non-linearity, radiation damping and interaction among other non-structural elements (Calvi et al., 2008). However, in order to introduce additional dissipation of the elastic substitute structure, which represents the original inelastic one, a hysteretic damping term is added to the elastic one, giving the total equivalent viscous damping of the structure, as noted in equation (5).

$$\xi_{eff} = \xi_{el} + \xi_{hyst} \tag{5}$$

The hysteretic behavior of a system is based on the force-displacement (or force-rotation) relation of a structural system. Figure 2.6 illustrates an elasto-plastic hysteretic loop, and defines the areas to compute the equivalent viscous damping, as indicated in equation (6) (Dwairi et al., 2007).
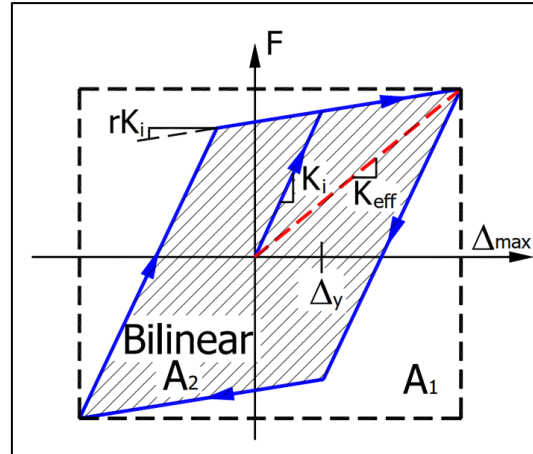
Figure 2.6. Elasto-plastic force-displacement hysteretic behavior (Dwairi et al., 2007).

$$\xi_{hyst} = \frac{2}{\pi} \cdot \frac{A_2}{A_1}$$

(6)

Certainly, the ratio between A_1 and A_2 in equation (6) depends on the particular hysteretic behavior of the structure, and the ductility of the system. Many hysteretic models are found in literature. Two common models are the Takeda model (Takeda et al., 1970), which is commonly used to model reinforced concrete members, and the elasto-plastic model, that may be appropriate for steel members. As concrete behavior is strongly dependent on axial force, modified Takeda hysteretic rules are used for beams or columns. The Thin Takeda is commonly used for column elements, which is less dissipative than the Thick Takeda, which is more appropriate for beam concrete elements, subjected to lower axial loads (Priestley et al., 1996).

Referring to Figure 2.7, the general Takeda model is characterized by the following behavior. An initial elastic branch with slope K_o proceeded by a plastic branch with slope rK_o (tangent stiffness). The intersection of these two branches defines the yield displacement Δ_y. Unloading branch has a slope K_u, dependent on the inverse of ductility and a parameter α, and descends down to zero force. Finally, the reloading branch reaches the plastic branch at a point which is at $\beta\Delta_p$ from maximum attained displacement (Δ_u), being Δ_p the difference between Δ_u and Δ_y.
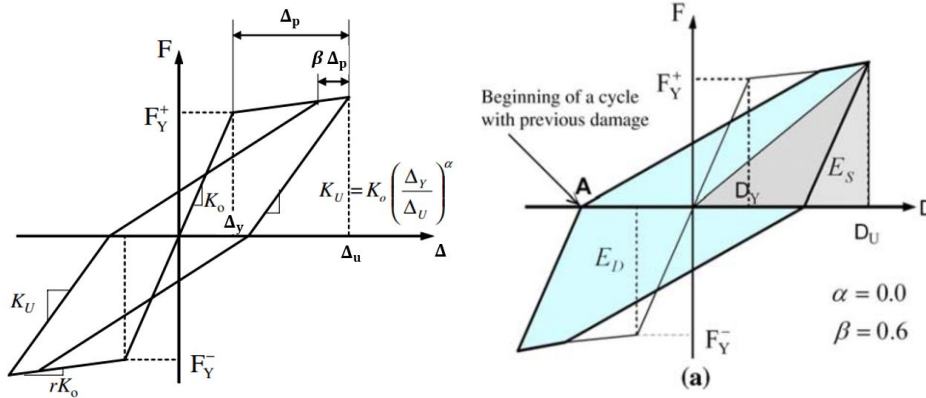
Figure 2.7. Takeda hysteretic model (left) and hysteretic loop (right) (Lu & Silva, 2006).

The resulting hysteretic loop is the area between plastic, reloading and unloading branches. By applying equation (6) to the general Takeda model, the equivalent hysteretic damping is obtained (Lu & Silva, 2006):

$$
\begin{aligned}
\xi_{hyst} &= \frac{1}{2\pi} \\
&\cdot \left(\frac{[1 + r(1-\beta)(\mu-1)]\{2\mu + \beta(\mu-1) - \mu^\alpha[1 + r(\mu-1)]\}}{\mu[1 + r(\mu-1)]} \right. \\
&+ \left. \frac{r\beta^2(\mu-1)^2 - \mu^\alpha[1 + r(\mu-1)]^2}{\mu[1 + r(\mu-1)]} \right)
\end{aligned}
\tag{7}
$$

The same approach can be followed with the elasto-plastic model, which is less geometrically complex. Referring to Figure 2.6, the model is characterized by an initial branch of slope K_i, followed by a plastic branch of tangent stiffness rK_i. The unloading and reloading branches have the same slope as the initial branch. Next equation gives the geometrical deduction of associated damping to the elasto-plastic model.

$$
\xi_{hyst} = \frac{2}{\pi} \cdot \frac{(\mu-1) \cdot (1-r)}{\mu \cdot (1 + r\mu - r)}
\tag{8}
$$

(Dwairi et al., 2007) finds that for low periods, previous expressions do not sufficiently agree with time history analyses, hence it proposes corrected expressions. The authors consider the specific case the Takeda model with $r = 0$, which is assuming that the concrete member behaves perfectly plastic on the first loading cycle after yielding. Parameters α and β are taken as 0,5 and 0, respectively. Equation (9) represents the Thin Takeda model (reinforced concrete columns), while equation (10) applies to elasto-plastic models (steel members). Note that these equations do not depend on r.

$$\xi_{hyst} = C_{LT}\left(\frac{\mu - 1}{\pi\mu}\right)\%$$
$$C_{LT} = 65 + 50\left(1 - T_{eff}\right) \qquad T_{eff} < 1\,s$$
$$C_{LT} = 65 \qquad T_{eff} \geq 1\,s$$

(9)

$$\xi_{hyst} = C_{EP}\left(\frac{\mu - 1}{\pi\mu}\right)\%$$
$$C_{EP} = 85 + 60\left(1 - T_{eff}\right) \qquad T_{eff} < 1\,s$$
$$C_{EP} = 85 \qquad T_{eff} \geq 1\,s$$

(10)

(Lu & Silva, 2006) proposes a simpler expression for the Thin Takeda model with $\alpha = 0{,}5$ and $\beta = 0$, an expression for any value of r. However, no correction is applied for low structural periods.

$$\xi_{hyst} = \frac{1}{\pi}\left(1 - \frac{1 - r}{\sqrt{\mu}} - r\sqrt{\mu}\right)$$

(11)

(Priestley et al., 2007) proposes next expression, which is also based on the Thin Takeda, although differently calibrated.

$$\xi_{hyst} = 0.444\left(\frac{\mu - 1}{\pi\mu}\right)$$

(12)

(M. J. N. Priestley, 2000) suggests that soil contribution to damping could also be considered in the equivalent hysteretic damping of the structure, and proposes a pondered contribution of both soil and structural elements to the global system. Being Δ_f displacement of foundation and Δ_s the displacement of the structure, considering a rigid foundation, and ξ_f and ξ_s respective hysteresis damping values, equation (13) represents the combined soil-structure hysteretic damping. The same approach can be followed to introduce additional damping from seismic isolation devices.

$$\xi_{hyst} = \frac{\xi_f \Delta_f + \xi_s \Delta_s}{\Delta_f + \Delta_s}$$

(13)

Damping expressions provided by the codes

Both ASCE 61-14 and POL-B provide expressions for total equivalent damping of the substitute structures. However, they do not mention which are the considered hysteretic assumptions. First, ASCE 61-14 mentions that it is allowed to use an increased damping, although it is not required, using equation (15). Certainly, if no additional damping is used in design, seismic displacement demand will be higher. By comparison with previous expressions, ASCE 61-14 considers an elastic damping of 5%, and matches the Thin Takeda model, leaving r as a variable to be obtained from the pushover curve, as in equation (14).

$$\xi_{eff} = 0.05 + \frac{1}{\pi}\left(1 - \frac{1-r}{\sqrt{\mu}} - r\sqrt{\mu}\right) \tag{15}$$

POL-A and POL-B propose an expression which is not dependent on tangent stiffness of the bilinear approximation of the capacity curve, on equation (16). The coefficient before the ductility term is slightly lower the resulting coefficient for a Thin Takeda model with $r = 0$, which would result from a horizontal secondary branch of the pushover curve, which may not be necessarily always the case. Note also that the elastic damping is taken as 10%.

$$\xi_{eff} = 0.1 + 0.565\left(\frac{\mu - 1}{\pi\mu}\right) \tag{16}$$

In summary, Figure 2.8 shows the equivalent damping corresponding to the exposed hysteretic models, for different levels of ductility.
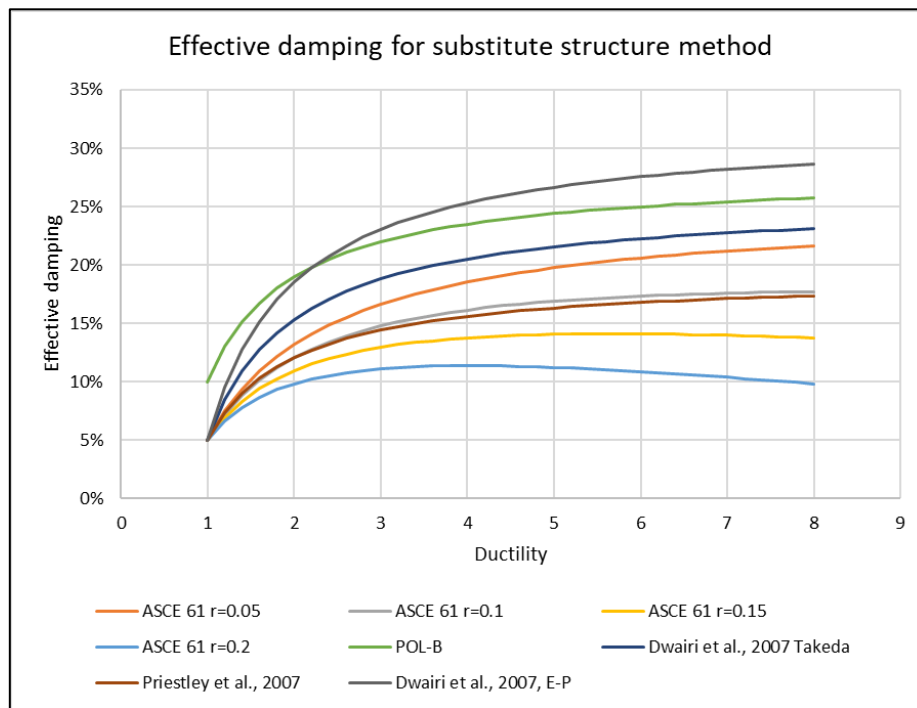
Figure 2.8. Effective equivalent damping comparison.

2.3.3. Design Spectrum Scaling Factor

Seismic design spectra are commonly defined for a fraction of critical damping of 5%. Thus, as the substitute structure may have larger effective damping, a tool for reducing spectra is needed for design.

Eurocode 8 (CEN, 2004), referred as EC8, proposes a damping scaling factor (DSF) which depends only on the equivalent damping of the structure, for structures with periods between 0,2s and 6s. This damping scaling factors are to be applied to spectral acceleration spectra. Being $S_a^{5\%}$ and S_a spectral accelerations for 5% damping and equivalent damping, respectively, equation

(17) relates these two magnitudes via the DSF. Note that the lower the DSF, the lower the spectral acceleration, hence lower displacement demand.

$$S_a = DSF \times S_a^{5\%} \tag{17}$$

Two versions have been proposed by Eurocodes, one introduced in 1994, equation (18), and the other in 2004, equation (19). (Kong & Kowalsky, 2016) indicates that displacement-based design has frequently used 1994 version, and that, compared to more complex DSF expressions, it is a reasonable expression for large magnitude earthquakes. (Calvi et al., 2008) proposes a modified expression for the 94 Eurocode expression, shown in equation (20).

$$DSF = \sqrt{\frac{7}{2 + \xi}} \tag{18}$$

$$DSF = \sqrt{\frac{10}{5 + \xi}} \tag{19}$$

$$DSF = \left(\frac{7}{2 + \xi}\right)^{0.25} \tag{20}$$

(Newmark & Hall, 1982) proposes alternative expressions for modifying design spectra. With the same notation as in the previous expressions, and considering an original damping of 5%, equation (21) is known as the velocity formula.

$$DSF = \frac{(2.31 - 0.41 \cdot \ln \xi)}{(2.31 - 0.41 \cdot \ln 5)} \tag{21}$$
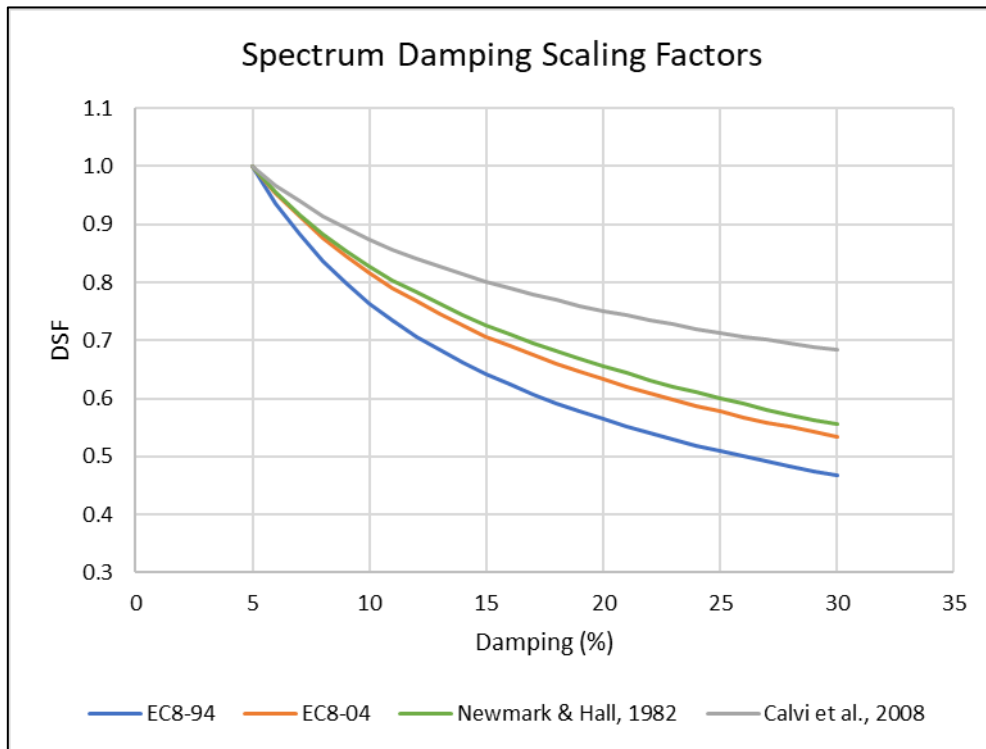
Figure 2.9. Spectrum Damping Scaling Factors for different levels of effective damping.

18

Finally, Figure 2.10 represents the flowchart to apply the substitute structure method. Note that the bilinear approximation of the pushover curve is part of the iteration process, as each displacement demand will imply different tangent stiffness (rk_i) and idealized yield displacement.
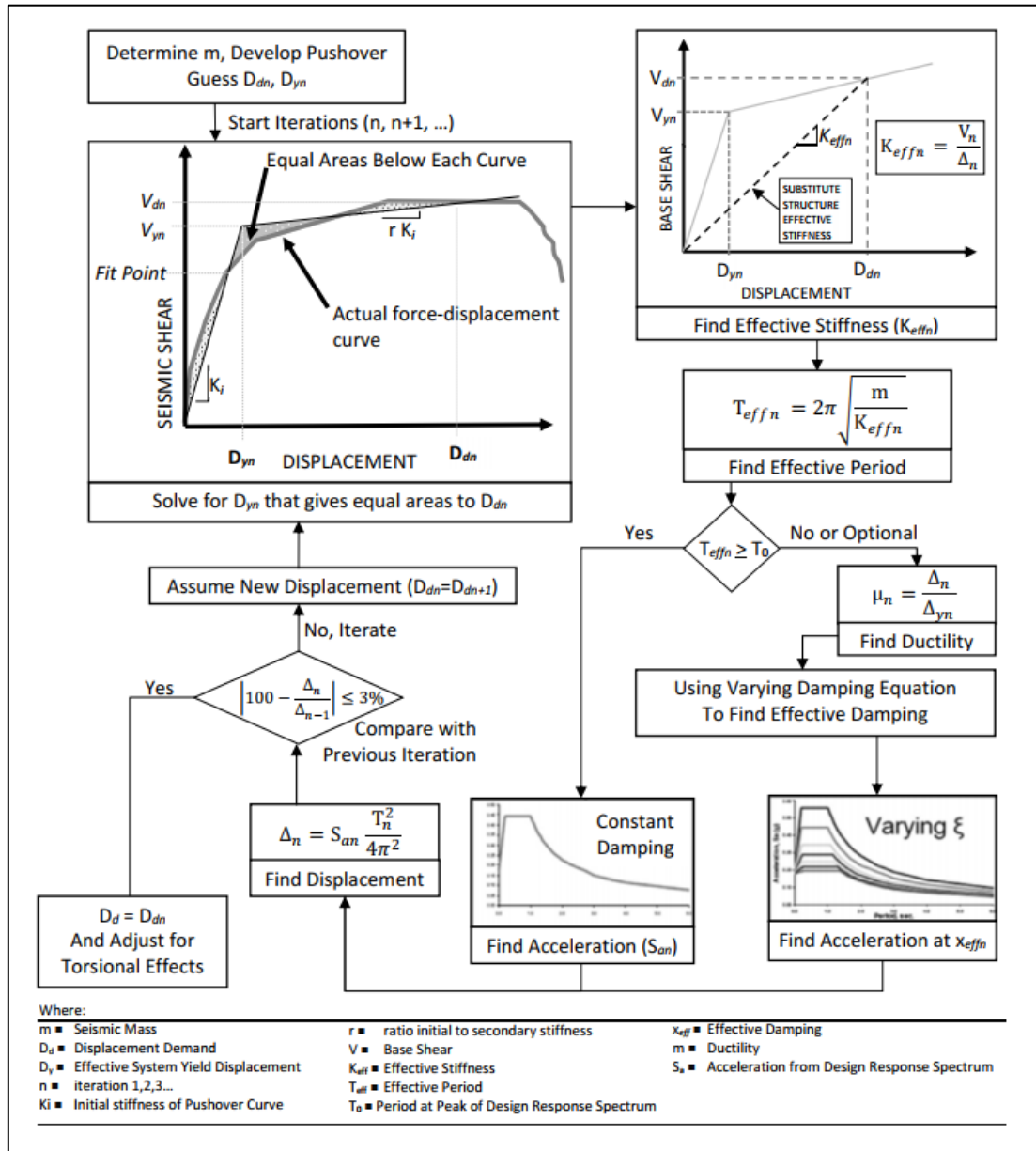
Figure 2.10. Substitute structure method flowchart (ASCE 61-14).

2.4.   DYNAMIC MAGNIFICATION FACTOR

Eccentricity between center of mass of the wharf and its center of rigidity will trigger torsional response when the wharf is excited longitudinally. In the transverse direction, as the wharf is supposed to be uniform (no structural stiffness variation nor significant soil changes), the center of rigidity and mass are expected to be aligned. Therefore, seismic actions along longitudinal direction of the wharf will cause both longitudinal and transversal displacements of piles, while transversal excitation will only cause transversal demand. Moreover, real seismic demand will not be unidirectional, hence combined effect of orthogonal directions shall be considered on the wharf.

The most solicited piles will be those on the corners of the wharf, due to torsional effects, as the distance to the center of rigidity is the largest. Additionally, shear keys, which connect consecutive wharf units, may also have an effect on displacement demand, being the most solicited piles those one the outer side of an external linked unit.

To the purpose of considering simultaneous longitudinal and transversal actions, as well as torsional effects due to stiffness eccentricity, a Dynamic Magnification Factor (DMF) is defined (Benzoni & Priestley, 2003). Considering only transversal seismic loading on the wharf, and being Δ_t the resultant displacement demand at the center of mass level, obtained by single mode transversal analyses, the aim is to obtain the corresponding maximum demand on a corner pile, Δ_{cr}, for the combined orthogonal loading seismic case. (Priestley et al., 2007) proposes a relation, shown in equation (22) between longitudinal displacement of the center of mass under pure longitudinal excitation, Δ_{ll}, and the resulting transversal demand due to torsional effects, Δ_{tl}, for the case of a single unit wharf over uniform soil conditions, and neglecting torsional inertia. It should be remarqued that ignoring torsional inertial effects is conservative, as displacement torsional demands will be necessarily larger.

$$\Delta_{tl} = \frac{6e}{L}\Delta_{ll} \tag{22}$$

Where eccentricity between center of mass is noted as e, and the length of the wharf by L. It should be noted that e may vary according to displacement demand, as yielding of shorter piles will reduce their rigidity. (Blandon, 2007) proposes an expression for obtaining the critical displacement of the corner pile considering the previous relation as well as simultaneous longitudinal and transversal excitation. Considering a seismic combination of 100% on the longitudinal direction and $X\%$ transversally, equation (23) gives the critical corner demand. On the other hand, equation (24) is the case for $X\%$ on longitudinal direction and 100% on the transversal.

$$\Delta_{cr} = \Delta_t \sqrt{1 + \left(\frac{X}{100} + \frac{6e}{L}\right)^2} \tag{23}$$

$$\Delta_{cr} = \Delta_t \sqrt{\left(\frac{X}{100}\right)^2 + \left(1 + \frac{X}{100} \cdot \frac{6e}{L}\right)^2} \tag{24}$$

(Priestley et al., 2007) affirms that time history analyses have shown that wharf design will be governed by full longitudinal seismic excitation with factored transversal load, giving maximum corner-pile demands. Additionally, considering that the value of $X = 30\%$ is most frequent in seismic design, the critical demand Δ_{cr} may be taken as indicated in equation (25). However, rotating the main seismic principal direction about 30 to 45 degrees with respect to the longitudinal axis may increment critical demand up to 15% compared to equation (25).

$$\Delta_{cr} = \Delta_t \times DMF$$
$$DMF = \sqrt{1 + \left(0.3 + \frac{6e}{L}\right)^2} \tag{25}$$

Previous DMF expressions only consider the influence of stiffness eccentricity, wharf length, and orthogonal factoring of seismic load. However, (Blandon, 2007) performed a series of inelastic time history analyses in order to evaluate the influence of other possible parameters. These analyses were performed on models with the following characteristics:

- Width (B): 33.5m
- Length (L): from 121m to 243m.
- Six rows of piles.
- Landside pile with a free length of 0.61m.
- Dike slope of 1.75H:1V.
- 610mm diameter prestressed octagonal piles.
- Center of mass: 16.9m (from landside pile).
- Center of rigidity: 2.1m
- Eccentricity: 14.48m

Results are summarized below of these studies are summarized below:

- DMF increases when upper bound soil properties are used.
- DMF is higher for OLE than CLE (higher DMF for lower intensity events).
- DMF is lower for linked segments than for single units.
- DMF is lower for the inner segment than for the exterior one for three-linked unit wharfs.
- DMF decreases linearly as segment length increases.
- DMF depends on the principal seismic direction orientation, and on the factoring along the two orthogonal directions.

On the other hand, (Blandon, 2007) concluded that the following aspects did not have significant effect on the DMF. First, the effect of elastic structural damping was inexistent for CLE levels, and very small for OLE. Second, the interaction between the deck and the soil on the coast line was found to have very little impact, and that complexity in modeling did not justify its

consideration in design. Finally, it was observed that shear forces on shear keys, which link consecutive wharf units, may be close to its maximum for low intensity events.

POL-B and POL-A propose a series of DMF expressions that consider the influence of ground motion intensity level, upper and lower bound soil conditions, and wharf width to length ratios. These expressions are based on the studies of (Blandon, 2007), and are listed below. Nonetheless, these expressions are restricted to the cases where:

- $121.9\ m < L < 243.8\ m$
- $30.48\ m < B\ < 36.58\ m$
- Initial elastic stiffness of piles varies less than 20% along the longitudinal direction.

Single Wharf Unit

$$DMF = 1.8 - 0.05\frac{L}{B} \geq 1.10 \text{ for OLE} \tag{26}$$

$$DMF = 1.65 - 0.05\frac{L}{B} \geq 1.10 \text{ for CLE or DE, and UB soil springs} \tag{27}$$

$$DMF = 1.50 - 0.05\frac{L}{B} \geq 1.10 \text{ for CLE or DE, and LB soil springs} \tag{28}$$

Linked Wharf Exterior Unit

$$DMF = 1.55 - 0.04\frac{L}{B} \geq 1.10 \text{ for OLE} \tag{29}$$

$$DMF = 1.35 - 0.02\frac{L}{B} \geq 1.10 \text{ for CLE or DE, and UB soil springs} \tag{30}$$

$$DMF = 1.16 - 0.02\frac{L}{B} \geq 1.10 \text{ for CLE or DE, and LB soil springs} \tag{31}$$

Linked Wharf Interior Unit

$$DMF = 1.10 \tag{32}$$

On the other hand, ASCE 61-14 proposes a single expression for the DMF, shown in equation (33). This expression is less restrictive on its applicability than those on POL-B, as the only condition is having a width to length ratio greater than 3, and not absolute values. By analogy with previous expressions, this DMF matches with (Priestley et al., 2007).

$$DMF = \sqrt{1 + \left(0.3\left(1 + \frac{20e}{L}\right)\right)^2} \tag{33}$$

It may be observed that ASCE 61-14 DMF expression only depends on the ratio between stiffness and mass eccentricity and wharf length, while POL-B uses the ratio between wharf length and width. Furthermore, note that the width of the wharf is quite restricted by POL-B, while ASCE 61-14 just requires that length over width ratio is larger than 3.

2.5. NON-LINEAR TIME HISTORY ANALYSIS CONSIDERATIONS

Direct integration of equilibrium equations may potentially give the most accurate results (POL-B). This approach allows to adapt to more complex geometries or irregularities in design, for instance changes of soil properties along the length of the wharf that may influence its dynamic behavior, or non-rectangular decks. However, time history models can be challenging to develop, and many parameters can influence design. According to (Priestley et al., 2007), the main aspects that might have an impact on results are summarized in the following:

- **Type of finite elements**. Three general types of elements representing structural components such as beams exist: line elements, fiber elements and three-dimensional elements. Line elements, typically found on consumer structural analysis software, are computationally simpler, but require explicit definition of moment-rotation hysteretic characteristics. Fiber elements discretize cross-sections in a finite number of bi-dimensional elements, which, by specifying constitutive equations to materials, are able to model directly non-linear moment-rotation behavior. However, these elements require considerably larger computing capacity than line elements. Finally, three-dimensional elements, which are the extension of fiber elements at the whole structural component scale. Applicability for production purposes is still limited.

- **Two-dimensional or three-dimensional structural representation**. Even if 3D models may provide richer results, their development is complex and many subjective modeling choices might need to be taken by the engineer. Two-dimensional models are simpler to develop and interpret, especially if line elements are used, where the hysteretic moment-rotation behavior has to be explicitly defined.

- **Hysteresis rules**. As reviewed in section 2.3.2, many models are available to represent hysteretic behavior of yielding sections of elements. These rules may be of the form of moment-rotation or stress-strain relations rather than force displacement. The choice of model can affect significantly results.

- **Elastic damping modeling**. The choice of initial (k_i) or tangent (rk_i) stiffness to define elastic damping, commonly as a fraction of critical damping, is relevant. Usually, this value is 5%. The damping coefficient, which multiplies velocity in motion equations, is defined as $c = 2\xi\sqrt{mk}$, being ξ the fraction of the critical damping. It is advised by (M. Priestley et al., 2007) to use tangent stiffness proportional damping. However, for multi-degree of freedom systems, a Rayleigh damping shall usually be specified, as pure tangent damping is usually not available in structural software. Rayleigh damping is defined at two modal frequencies. Being α' and β' the mass proportional and stiffness proportional coefficients, the fraction of the critical damping is defined for the n mode angular frequency ω_n as:

$$\xi = \frac{1}{2}\left(\frac{\alpha}{\omega_n} + \beta\omega_n\right) \tag{34}$$

  However, this formulation yields to low relative influence of stiffness proportional damping compared to mass proportional damping for lower modes. As a result, the influence of tangent stiffness when inelasticity occurs in the structure is not properly

modeled, overestimating damping. (Priestley et al., 2007) suggests the possibility of artificially assigning low damping coefficients for the fundamental mode, by using a reduced critical damping according to following expression:

$$\xi^* = \frac{\xi\big(1 - 0.1(\mu - 1)(1 - r)\big)}{\sqrt{\dfrac{\mu}{1 + r\mu - r}}} \tag{35}$$

Being μ the system's ductility and r the parameter defining the tangent stiffness with respect to initial stiffness. However, note that this formulation is rather of little interest if demand is not known in advance. If, for instance, demand has been obtained by other means, such as the substitute structure method, then this formulation may be useful.

- **Accelerogram choice**. The number of records, its scaling to design spectra and the coupling between orthogonal directions can have an influence in results. It is common practice, and coherent with ASCE 61 and POL-B guidelines, to use 3 or 7 records for each seismic level. The envelope of results is taken when three records are considered, while results are averaged if 7 analyses are performed. Moreover, when three-dimensional analyses are performed, orthogonal components of accelerogram should be appropriately coupled.

Both ASCE 61 and POL-B allow time history analyses. However, their complex nature is recognized, and they are required to be performed along another simpler type of analysis, for instance the substitute structure method. ASCE 61 allows to use in design results of time history analyses, as long as they are not smaller than 2/3 of results in a response spectrum analysis (linear). On the other hand, POL-B states that results from time histories should present up to 20% differences of results with other less complex analyses. POL-B also allows to perform time history analyses to simplified structural models using the Super-Pile approach (section 4.4). Peer reviewing is also required by POL-B.

2.6.   SOIL-STRUCTURE INTERACTION

Soil-pile interaction in seismic conditions is a very complex phenomenon. During an earthquake, the whole system, soil and structure, will be excited in a coupled fashion. The superstructure, foundations and the soil layers are all deformable entities. It is clear that strong accelerations produced by seismic waves approaching from deep geological layers will produce deformations and changes in stresses in all elements at the surface.

Although the complete coupled problem is certainly very complex, for design purposes engineers need a practical methodology to assess pile dimensioning. A common approach for soil-pile interaction is the use of non-linear p-y springs (Martin & Lam, 1995). These springs model the non-linear force-displacement relation between the pile and the soil, usually from experimental data. During seismic loading, the deck will oscillate (inertial effects), and soil will offer some lateral reaction.
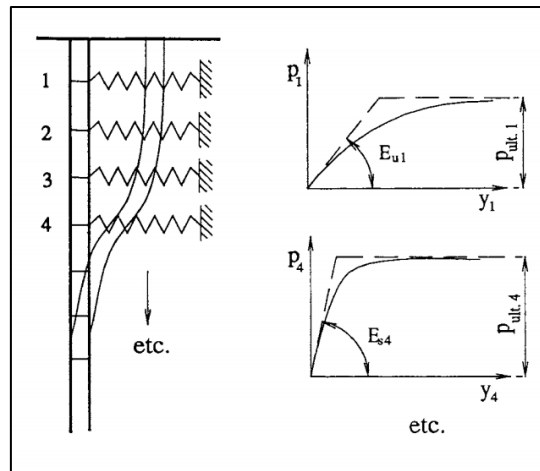
Figure 2.11. P-Y springs for a column type element (Martin & Lam, 1995).

A part from inertial effects, geotechnical failures of soils such as lateral spreading will cause lateral loading on piles. Although relevant standards and design guides state that kinematic forces need to be considered in design, there is little clearance on how one should evaluate them in a project. Furthermore, they express that both kinematic and inertial effects should be combined.

One first approach could be to use a dynamic finite element model considering effective stresses analysis in the soil coupled with structural elements representing the piles using a seismic time-dependent accelerogram (Cubrinovski et al., 2010). This is probably the most precise approach that can be currently followed, but has significant drawbacks. First, they need exhaustive soil characterization in order to introduce pertinent constitutive models in the program, which need extensive site surveying. Secondly, they require a substantial amount of expertise from the geotechnical point of view, thus making it less accessible from the structural side. Furthermore, the calibration of such models is not simple, and might take weeks to make it fully operational Finally, the computing demand of a coupled dynamic analysis is very high, requiring times of the order of days (Besseling & Lengkeek, 2012). Although results may be the most accurate available, all factors listed above make this method impractical for design purposes.

Another simpler possible approach to the problem is an uncoupled static structural analysis using non-linear Winkler springs (Percher & Iwashita, 2016). In a first step, displacements in the soil due to the seismic event are obtained by means of simplified geotechnical methods or by finite element analysis in a commercial software or via simplified methods as the Newmark sliding block analysis (N. M. Newmark, 1965).

(Percher & Iwashita, 2016) exposes two methods for considering kinematic forces using p-y springs: the displacement method and the pressure method. The former consists on using two node p-y springs, one being attached to the pile and the other to the soil node displacement. This approach assumes that the sliding block above the failure line maintains its capacity resistance. On the other hand, pressure method consists on applying the maximum corresponding load of p-y springs to piles, therefore is considered as a more conservative approach. Figure 2.12 illustrates both methods.
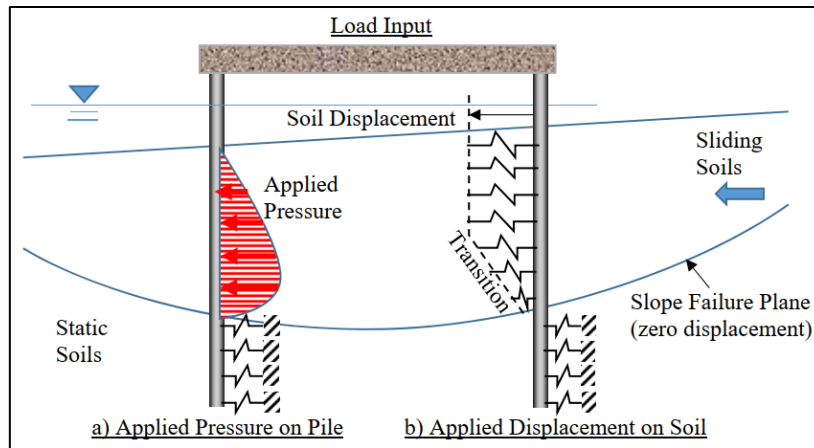
Figure 2.12. Methods for modeling kinematic forces with p-y springs (Percher & Iwashita, 2016).

(Percher & Iwashita, 2016) proposes an approach to combinate inertial and kinematic methods in two phases. First, the full kinematic load shall be applied to the model. From that displaced position, a non-linear static pushover analysis may be performed to analyze capacity of the wharf. However, it recognizes the need of further research.

3. METHODOLOGY AND MODELING

The development of numerical structural models for seismic analysis according to ASCE 61 and the principles of displacement-based design is the main purpose of this section. SAP2000 software is used for developing structural models, although the presented methodology is applicable to other programs.

In the first place, the particular case of study is presented, which consists on a regular pile-supported wharf situated on a sloped dike. Specific characteristics are described, as the wharf geometry, constitutive materials, structural elements cross sections, type of pile-to-deck connection, as well as design loads and geotechnical specifications. Next, general modeling methodology is presented, with special emphasis on plastic hinge definitions, both for concrete and steel, as well as soil-structure interaction. Finally, assembly of numerical structural models is performed.

3.1. CASE STUDY DESCRIPTION

The objective of this section is to establish the structural characteristics of the particular wharf to be analyzed, the geotechnical considerations of the dike, and code-specific seismic assessment.

3.1.1. Description of the Wharf and Geometry

The wharf of study is assumed to be a container terminal classified as a "High" structure, according to §2.2 of ASCE 61. Therefore, it is supposed to be a very relevant structure to the local economy, which involves to design the structure for three different seismic levels: Operational Level Earthquake, Contingency Level Earthquake, and Design Earthquake.

The structure to be studied is a regular pile-supported unit, situated on a sloped dike. As on the majority of quays, the direction parallel to the shore is considerably longer than the transversal direction. In order to be able to fall into the regular geometric characteristics stated in ASCE 61-14 and POL-B, the characteristics of the wharf that have been chosen are summarized below:

- Length of the unit (L): 126m.
- Width of the unit (B): 36m.
- Distance between first and last pile rows: 30.5m (typical width of ship-to-shore crane).
- Sea cantilever: 3.5m.
- Land cantilever: 2m.
- Number of piles in a transversal row: 6
- Transversal distance between piles: 6.096m.
- Distance between water level and deck soffit (lowest part of the superstructure): 3,0m.
- Deck depth: 1.6m.
- Separation between transversal rows: 6m.

Many different solutions may be possible to design a container wharf. For this study, steel piles are used, and the superstructure is assumed to be made of reinforced concrete. The connection between steel piles and the deck is performed by using cast-in-situ concrete plugs. The concrete plug is assumed to have a length of 3m, from the deck soffit. Additionally, a gap of 3cm is assumed between the deck soffit and the beginning of the steel pile. Therefore, a connection of type isolated shell, according to ASCE 61, is considered. Additionally, steel pile corrosion is not considered, assuming that cathodic protection devices are implemented.

Moreover, it is assumed that the wharf has been previously designed for service situation. Therefore, loads such as gravity loads, berthing and mooring of vessels, temperature, shrinkage, waves and current, among others, are supposed to be admissible. No ship-to-shore crane is assumed to operate on the wharf. The length of piles is assumed to be governed by bearing capacity of soils, not studied in this project, and the toes of piles are supposed to be at a depth of 45m, with respect to the sea level. Additionally, driving conditions are assumed to be already assessed.

Finally, for the definition of seismic loads on the wharf, the structure is located at the coastal province of Machala, Ecuador. Regarding earthquake definitions, they are considered according NEC-SE-DS (Ministerio de Desarrollo Urbano y Vivienda, 2014), due to availability that this study has on particular seismic data, including time-history records, at Ecuador. From this standard, acceleration and displacement spectra are obtained, and used as an input for seismic design.
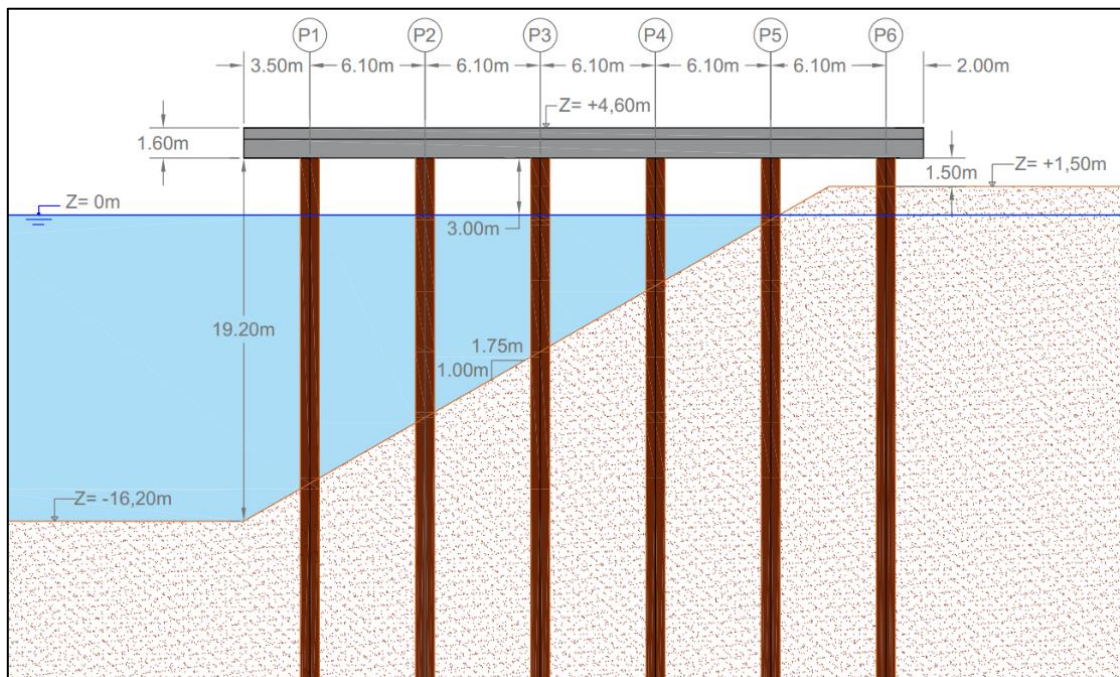
Figure 3.1. Wharf transversal dimensions.

28
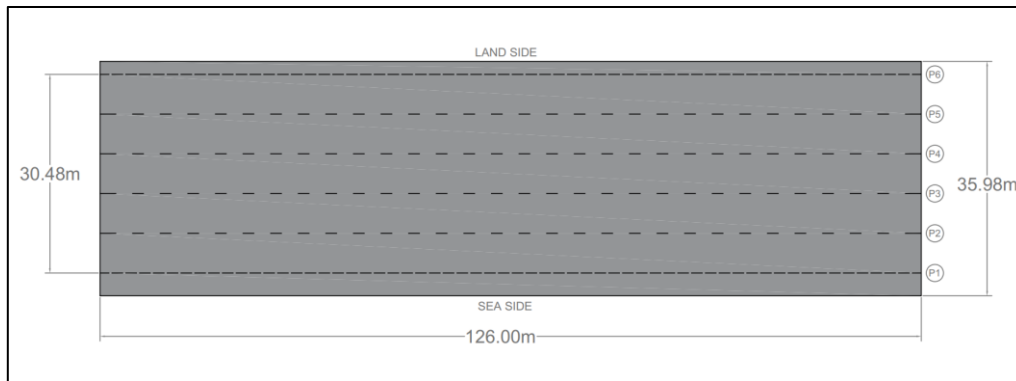
Figure 3.2. Plan view of the deck.

3.1.1.1.   Materials

Structural steel

Structural steel is used for piles, while for the deck and pile-plugs reinforced concrete is used.

The structural steel for piles is API 5L Grade B, whose properties are:

- Yield limit: 245 MPa
- Tensile limit: 415 MPa
- Elastic modulus: 200000 MPa
- Density: 7850 kg/m3
- Poisson ration: 0.3
- Thermal expansion coefficient: 1.17 x 10^{-5}

For the seismic analysis, expected properties of steel are used when determining the seismic demand and capacity of the members, with exception of shear forces. These properties are taken according to section 6.5 of ASCE 61 and section 4.6.2 in POLB, being:

$$f_y = 245 MPa$$
$$f'_{ye} = 1.1 \times 290 MPa = 269.5 MPa$$
$$f_u = 415 MPa$$
$$f'_u = 1.1 \times 415 MPa = 456.5 \ MPa$$

Where:

f_{ye} and f_{ue} are the expected yield limit and the tensile limit, respectively.

f_y and f_u are the characteristic yield limit and the tensile limit, respectively.
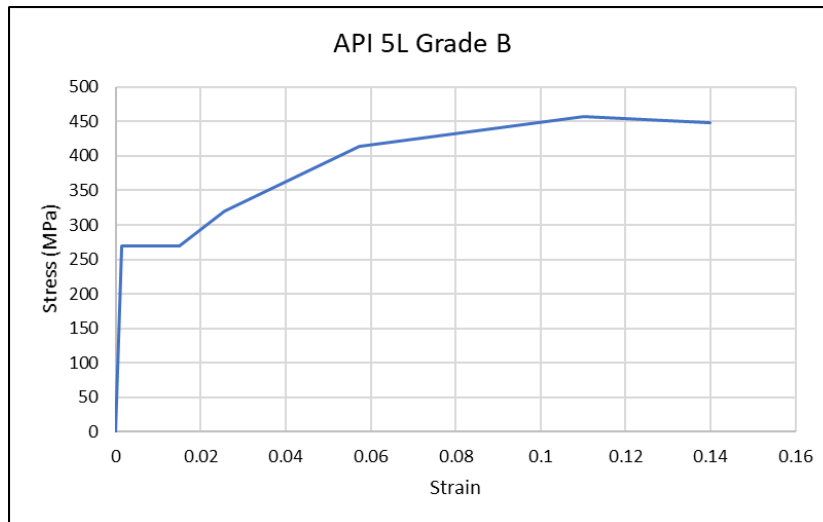
Figure 3.3. Stress-strain relationship for structural steel (API 5L Grade B), with expected properties.

Concrete

The concrete for reinforced concrete structures is C40/50 whose properties are:

- Characteristic compressive strength: $f'_c = 40 MPa$
- Elastic modulus: $E_c = 5000\sqrt{f'_{ce}} = 36056 MPa$
- Density: $\rho_c = 2500\ kg/m^3$
- Poisson ration: $\nu_c = 0.2$
- Thermal expansion coefficient: $\alpha_c = 1.0 \times 10^{-5}$

Particularly, for the seismic analysis, the expected compressive strength of the concrete material is considered according ASCE 61 and POLB, being:

$$f'_{ce} = 1.3 f'_c = 1{,}3 \times 40 = 52\ MPa$$

Where:

f'_{ce} is the expected compressive strength at 28 days.

f'_c is the characteristic compressive strength at 28 days.

The stress-strain relationship of the concrete is dependent on confinement provided by steel piles, which is assessed on section 3.2.1.1.

Reinforcing steel

The steel reinforcement for reinforced concrete structures is ASTM A706 Grade 60, whose characteristic properties are:

- Yield limit: 420 MPa
- Tensile limit: 620 MPa
- Elastic modulus: 200000 MPa

Again, for the seismic analysis, the expected properties of the steel reinforcement are used when determining the seismic demand and capacity of the members, except for shear forces, according ASCE 61 and POLB, being:

$$f_{ye} = 1.1 f_y = 1.1 \times 420 = 462 \, MPa$$

$$f_{ue} = 1.4 f_{ye} = 1.4 \times 462 = 647 \, MPa$$

$$f_{yhe} = 1.0 f_{yh} = 1.0 \times 420 = 462 \, MPa$$

Where:

f_{ye} and f_{ue} are the expected yield limit and the tensile limit for vertical reinforcement, respectively.

f_y is the characteristic yield limit for vertical reinforcement, respectively.

f_{yhe} and f_{yh} are the expected yield limit and the characteristic yield limit for transversal confining reinforcement, respectively.

The strain at maximum stress, ε_{smd}, depends on the bar reinforcement diameter:

$$\varepsilon_{smd} = \begin{cases} 0.120, & \text{Ø32 or smaller} \\ 0.090, & \text{Ø35 or larger} \end{cases} \tag{36}$$

For strain-hardening law of reinforcement steel, the onset of strain hardening is taken as $\varepsilon_{sh} = 0,01$.
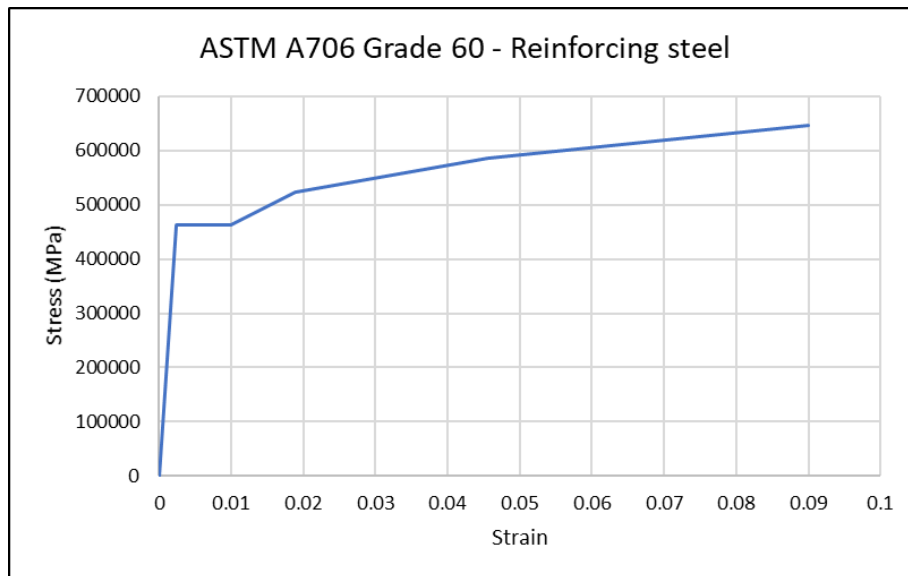
Figure 3.4. Stress-strain relationship for reinforcing steel (ASCE 61-14).

3.1.1.2.   Cross section definition

Steel piles

The piles that are used for the design are catalogued in API Specification 5L (American Petroleum Institute, 2000), with the following characteristics:

- Pile outer diameter: D=1016.0 mm
- Pile thickness: t=22.2 mm

Considering the structural steel that is used, with a characteristic yield stress of $245\ MPa$, it is important to check for the classification of the cross section. According to (AISC 360-16, 2016) §B4, the section may be classified as compact or non-compact for flexure, and slender or non-slender for compression, as a function of the diameter-to-thickness ratio.

For compression:

$$\frac{D}{t} = \frac{1016}{22.2} = 45.77 < 0.11\frac{E}{f_y} = 0.11\frac{200000MPa}{245MPa} = 89.8 \tag{37}$$

Therefore, the section is non-slender.

For flexure:

$$\frac{D}{t} = \frac{1016}{22.2} = 45.77 < 0.07\frac{E}{f_y} = 0.07\frac{200000MPa}{245MPa} = 57.1 \tag{38}$$

Therefore, the section is compact.

As a result, the section is able to develop plastic resistance without previously suffering from local buckling (the equivalent to a minimum of Class 2 from EC3).

Pile plugs

For the pile-deck connection, the design proposes a cast-in-situ concrete plug that uses shear rings for ensuring the adherence between the steel pile and the concrete plug, following an isolated shell connection scheme.

Reinforcement of the plug is supposed to be 12 bundles of two bars #10 (Ø32mm), with a total of 24 longitudinal bars, using ASTM A706 Grade 60 reinforcing steel, which gives a total area of longitudinal reinforcement of 0,0196m². Regarding transversal reinforcement, hoops of #5 (Ø16mm), with a separation of 100mm, are considered.

Regarding reinforcement ratio under seismic situation, Caltrans Seismic Design Criteria 2013 §3.7 (Caltrans, 2013) is taken as reference. Being A_g the gross cross-section area of the plug, the minimum and maximum ratio for longitudinal reinforcement for columns are, respectively:

$$A_{st,min} = 0.01A_g = 0.0074m^2 \tag{39}$$

$$A_{st,max} = 0.04A_g = 0.0297m^2 \tag{40}$$

Being the total area of longitudinal reinforcement 0.0196m^2, the plug complies with these ratios.

The concrete cover is taken, according to ACI 318-19 §20.5 (ACI Committee 318, 2019), for deep foundation members exposed to seawater, as 65mm.

Superstructure

The deck of the wharf is assumed to be composed by a solid slab of 60cm of depth and a family of beams underneath, both using reinforced concrete. On the one hand, transversal beams are situated aligned with each row of piles (P1 to P6), with a length of 36m. On the other hand, longitudinal beams are situated under rows P1 and P6, for the whole length of the wharf, 126m. Both beams are assumed to have the same cross-section, of width 2m and depth 1m. Additionally, the beams and the slab are supposed to be continuous and monolithically connected, thus behaving as a single element.

3.1.1.3.   Loads

As previously mentioned, it is assumed that the wharf complies with operational loads, which is not the aim of this study. As a result, only those loads that are relevant to the seismic situation are considered.

- Self-weight.
- Dead-load: $2.5 kN/m^2$
- Uniform live load at the deck: $50 kN/m^2$
- Seismic loads:
    - Horizontal.
    - Vertical.

Seismic loads may be expressed by employing design acceleration spectra, or also time dependent accelerogram records. Refer to section 3.1.3 for further details regarding seismic actions.

According to ASCE 61-14, the seismic design is to be verified under the following load combination:

$$(1.0 \pm 0.5 PGA)D + 0.1L + 1.0H + 1.0E \tag{41}$$

Where:

- D: dead loads.
- L: uniform live loads.
- H: soil pressure loads
- E: horizontal earthquake loads.
- PGA: peak ground acceleration (g).

It is also assumed that piles are open-ended, therefore they will be filled with soil and/or water. As a result, soil pressure loads will be disregarded, since they will be compensated between the inner and outer sides of piles. Additionally, ASCE 61-14 mentions that seismic loads are not to be combined with mooring, berthing and environmental loads (wind, currents, etc.). Consequently, the load combination may be simplified as:

$$(1.0 \pm 0.5PGA)D + 0.1L + 1.0E \qquad (42)$$

Vertical seismic actions are considered via the peak ground acceleration, which increases or decreases the axial load on structural elements, especially on piles.

3.1.2. Geotechnical Provisions

A simplified soil profile has been selected such that the design approach can be applied without excessive and unnecessary data. Two kinds of sands and one soft clay have been considered. The first sand (SAND 1), which will be situated towards the surface of the dike, has worse properties than the second (SAND 2). On the other hand, the soft clay (CLAY) has poor properties, and will be concentrated at a thinner layer. The soil profile is illustrated in Figure 3.5. Next tables provide relevant soil properties for modeling its interaction with the structure. For sands, the internal angle of friction ϕ', the specific weight γ and the initial modulus of subgrade reaction k. For clay, the undrained shear strength c_u and the specific weight.

Table 3.1. Sand relevant properties for soil-structure interaction modeling.

	ϕ'	γ	k
SAND 1	30°	$18\ kN/m^3$	$90\ lb/in^3$
SAND 2	35°	$19.5\ kN/m^3$	$90\ lb/in^3$

Table 3.2. Clay relevant properties for soil-structure interaction modeling.

	c_u	γ
CLAY	$40\ kN/m^2$	$17\ kN/m^3$
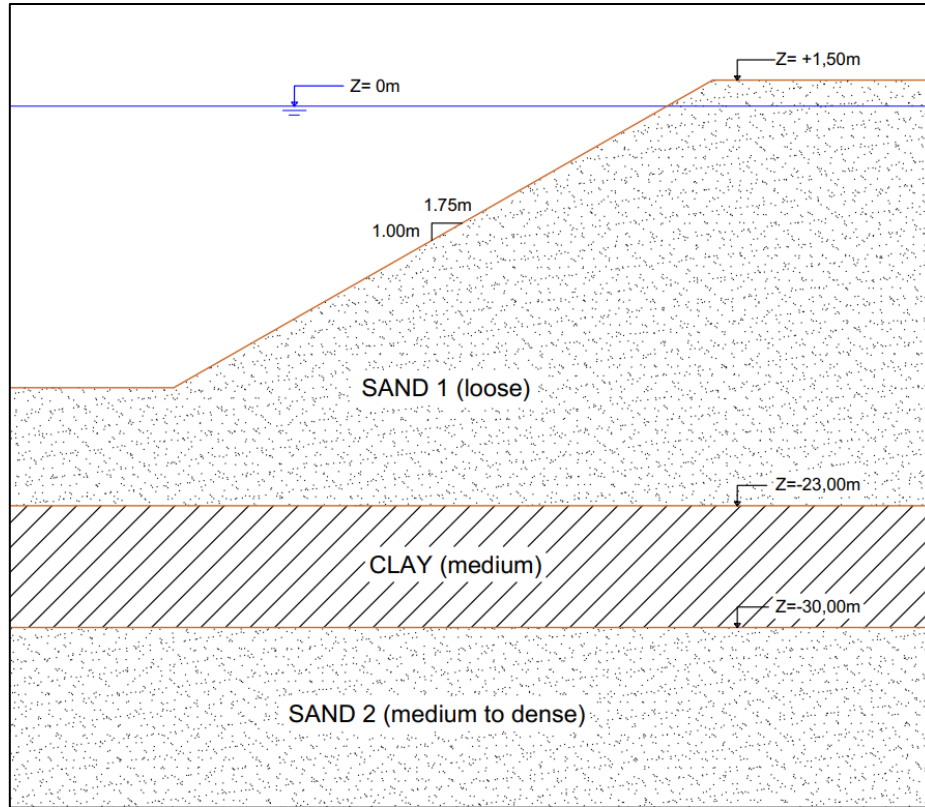
Figure 3.5. Geotecnical profile of the dike.

3.1.3. Seismic Provisions

Three different seismic levels are considered, according to ASCE 61-14, as the structure is classified as "high". These seismic levels are given in the standard in terms of ground motion probability of exceedance. Specific design spectra for the wharf are obtained using NEC-SE-DS. This local standard provides seismic hazard curves in terms of annual exceedance probability. To translate probability of exceedance into annual probability, a probabilistic approach is followed. The occurrence of seismic events can be modelled using Poisson distributions. Being x the number of seismic events occurred in an observation period of t, and noting λ the annual exceedance probability (inverse of the return period), the probability of occurrence of x is given by.

$$P_X(x) = \frac{(\lambda t)^x}{x!} e^{-\lambda t} \tag{43}$$

Therefore, the probability of exceedance can be written as:

$$P_X(x \geq 1) = p = 1 - e^{-\lambda t} \tag{44}$$

From which the annual exceedance probability, as well as the return period, may be obtained.

$$\lambda = \frac{1}{T} = -\frac{\ln(1-p)}{t} \tag{45}$$

Referring to NEC-SE-DS §10.4, the peak ground acceleration (PGA) at Machala is obtained for each seismic scenario, according to computed annual exceedance probabilities.

Table 3.3. Seismic hazard at Machala, and Peak Ground Acceleration.

	PROBABILITY OF EXCEEDENCE IN 50 YEARS	ANNUAL EXCEEDANCE PROBABILITY	RETURN PERIOD (years)	Z or PGA (g)
OLE	50%	0.01389	72	0.15
CLE	10%	0.00211	475	0.375
DE	2%	0.0004	2500	0.61
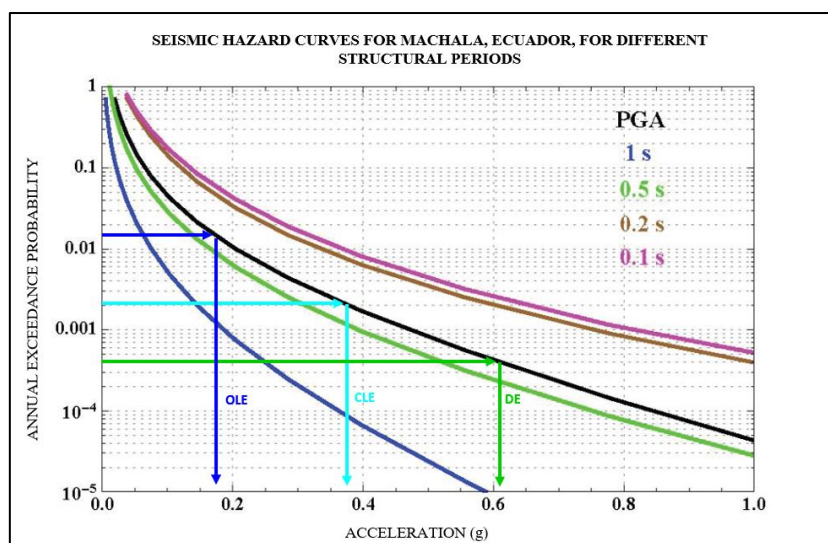
Figure 3.6. Seismic hazard curves for Machala, Ecuador, according to NEC-SE-DS.

For defining design spectra, the soil must be classified in one of six categories. According to the geotechnical profile introduced in section 3.1.2, it has been classified as type E, as the total thickness of soft clay layers is greater than 3m, according to NEC-SE-DS. Three coefficients are to be considered, which are dependent on the soil classification and seismic intensity:

- F_a: soil amplification coefficient at low periods.
- F_d: elastic spectrum amplification coefficient for rock design.
- F_s: nonlinear behavior of soils.

According to 3.2.2 of NEC-SE-DS, and for the three seismic levels considered in design, Table 3.4 summarizes the values of soil profile coefficients.

Table 3.4. Spectrum coeficients for the three seismic hazards according to NEC-SE-DS.

	F_a	F_d	F_s
OLE	1.8	2.1	1.5
CLE	1	1.6	1.9
DE	0.85	1.5	2

The spectral acceleration and displacement spectrum have the following structure, according to NEC-SE-DS § 3.3.1.
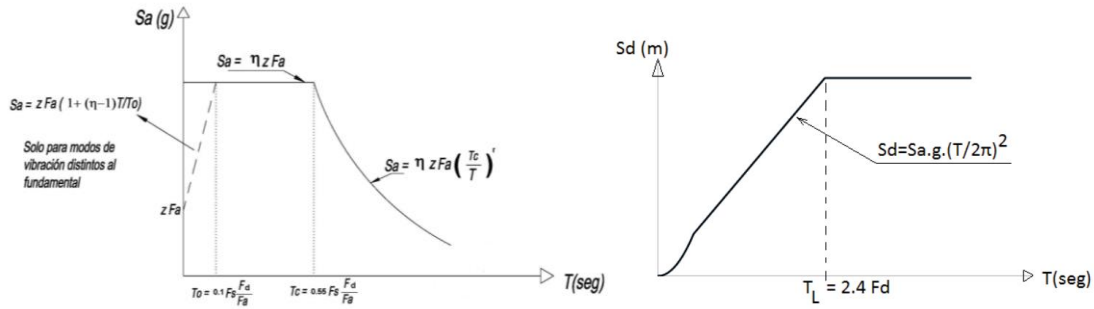
Figure 3.7. Design acceleration (left) and displacement (right) spectra according to NEC-SE-DS.

For soil type E, the coefficient r is fixed to 1,5, and η, which provides the relation between PGA and spectral acceleration, is fixed to 1,8 for coastal locations.

Table 3.5. Parameters defining acceleration and displacement spectra according to NEC-DS-SE.

	η	r	T_c (sec)	T_0 (sec)	T_L
OLE	1.8	1.5	0.963	0.175	4.00
CLE	1.8	1.5	1.672	0.304	3.84
DE	1.8	1.5	1.941	0.353	3.60

Finally, the three design acceleration spectra and displacement spectra are shown in the following figures.
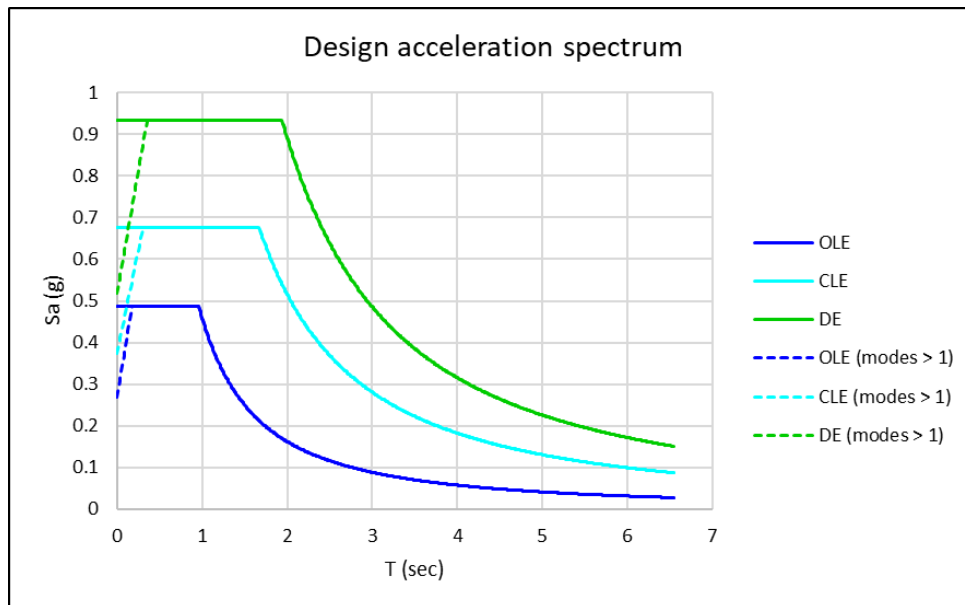
Figure 3.8 Design acceleration spectra for OLE, CLE and DE, according to NEC-SE-DS.
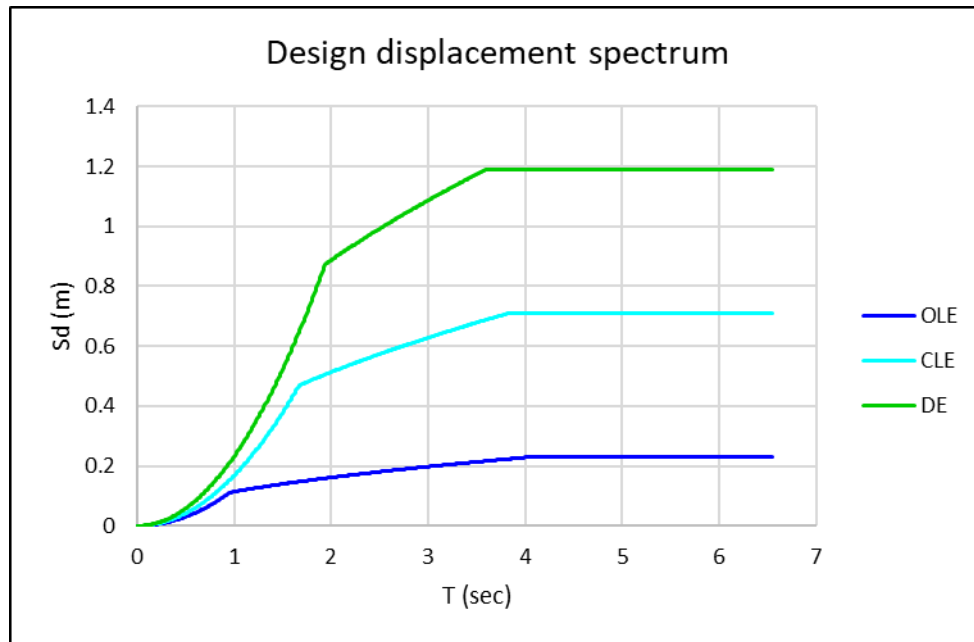
Figure 3.9. Design displacement spectra for OLE, CLE and DE, according to NEC-SE-DS.

3.2.   GENERAL MODELING

This section is devoted to obtaining moment-rotation relationships for plastic hinges, as well as modeling non-linear p-y spring properties.

3.2.1. Plastic Hinges

This part of the document aims to model the yielding behavior of structural elements defined in 3.1.1. It is divided on three sections. The first one obtains stress-strain relationships for confined-concrete, considering steel pipe confinement. Second, particular modeling of the concrete plug hinge is performed. Finally, the steel pile hinge is assessed.

3.2.1.1.   *Confined-concrete stress-strain relation*

Regarding concrete stress-strain relations, ASCE 61 proposes in §6.5.2.1 the model of confinement by steel hoops or spirals originally introduced by (Mander et al., 1988). However, it specifies that other models found in literature may be appropriate. This confined concrete model does not represent originally the particular situation of a concrete plug confined by a steel pile; however, it is based on simple principles that are modifiable in order to model. this behavior. Below, the original formulation of the confined concrete model is presented. Then, modifications based on literature are introduced to model the confinement provided by the steel pile.

38
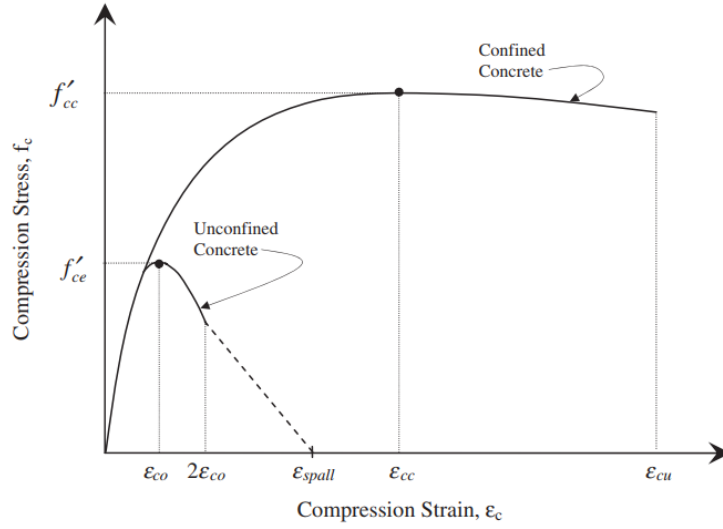
Figure 3.10. Stress-strain curves for confined and unconfined concrete (ASCE 61).

The previous confined relationship is given by next equations:

$$f_c = \frac{f'_{cc}xr}{r - 1 + x^r} \tag{46}$$

$$x = \frac{\varepsilon_c}{\varepsilon_{cc}} \tag{47}$$

$$r = \frac{E_c}{E_c - E_{sec}} \tag{48}$$

$$E_c = 5000\sqrt{f'_{co}} \ (MPa) \tag{49}$$

$$E_{sec} = \frac{f'_{cc}}{\varepsilon_{cc}} \tag{50}$$

$$\varepsilon_{cc} = \varepsilon_{co}\left[1 + 5\left(\frac{f'_{cc}}{f'_{co}} - 1\right)\right] \tag{51}$$

- f'_{cc}: compressive strength of confined concrete
- ε_c: longitudinal compressive concrete strain
- ε_{cc}: strain at maximum stress for confined concrete
- E_c: tangent modulus of elasticity of the concrete
- E_{sec}: secant modulus of elasticity of the concrete
- f'_{co}: unconfined concrete strength
- ε_{co}: unconfined concrete ultimate strain (usually 0.002)

The compressive strength of confined concrete is given by equation (52).

$$f'_{cc} = f'_{co}\left(-1.254 + 2.254\sqrt{1 + \frac{7.94f'_l}{f'_{co}}} - 2\frac{f'_l}{f'_{co}}\right) \tag{52}$$

Where:

- f'_{co}: unconfined concrete compressive strength
- f'_l: effective lateral confining pressure on concrete

The original fundamental hypothesis of the model is that the transversal reinforcement applies a lateral pressure on the core of the column, and therefore provides confinement. The area of concrete that is surrounded by transverse hoops is called concrete core. The average confining stress for circular sections can be obtained from the following diagram.
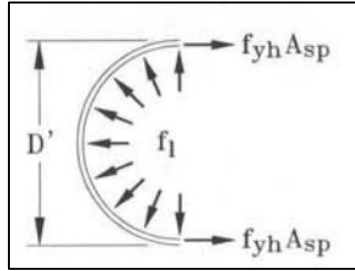
Figure 3.11. Confinement provided by steel hoop (Priestley et al., 1996).

$$f_l = \frac{2f_{yh}A_{sp}}{D's}$$

(53)

Where f_l is the lateral confining pressure on concrete, D' is the hoop diameter and s is the hoop or spiral separation, and f_{yh} and A_{sp} are the yield stress and the area of the transversal reinforcement, respectively.

However, due to hoop separation, only part of the lateral confinement pressure is effectively provided (f'_l):

$$f'_l = k_e f_l$$

(54)

$$k_e = \frac{A_e}{A_{cc}}$$

(55)

$$A_e = \frac{\pi}{4}\left(d_s - \frac{s'}{2}\right)^2$$

(56)

$$A_{cc} = A_c(1 - \rho_{cc})$$

(57)

$$\rho_{cc} = \frac{A_s}{A_c}$$

(58)

Where:

- k_e: confinement effectiveness coefficient
- A_e: area of effectively confined concrete core
- A_{cc}: area of the concrete core
- A_c: area of core of section enclosed by the center lines of the perimeter spiral or hoop
- ρ_{cc}: ratio of area of longitudinal reinforcement to area of core section

Being ρ_s the ratio of the volume of transverse confining steel to the volume of confined concrete core, then:

$$\rho_s = \frac{A_{sp}\pi d_s}{\frac{\pi}{4}d_s^2 s} = \frac{4A_{sp}}{d_s s} \tag{59}$$

$$f_l = \frac{1}{2}\rho_s f_{yh} \tag{60}$$

Finally, (Priestley et al., 1996) introduces a conservative estimate for ultimate compression strain, based on the failure strain of the hoops:

$$\varepsilon_{cu} = 0.004 + \frac{1{,}4\rho_s f_{yh}\varepsilon_{su}}{f'_{cc}} \tag{61}$$

Where ε_{su} steel strain at ultimate tensile stress.

(Li et al., 2005) proposes that on sections with both steel jacketing and transverse reinforcement, based on the (Mander et al., 1988) model. Steel jacketing consists on installing steel sheets on a concrete column, which may be compared to the steel pile and concrete plug situation. The equivalent lateral load on the concrete can be expressed as:

$$f_l' = f_{l1}' + f_{l2}' \tag{62}$$

Where f_{l1}' is the effective confining strength provided by the lateral steel reinforcement, while f_{l2}' is the effective lateral confining strength provided by the steel pile. They can be expressed as:

$$f_{l1}' = \frac{1}{2}k_e\rho_s f_{yh} \tag{63}$$

$$f_{l2}' = \frac{2}{D}k_c t f_{yj} \tag{64}$$

Where f_{yj} is the steel jacket strength, D its diameter and k_c a shape factor, which is equal to 1 for perfectly circular sections.

(Priestley et al., 1996) then adapts the ultimate curvature of concrete to the steel jacketing case:

$$\rho_s = \frac{4t_j}{D} \tag{65}$$

$$\varepsilon_{cm} = 0.004 + \frac{5.6t_j f_{yj}\varepsilon_{sm}}{Df'_{cc}} \tag{66}$$

Where:

- t_j: steel jacket (or pile) thickness
- f_{yj}: steel jacket (or pile) yield stress
- ε_{sm}: strain at maximum stress of steel jacket (or pile).

Since in the concrete plug there will be both a steel jacket and transverse reinforcement, we may still distinguish between two zones: the core and outside concrete, even if both will be considered as confined concrete.

In the outside concrete, only the effect of the steel pipe-pile will be considered. As a result, the lateral confining stress may be expressed as follows:

$$f_l' = f_{l2}' = \frac{2}{D}tf_{yj} \tag{67}$$

$$\rho_s = \frac{4t_j}{D} \tag{68}$$

$$\varepsilon_{cm} = 0.004 + \frac{5.6t_jf_{yj}\varepsilon_{sm}}{Df_{cc}'} \tag{69}$$

On the other hand, the core section will be confined both by the steel jacket and the transverse reinforcement. Thus, both contributions should be aggregated:

$$f_l' = f_{l1}' + f_{l2}' = \frac{1}{2}k_e\rho_sf_{yh} + \frac{2}{D}tf_{yj} \tag{70}$$

$$\varepsilon_{cu} = 0.004 + \frac{1.4\rho_s^{hoop}f_{yh}\varepsilon_{su} + 1.4\rho_s^{pile}f_{yj}\varepsilon_{sm}}{f_{cc}'} \tag{71}$$

Applying the previous expressions to the cross-section properties of the pile plug and the steel pile that are considered in this study, the following values and curves are obtained.

Table 3.6. Confined strength, associated strain, and ultimate strain.

	f_{cc}'	ε_{cc}	ε_{cu}
Core concrete	113 MPa	0,016	0,036
Outside concrete	107 MPa	0,015	0,032
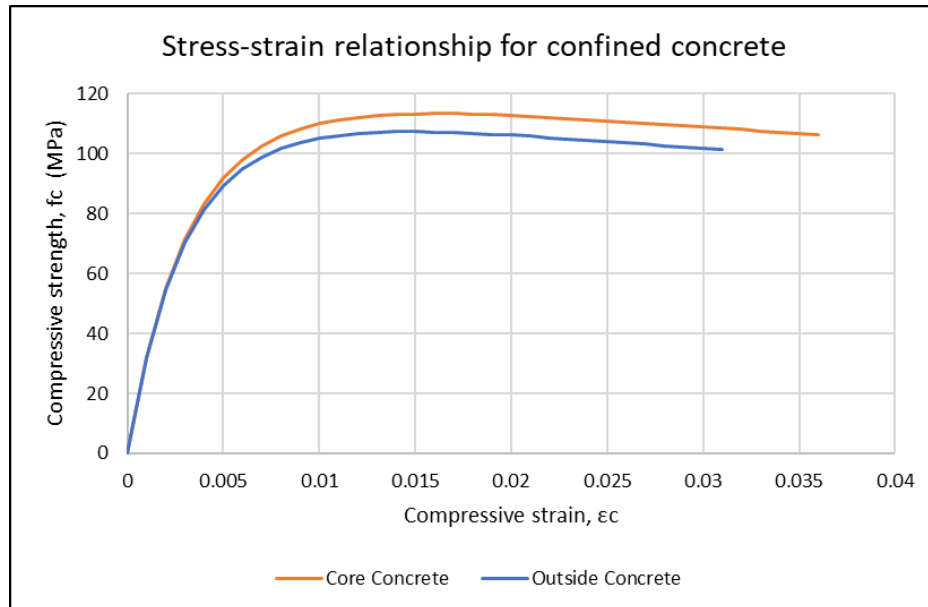
Figure 3.12. Stress-strain relationship for concfined concrete at the pile-to-deck connection.

3.2.1.2.   Concrete-plug hinge

According to ASCE 61-14 §7.4.2.3, in the case of an isolated shell connection (concrete plug with small gap between the steel pile top and the deck soffit), the effect of steel piles on the confinement of the concrete shall be considered. However, steel pile resistance is not considered for the bending resistance of the connection, as there is no continuity between the deck and the steel pile. Finally, "Method B" shall be used for this connection for moment-curvature analysis, as per ASCE 61 §6.6.2.

"Method B" is appropriate for concrete members that do not experience a loss of resistance after yielding, as cover spalling is avoided by the steel casing. The exact moment-curvature relationship is approximated by a bilinear curve, following an equal area approach. An initial elastic branch of the section from the origin passes through the point at first yield of steel reinforcement or when concrete reaches a strain of 0,002, which is defined as the curvature at first yield (ϕ_{yi}). A second branch, which is horizontal, defines the plastic range of the section. This branch corresponds to the plastic moment (M_p) on the ordinate axis, which is defined such that the areas under the bilinear approximation and the original relationship are equal. This plastic branch extends on the abscissa axis up to the ultimate curvature of the section (ϕ_u), which is defined as the curvature at ultimate strain of the reinforcing steel or the confined concrete, whichever arrives first. The intersection between the initial branch and the plastic branch defines the idealized yield curvature (ϕ_y). Figure 3.13 illustrates this method.
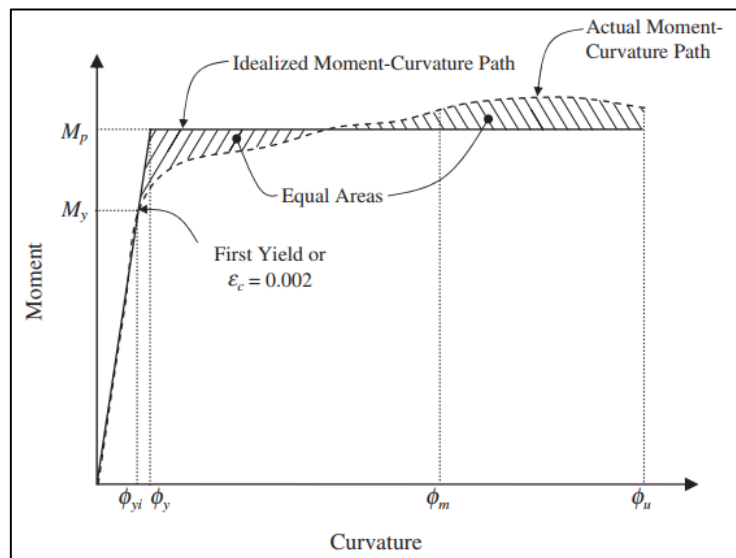
Figure 3.13. Moment-curvature analysis "Method B" (ASCE 61-14).

ASCE 61 provides strains for concrete and steel as the damage indicator. Thus, correlation between strains and curvature is necessary. Additionally, for convenience of modelling in most analysis software, the magnitude of interest is plastic rotation, and not section curvature. Thus, it is assumed by ASCE §6.6.3 that the section curvature is constant along a certain length, defined as the plastic hinge length (L_p), which allows to obtain the plastic curvature in a simple manner. The generic relation between curvature (ϕ) and rotation (θ) is given in next equation:

$$\phi = \frac{d\theta}{dx} \tag{72}$$

Assuming a constant curvature between $x = 0$ (start of plastic hinge) and $x = L_p$ (end of plastic hinge), the previous expression is integrated, giving the relation between plastic rotation ($\theta_{p,m}$), and section curvature (ϕ_m) at a given performance level m (OLE, CLE or DE), using the introduced notation in the previous paragraph:

$$\theta_{p,m} = L_p \phi_{p,m} = L_p(\phi_m - \phi_y) \tag{73}$$

$$\theta_y = L_p \phi_y \tag{74}$$

$$\theta_{p,u} = L_p \phi_{p,u} = L_p(\phi_u - \phi_y) \tag{75}$$
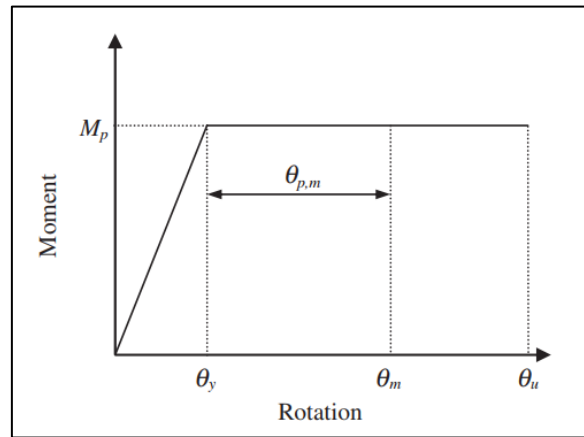
Figure 3.14. Idealized moment-rotation relationship (POLB).

Lastly, the particular value of the plastic hinge length, L_p, is taken according to ASCE 61 §6.6.4.

The length of the top hinge, situated on the concrete plug, is given by:

$$L_p = 0,3 f_{ye} d_b + g \tag{76}$$

The previous particular expression is given for Imperial units. Where f_{ye} is the expected yield stress of longitudinal reinforcement, d_b the longitudinal reinforcement bar size, and g the gap between the end of the steel pile and the deck-soffit.

Being $f_{ye} = 462 MPa = 66,99 kip/in^2$, $d_b = 32\ mm = 1,26\ in$ and $g = 3cm = 1,18\ in$:

$$L_p = 0,3 \cdot 66,99 \cdot 1,26 + 1,18 = 26,5\ in = 673mm \tag{77}$$

The previously described procedure is illustrated below for the specific cross-sections of the plug that are considered in this study, using SAP2000 section designer for section analysis.
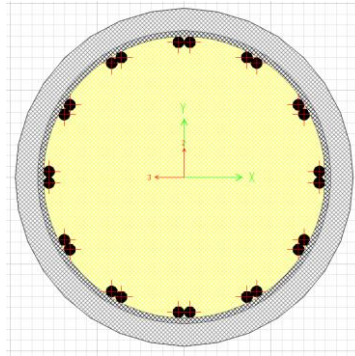
Figure 3.15. Concrete plug modeled in SAP2000 (D=972mm, 24Ø32).

Once all constitutive data is introduced in SAP2000 Section Designer, the section is analyzed for moment-curvature, with exact integration. The procedure is described below:

1. Selection of axial load.
2. Moment-curvature analysis.
3. Obtain strain-curvature relationships.
4. According to limiting strains at each seismic level, determine limiting curvatures.
5. Bilinear approximation of the moment-curvature curve.

This procedure is illustrated for a particular axial load of $P = 1000kN$ (compression).

Table 3.7. ASCE 61-14 strain performance limitations for concrete hinges.

CASE	CONCRETE STRAIN ε_c	STEEL STRAIN ε_s
OLE	0.01	0.015
CLE	0.025	$\min(0.6\varepsilon_{smd}; 0,06) = 0,06$
DE	-	$\min(0.8\varepsilon_{smd}; 0,08) = 0,08$
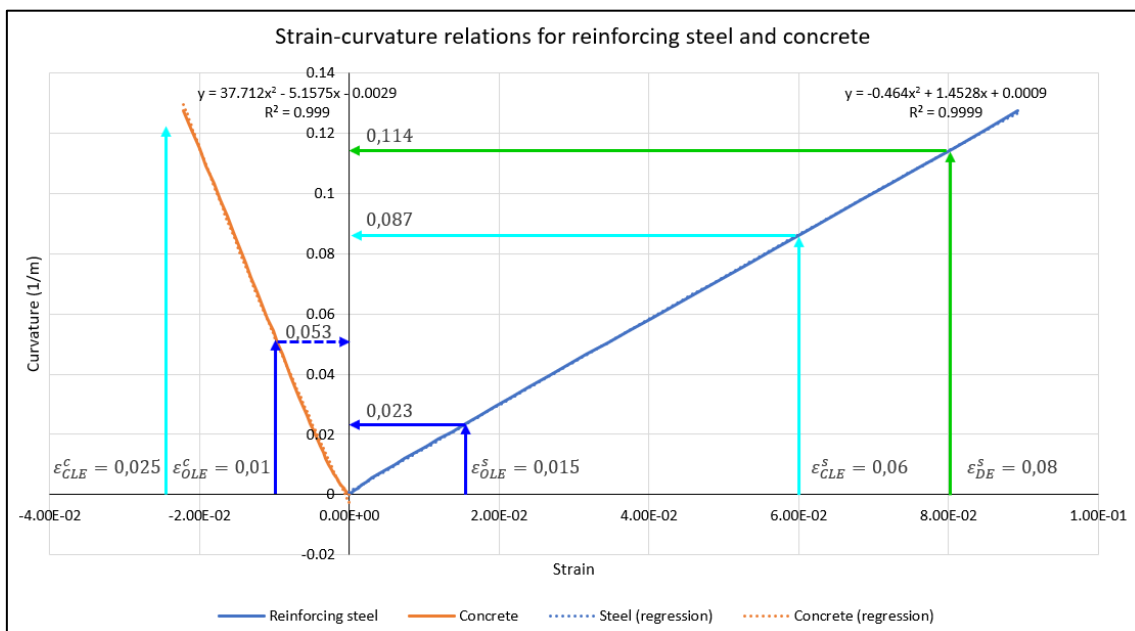
Figure 3.16. Strain-curvature relation of concrete plug for axial load of 1000kN, and performance strains.

Table 3.8. Maximum curvatures for each seismic level, according to concrete and reinforcement limitations.

SEISMIC CASE	MAX CONCRETE CURVATURE	MAX STEEL CURVATURE	LIMITING CURVATURE
	1/m	1/m	1/m
OLE	0.053	0.023	0.023
CLE	0.151	0.086	0.086
DE	-	0.114	0.114

With these results, the bilinear approximation of the exact moment-curvature is obtained, with a resulting idealized plastic moment of $M_p = 4384{,}1\ kNm$.

As the axial load is at this stage unknown, and it may change in different design situations or structure locations, the previously described procedure is performed for a range axial forces.
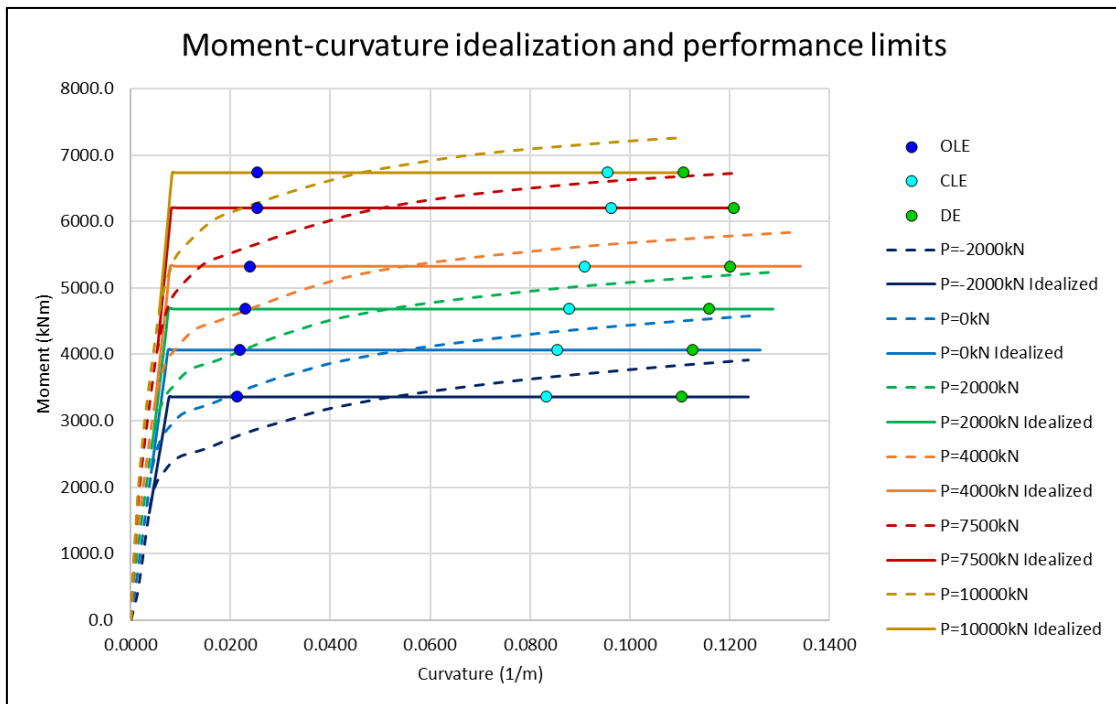
Figure 3.17. Moment-curvature idealization and performance limits of concrete plug plastic hinges.

Table 3.9. Moment-curvature idealization and performance limits for the concrete plug (compression axial load is positive).

P	M_{pl}	ϕ_{OLE}	ϕ_{CLE}	ϕ_{DE}	ϕ_{yi}	ϕ_y	$\theta_{p,OLE}$	$\theta_{p,CLE}$	$\theta_{p,DE}$
kN	kNm	1/m	1/m	1/m	1/m	1/m	rad	rad	rad
-2000	3360.3	0.0213	0.0833	0.1104	0.0037	0.0076	0.0092	0.0509	0.0692
-1000	3693.9	0.0218	0.0842	0.1114	0.0039	0.0075	0.0096	0.0516	0.0700
0	4068.0	0.0219	0.0854	0.1125	0.0041	0.0075	0.0097	0.0524	0.0707
1000	4384.1	0.0226	0.0864	0.1142	0.0043	0.0075	0.0101	0.0531	0.0718
2000	4686.0	0.0230	0.0878	0.1160	0.0044	0.0076	0.0103	0.0539	0.0729
3000	5038.2	0.0235	0.0894	0.1182	0.0046	0.0078	0.0106	0.0550	0.0743
4000	5324.6	0.0239	0.0910	0.1201	0.0048	0.0079	0.0108	0.0559	0.0756
5000	5599.9	0.0243	0.0925	0.1223	0.0049	0.0079	0.0110	0.0569	0.0769
7500	6196.5	0.0254	0.0963	0.1208	0.0053	0.0081	0.0117	0.0594	0.0759
10000	6739.2	0.0253	0.0956	0.1108	0.0057	0.0083	0.0115	0.0587	0.0690

As it is shown in Figure 3.17, axial load on concrete plugs increases its plastic moment, as well as the limit curvatures for the three seismic performance levels, up to a certain value. Being P' the gross axial expected resistance of the pile, with a value of 40803kN, Figure 3.18 represents the evolution of the limiting curvatures according to performance levels with the axial load ratio, defined as the ratio between the axial load (P) and axial resistance (P').
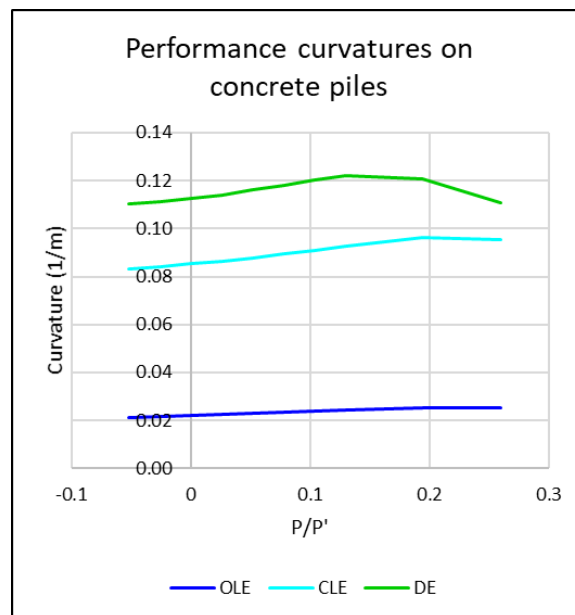
Figure 3.18. Evolution of performance curvatures with axial load ratio (P'=40803kN).

Finally, for modeling purposes in SAP2000, a yield surface needs to be defined. This surface defines the limiting combinations of axial force and bending moment that cause yielding of the section, and therefore the beginning of plastic deformation. This is important because in SAP2000, elastic and plastic deformation are considered using different types of elements. On the one hand, elastic deformation is carried by "frame" elements (beam elements). On the other hand, post-yield plastic deformation is carried by "hinge" elements. As long as the internal forces

in "frame" elements are within the yield surface, "hinge" elements remain inactive. Using idealized values of yield curvature and plastic moment from Table 3.9, the yield surface is shown in Figure 3.19, which is symmetric with respect to the axial load axis.
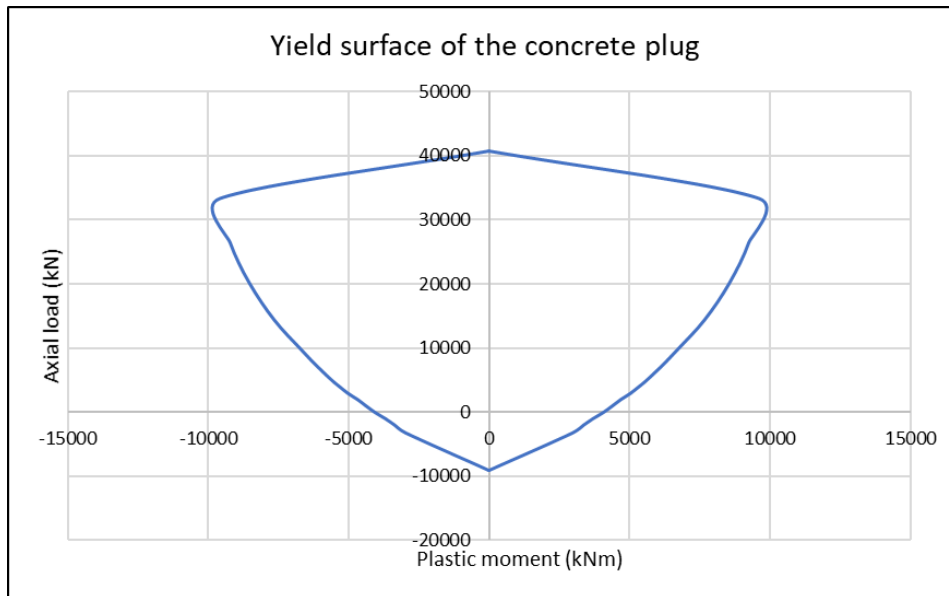
Figure 3.19. Yield surface of the concrete pile. Compression axial load is positive.

3.2.1.3. Steel-pile hinge

In-ground hinges will be constituted exclusively by structural steel. However, neither ASCE 61-14 nor POL-B give much guidance on the modelling of steel hinges. Additionally, limiting strains at each performance level for steel piles provided by ASCE 61 are significantly unconservative and do not consider local buckling. Thus, they should only be taken as an upper bound of the strains, as they can overestimate the ductility capacity of the section.

Firstly, the proposed pile section, of diameter 1016mm, thickness 22,2mm and $f_y = 245MPa$, is classified as a compact and non-slender section as per AISC 360-16 §B4. Thus, the section shall develop plastic resistance without previously suffering from local buckling. On the other hand, plastic rotation after yielding is less clearly defined. AISC 360-16 just states that the rotation capacity of a compact section, defined as the ratio between the total rotation and the yield rotation, shall be larger than 3.

According to (AISC 341-16, 2016) §D1, compact steel sections may be classified as highly ductile and moderately ductile members. For the first category, plastic rotation during seismic event is expected to be of 0,02 radians or less. For highly ductile members, plastic rotation may be 0,04 radians or more. Nevertheless, it states that member rotation may result from either flexure or flexural buckling. This classification is done according to the diameter to thickness ratio.

Highly ductile member:

$$\frac{D}{t} < 0.053 \frac{E}{R_y f_y} \tag{78}$$

Moderately ductile member:

$$\frac{D}{t} < 0.077 \frac{E}{R_y f_y} \tag{79}$$

Where R_y is the ratio between the expected yield stress and the specified minimum yield stress.

Particularly for the case study, $E = 200000 MPa$, $R_y = 1,1$ and $f_y = 245 MPa$. Therefore, the section is classified as moderately ductile.

$$0.053 \frac{E}{R_y f_y} = 39.33 < \frac{D}{t} = \frac{1016mm}{22.2mm} = 45.76 < 0.077 \frac{E}{R_y f_y} = 57.14 \tag{80}$$

On the other hand, PIANC WG 34, specifically for pile-supported wharves, gives the following limitation to the maximum strain at design earthquake situation, which is found to be slightly less conservative than the rotations given by AISC 341-16.

$$\varepsilon_{DE} < 0.44 \frac{t}{D} = 0.0096 \tag{81}$$

Additionally, PIANC states that for operational level earthquake, no in-ground hinges should develop, as its repairability is more difficult.

It is found that all these performance criteria are much more conservative than limiting strains given by ASCE 61. Consequently, the following criteria are adopted for this particular study:

- OLE: $\phi_{OLE} < \phi_y$ (from PIANC)
- CLE: $\phi_{CLE} < 3\phi_y$ (from AISC 360-16)
- DE:
  - $\varepsilon_{DE} < 0.44 \frac{t}{D} = 0.0096$ (from PIANC)
  - $\theta_{p,DE} < 0.04 \, rad$ (from AISC 341-16)

It is however noted that (Harn et al., 2019) suggests that next version of ASCE 61, unavailable at the moment of the development of this study, may propose new strain limitations for steel piles that might take into account local instability.

On the other hand, the plastic hinge length for the steel pile (in-ground), according to ASCE 61 §6.6.4, is obtained from the following expression:

$$L_p = 2D = 2 \cdot 1016mm = 2032mm$$

Where D is the pile diameter.

SAP2000 Section Designer has also been used to analyze moment-curvature of the steel pile. It is however noted that this software does not consider any local instability effects, and only considers material resistance and the stress hardening constitutive law of steel. Due to low performance limiting strains, the maximum curvatures fall on the horizontal line of the moment-curvature curves, therefore before strain-hardening. As a result, a simplified elasto-plastic approximation of moment-curvature relationships is adopted. This is first illustrated by a particular case with compression axial load of 1000kN.

The bilinear approximation starts by an elastic initial branch, tangent to the origin. Then, a horizontal plastic branch, situated at an ordinate corresponding to the plastic moment at a specific axial load. The intersection between these two branches defines the idealized yield curvature of the section. Additionally, in order to model loss of strength after local buckling, the strength of the section is arbitrarily taken as 20% of the plastic moment, immediately after the DE limit curvature.

From strain-curvature analysis of the section, it is corroborated that ASCE 61-14 strain limitations for steel piles are much less conservative than the other criteria that has been presented. Next tables summarize the limiting strains and curvatures for each seismic level, according to ASCE 61-14, PIANC and AISC 316 AND 341.

Table 3.10. Limiting strains and curvatures for each performance level according to ASCE 61-14, for a compression axial load of 1000kN.

	OLE (ASCE 61)	CLE (ASCE 61)	DE (ASCE61)
Strain ε	0.010	0.025	0.035
Curvature ϕ	0.019	0.046	0.065

Table 3.11. Alternative conservative limiting strains and curvatures for each performance level, for a compression axial load of 1000kN.

	OLE (PIANC)	CLE (AISC 360)	DE (PIANC)	DE (AISC 341)
Strain ε	0.002	0.007	0.010	0.010
Curvature ϕ	0.003	0.014	0.018	0.020

Therefore, limiting values from Table 3.11, are considered.
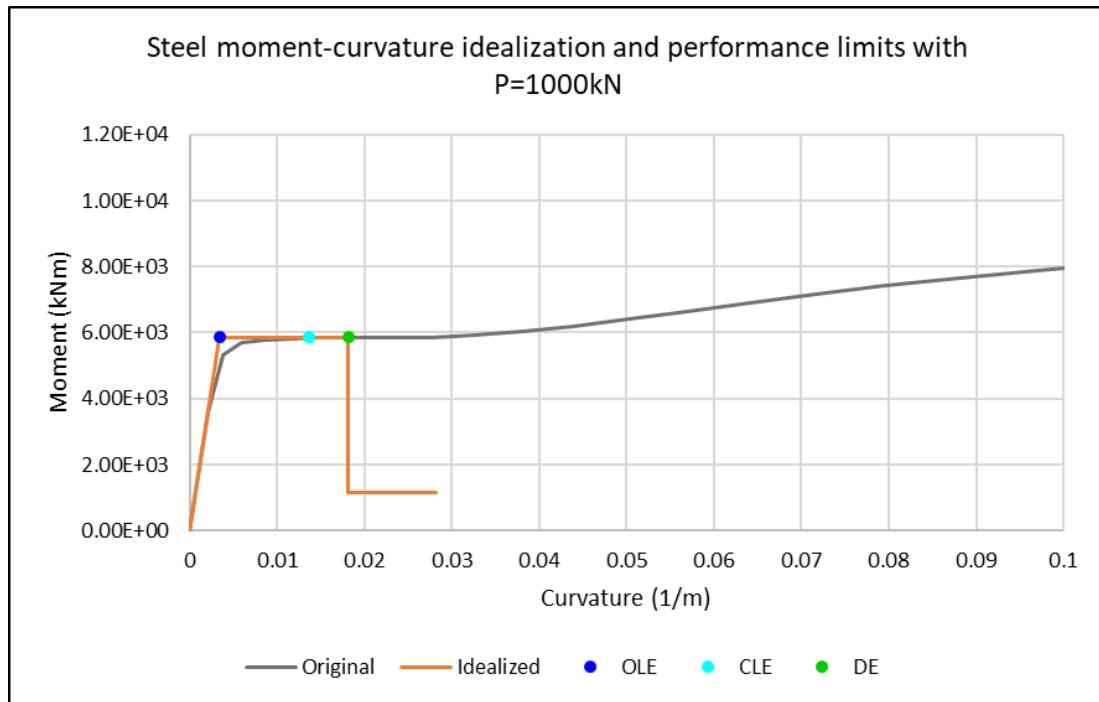
Figure 3.20. Steel pile moment-curvature idealization and performance limits for a compression axial load of 1000kN.

This process may be repeated for the same range of axial loads than for the concrete plug.
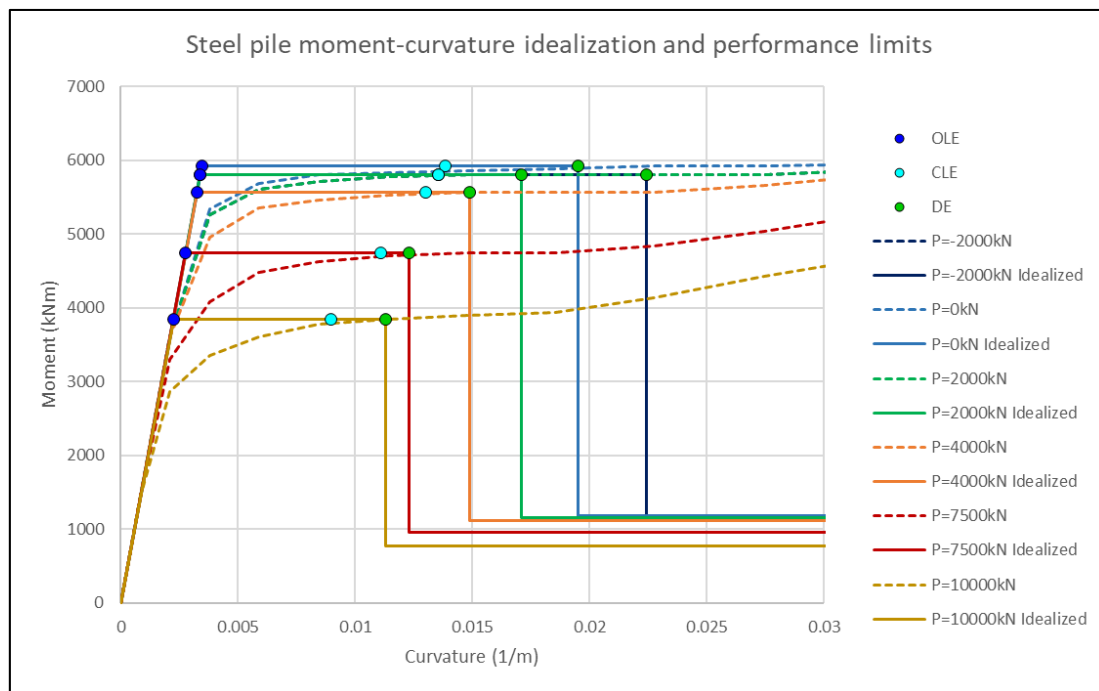
Figure 3.21. Steel pile moment-curvature idealization and performance limits (compression load is positive).

As it is shown in Figure 3.21, moment resistance is maximum with zero axial load, and decreases equally for positive or negative axial loads. However, it can be observed that for an axial tension load of -2000kN, performance limitations for DE are higher than for the same axial load but in

compression. This is due to the fact that this performance limitation has been introduced in terms of maximum strains in order to avoid local buckling. Thus, as only the compressed side of the section may suffer local instability, for a same value of axial load, compression is less favorable than tension. This is not the case with the concrete plastic hinge. Finally, Table 3.12 summarizes results of bilinearization, with the plastic moment, performance and yielding curvatures, and plastic rotations for each seismic level.

Table 3.12. Moment-curvature idealization and performance limits for the steel pile (compression axial load is positive).

P	M_{pl}	ϕ_{OLE}	ϕ_{CLE}	ϕ_{DE}	ϕ_{yi}	$\theta_{p,OLE}$	$\theta_{p,CLE}$	$\theta_{p,DE}$
kN	kNm	1/m	1/m	1/m	1/m	rad	rad	rad
-2000	5797.7	0.0034	0.0136	0.0224	0.0034	0.0000	0.0207	0.0387
-1000	5858.3	0.0034	0.0137	0.0213	0.0034	0.0000	0.0209	0.0362
0	5918.8	0.0035	0.0138	0.0195	0.0035	0.0000	0.0211	0.0326
1000	5858.3	0.0034	0.0137	0.0182	0.0034	0.0000	0.0209	0.0300
2000	5797.7	0.0034	0.0136	0.0171	0.0034	0.0000	0.0207	0.0278
3000	5727.5	0.0033	0.0134	0.0164	0.0033	0.0000	0.0204	0.0265
4000	5557.9	0.0032	0.0130	0.0149	0.0032	0.0000	0.0198	0.0236
5000	5364.0	0.0031	0.0125	0.0130	0.0031	0.0000	0.0191	0.0200
7500	4745.2	0.0028	0.0111	0.0123	0.0028	0.0000	0.0169	0.0193
10000	3842.8	0.0022	0.0090	0.0113	0.0022	0.0000	0.0137	0.0184

Using the results from Table 3.12, a yield surface for the steel plastic hinge. Note that the curve that defines the surface is symmetric with respect both axes.
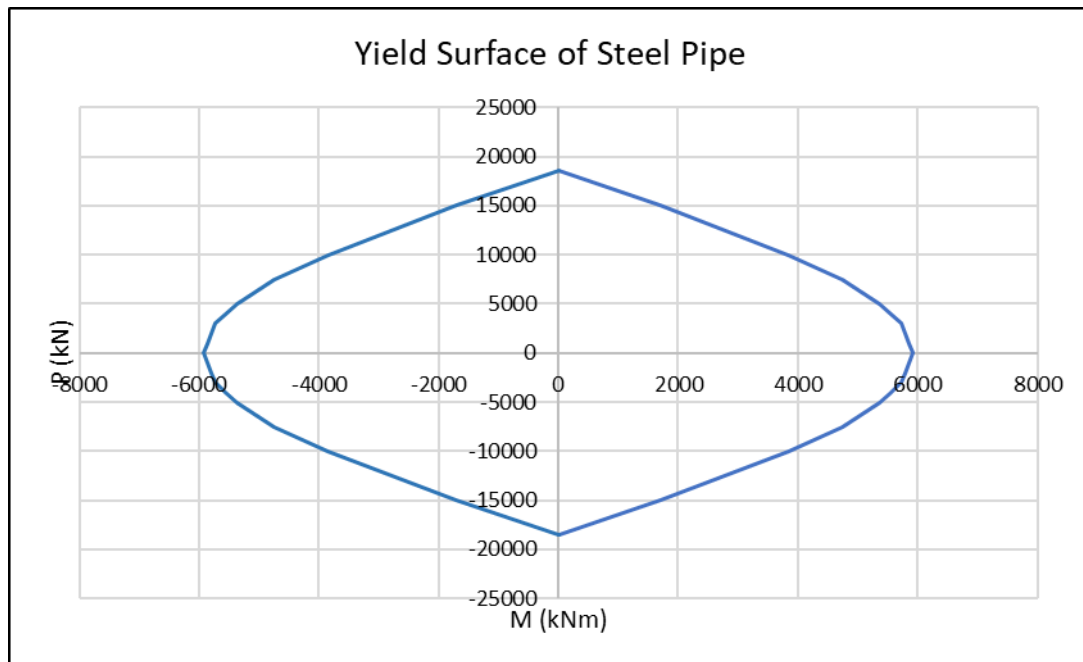
Figure 3.22. Yield surface of the steel pile.

3.2.2. Soil Springs

Interaction between soil properties and the structural model is considered using non-linear p-y curves. These force-displacement relationships are obtained from (API, 2007).

For soft clays, the lateral bearing capacity curve is determined by two parameters: the ultimate resistance (p_u), and the displacement at half resistance (y_c).

$$p_u = f(x) = \begin{cases} 3c + \gamma X + J\dfrac{cX}{D}, & X < X_R \\ 9c, & X \geq X_R \end{cases} \tag{82}$$

$$y_c = 2.5\varepsilon_c D \tag{83}$$

Where:

- c: undrained shear strength.
- γ: effective unit weight.
- X: depth below surface.
- J: dimensionless empirical constant.
- D: pile diameter.
- X_R: depth of reduced resistance zone.
- ε_c: strain at one half of the maximum stress of undisturbed soil samples testing.

Being:

$$X_R = \frac{6D}{\dfrac{\gamma D}{c} + J} \tag{84}$$

$X > X_R$		$X < X_R$	
P/p_u	y/y_c	p/p_u	y/y_c
0.00	0.0	0.00	0.0
0.23	0.1	0.23	0.1
0.33	0.3	0.33	0.3
0.50	1.0	0.50	1.0
0.72	3.0	0.72	3.0
0.72	∞	0.72 X/X_R	15.0
		0.72 X/X_R	∞

Figure 3.23. P-Y definition for clay materials (API, 2007).

On the other hand, p-y curves for sands are obtained using the following expressions. Regarding the ultimate resistance:

$$p_u = \min(p_{us}, p_{ud}) \tag{85}$$

$$p_{us} = (C_1 \cdot X + C_2 \cdot D) \cdot \gamma \cdot X \tag{86}$$

$$p_{ud} = C_3 \cdot D \cdot \gamma \cdot X \tag{87}$$

Where the same notation is used as for clays. C_1, C_2 and C_3 are empirical coefficients as a function of the angle of internal friction (ϕ'). For sand materials introduced in section 3.1.2, the corresponding coefficients are shown in Figure 3.24.
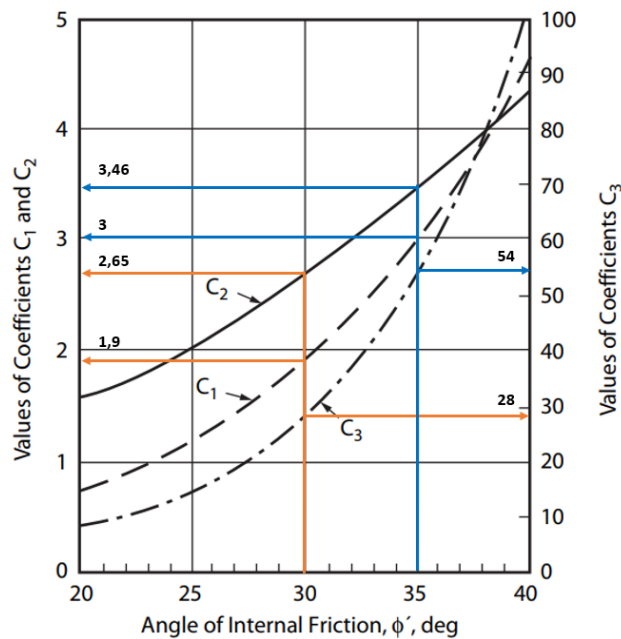
Figure 3.24. Values of coefficients C1, C2 and C3 as a function of ϕ'.

The resulting force-displacement relation is given by the following expression:

$$p = A \cdot p_u \cdot \tanh\left[\frac{k \cdot X}{A \cdot p_u} \cdot y\right] \tag{88}$$

Where $A = 0,9$ for cyclic loading, and k is the initial modulus of subgrade reaction.

Figure 3.25, Figure 3.26 and Figure 3.27 show particular results for pile P3. Although not shown, p-y springs are defined every meter for the six rows of piles.
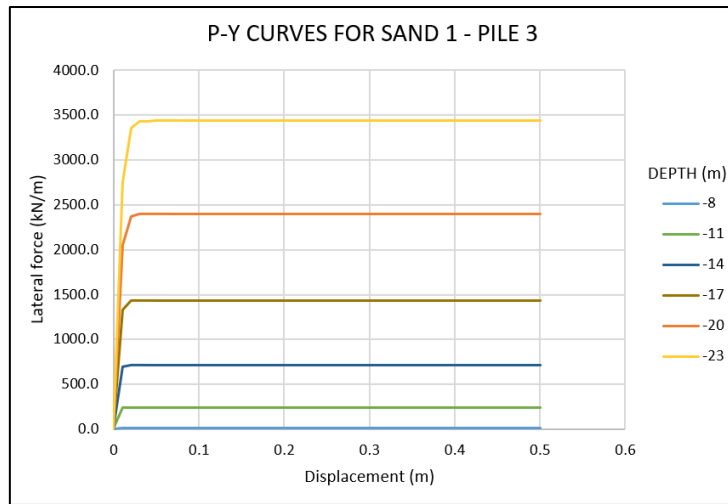
Figure 3.25. P-Y curves for SAND 1 soil type, for Pile P3.
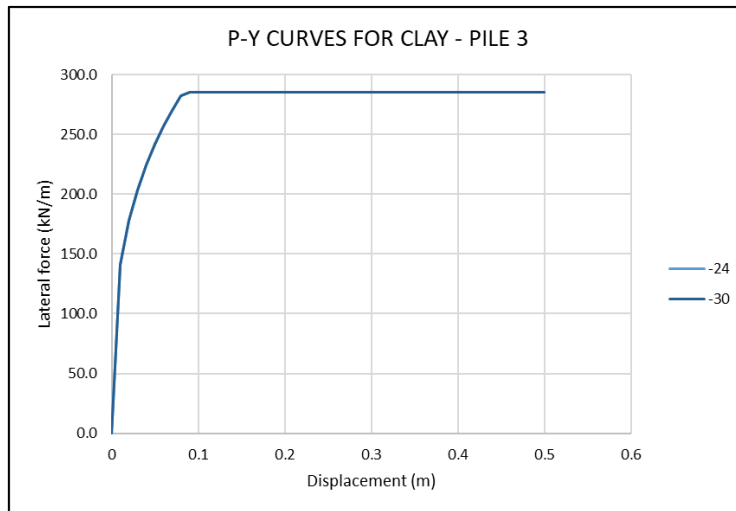
Figure 3.26. P-Y curves for CLAY soil type, for Pile P3.
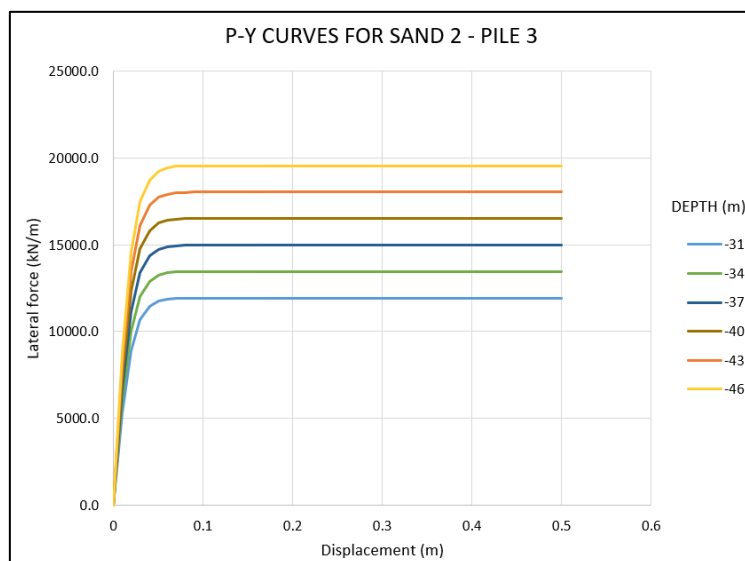
Figure 3.27. P-Y curves for SAND 2 soil type, for Pile P3.

55

3.3.   MODELING ASSEMBLY IN SAP2000

Three types of elements are used in SAP2000 to model the structure transversally:

- Beam elements (frame elements in SAP2000).
    - Steel piles.
    - Concrete plug.
    - Composite section (concrete plug embedded by steel pile).
    - Equivalent superstructure (slab + transversal beam).
    - Longitudinal beams.
    - Rigid connection between end of pile and superstructure.
- Non-linear spring elements (one-joint multilinear link in SAP2000).
    - Lateral soil-pile interaction.
- Plastic hinges
    - Pile-deck connection (concrete hinge).
    - In-ground (steel hinge).

3.3.1. Elastic properties

Member stiffness is determined according to ASCE 61 §6.6.1. On the one hand, elastic properties are modeled with effective elastic properties, in order to consider cracking of concrete members.

For the concrete plug:

$$\frac{EI_{eff}}{EI_g} = 0.3 + \frac{N}{f_c' A_g} \sim 0.42 \tag{89}$$

Where eff denotes effective properties, and g gross properties. Note that ASCE 61 allows approximating the previous expression, dependent on axial load, by a constant, of value 0,42.

Composite section (plug and steel pile):

$$\frac{EI_{eff}}{EI_g} = \frac{E_s I_s + 0{,}25 E_c I_c}{E_s I_s + E_c I_c} = 0.7 \tag{90}$$

Where E_s and I_s are the modulus of elasticity and inertia of the steel pile, while E_c and I_c are the modulus of elasticity and gross inertia of the concrete plug.

Superstructure:

$$\frac{EI_{eff}}{EI_g} = 0.5 \tag{91}$$

3.3.2. Pile-to-deck connection

The pile-deck connection is modeled following the guidelines provided in POL-B. Strain penetration shall be considered for non-rigid pile-to-deck connections, which include dowelled steel pipe pile with isolated shell, according to ASCE 61. The consequence of strain penetration is that the concrete plug is not perfectly rigid against rotation at the deck soffit, but rather there is a virtual fixed point inside the deck superstructure.

The strain penetration length L_{sp} is obtained according to ASCE 61 using the following expression, in Imperial units, being d_b the diameter of longitudinal reinforcement bars:

$$L_{sp} = 0.1 \cdot \frac{f_{ye}}{d_b} = 0.1 \cdot \frac{70 \; kip/in^2}{1.26 \; in} = 8.44 \; in = 214mm \tag{92}$$

Therefore, the top of the concrete pile is modeled higher than it should be in reality. From this higher point to the center of gravity of the section, a rigid frame is used to link the pile to the superstructure, without inducing additional deformations. However, in order to not depend explicitly on the center of gravity of the superstructure, the superstructure frame is modeled with respect to the top center of the cross section, using "insertion point" feature in SAP2000. As a result, the deck frame in the model is situated at the higher level, which is 4,6m above water level. Below the superstructure, the concrete plastic hinge is expected to develop. As the steel pile is not directly connected to the deck but only through the concrete pile, only concrete structural properties are considered. However, as previously exposed, the steel pile has an effect on concrete confinement, which is advantageous to its resistance. Hence, a frame of length the plastic hinge length given by ASCE 61 §6.6.4 is modeled from the end of the rigid frame downwards. As the concrete plug measures 3m from the deck soffit and the plastic hinge is only 673mm, another frame below the previous one models the combined structural contribution of the steel pile and concrete properties. Finally, from the end of the concrete plug to the bottom of the pile, a continuous frame with steel cross section properties is considered. Figure 3.28 represents graphically the modeling approach of the pile-to-deck connection.

Summarizing, for each pile, four "frame" elements are used:

- Frame A: rigid frame.
- Frame B: confined concrete properties, without structural contribution of steel.
- Frame C: composite section with both concrete and steel.
- Frame D: round hollow steel section.
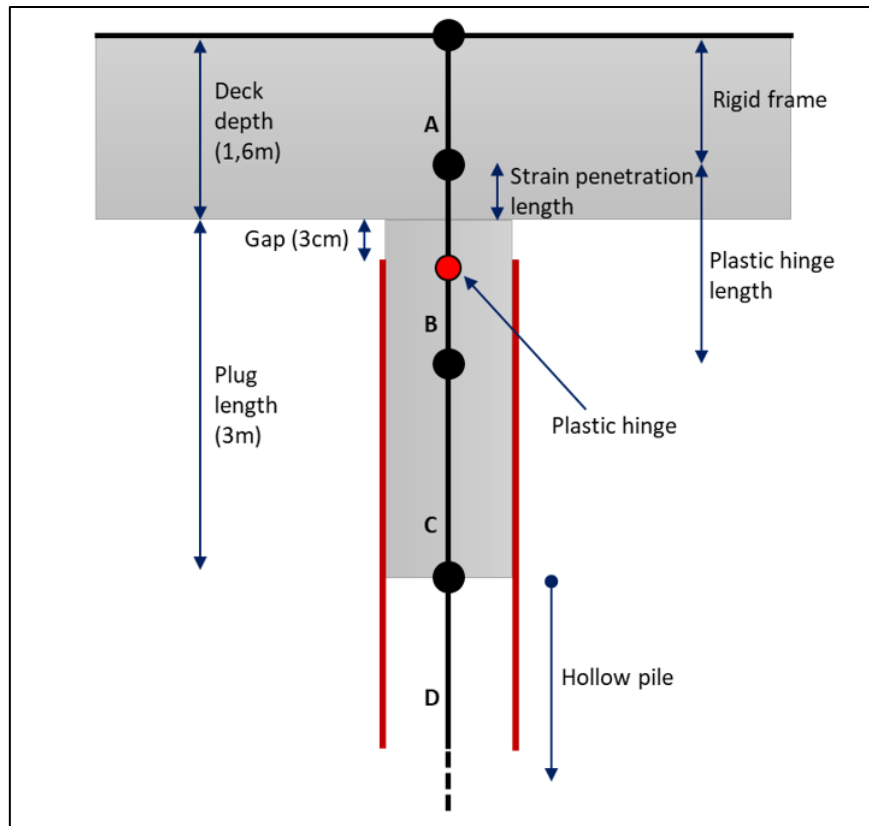
Figure 3.28. Pile-to-deck connection modeling.

Figure 3.29, Figure 3.30 and Figure 3.31 show transverse structural models in SAP2000. These models are the base for developing non-linear static pushover analyses.
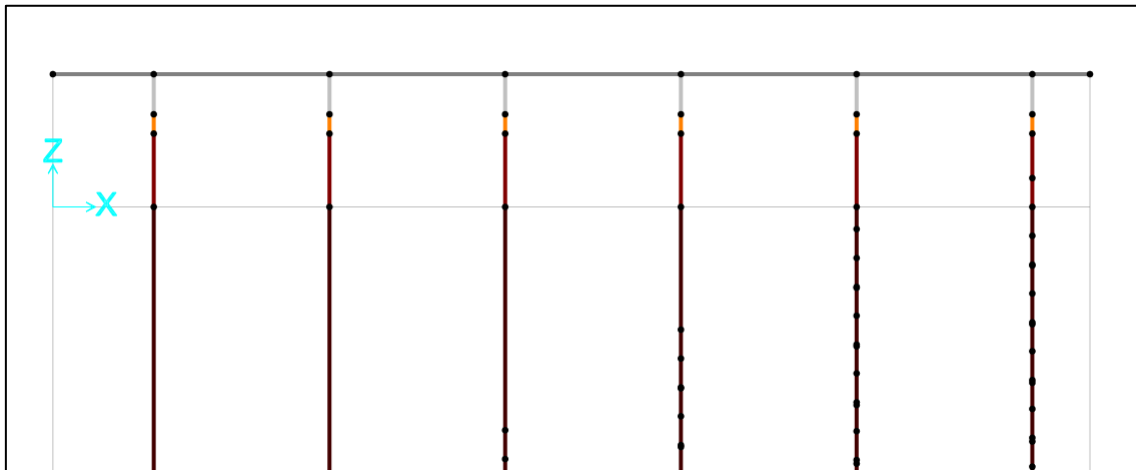
Figure 3.29. Pile-to-deck connection in SAP2000.
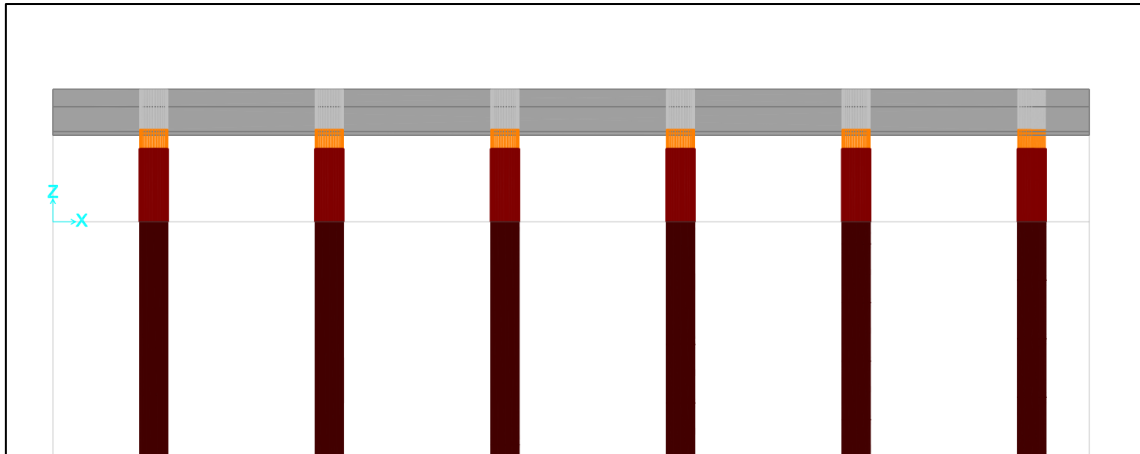
Figure 3.30. Pile-to-deck connections in SAP2000, extruded view.
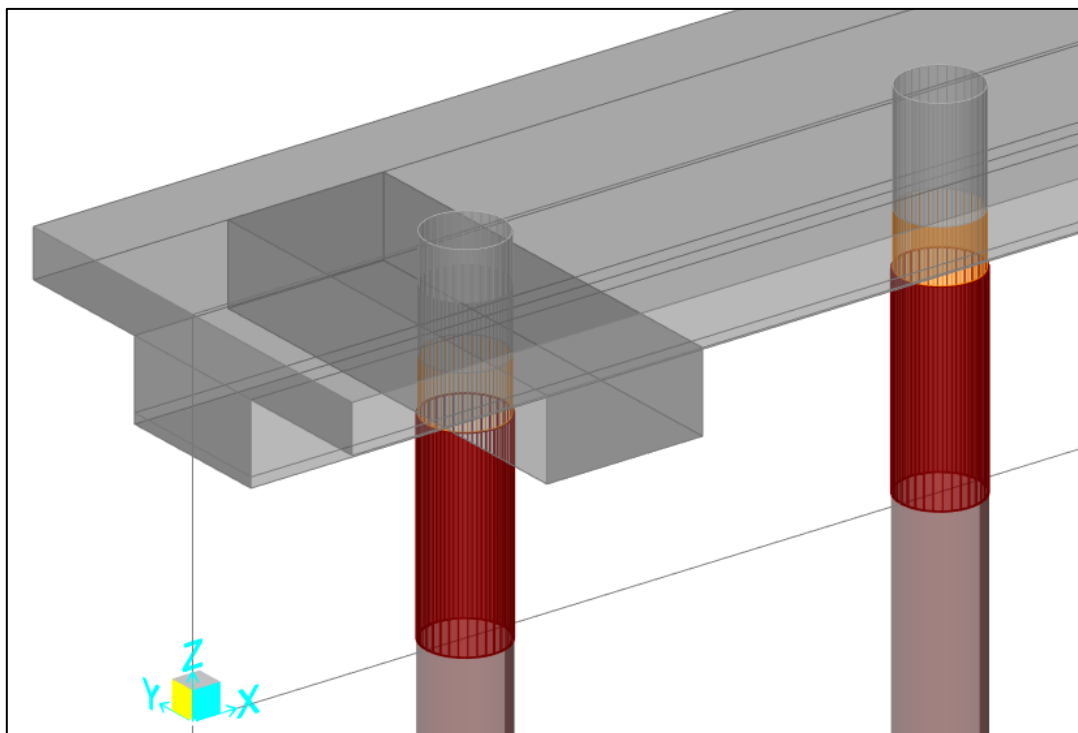
Figure 3.31. Superstructure and beams modeling in SAP2000, extruded view.

3.3.3. Soil springs

Non-linear springs are distributed along the buried part of piles, modeled according to section 3.2.2. Lateral resistance of soils against pile movement has been obtained as a force per unit of length. According to ASCE 61-14, for the considered dike slope, two scenarios shall be considered: Upper Bound (UB) and Lower Bound (LB). Being f_{soil} the lateral force per unit of length for a particular displacement, the resulting force applied by the nonlinear spring in the model, F_{soil} will be given by:

$$F_{soil} = C_{soil} \times L_{spring} \times f_{soil} \qquad (93)$$

Where C_{soil} is 2 for the upper bound situation, and 0,3 for lower bound, and L_{spring} is the separation between springs, which has been taken as 1m in the general model.

Additionally, the bottom end condition of piles has been considered a simple support, which blocks all translations, but allows rotation.
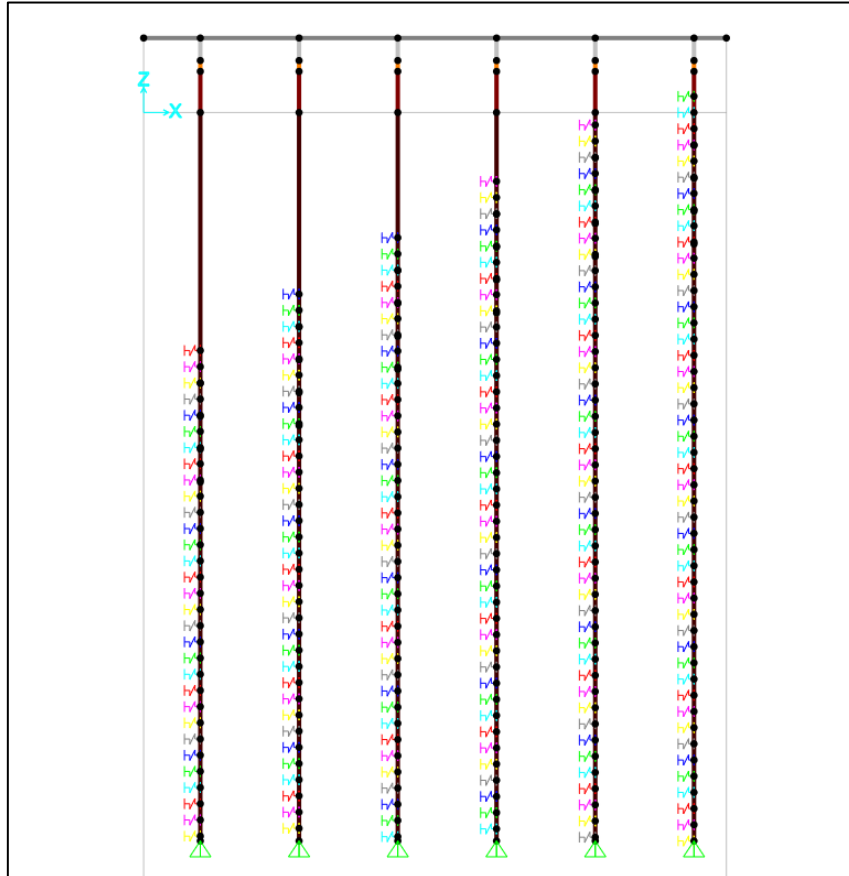
Figure 3.32. Non-linear springs in transverse model, separated 1m.

3.3.4. Plastic hinges

In SAP2000, plastic hinges may be manually defined, and then assigned to a particular frame. Then, all deformation before reaching the yield surface is carried by the frame element. Next, when stresses reach yielding in the frame, the plastic hinge element is activated, and plastic deformation is carried by it. Following this approach, one plastic hinge is assigned to the middle of each frame "B" (confined concrete properties). On the other hand, as the position of in-ground plastic hinges is not known precisely in advance, the steel pile frame elements below the soil (from the first soil spring), are split in multiple continuous frames of length the steel plastic hinge length, which is two times the pile diameter, 2032mm. Maximum in-ground moments due to inertial seismic actions are expected to be approximately 5 times the pile diameter deep,

according to POL-B. Six hinges have been assigned to each pile, therefore covering a length of 12,2m below ground. It is also noted that on pile P6, which has part of the composite plug and pile section embedded in the ground, the plastic hinge location is only considered from the beginning of the hollow pile section. In fact, resistance of the composite section is considerably higher than the pile alone, therefore no plasticity is expected.
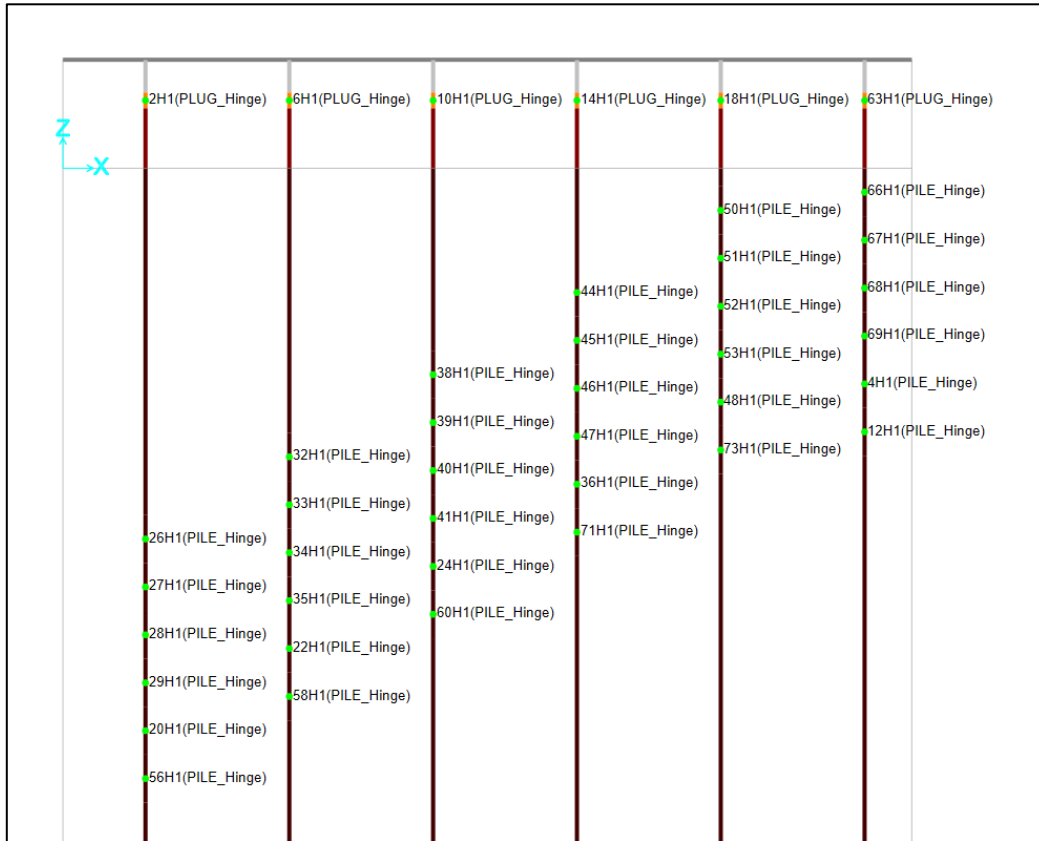
Figure 3.33. Plastic hinge assignments in the transverse model.

3.3.5. Seismic mass

This mass considers the mobilized part of the total mass of the wharf when the structure vibrates, as well as the contribution of applied loads. According to ASCE 61, this mass considers:

- Structural self-weight.
  - Deck.
  - One third of the piles mass from the deck soffit down to 5 pile diameters deep in-ground.
- Permanently attached equipment.
- 10% of the design uniform live load.
- Hydrodynamic mass of piles.

All these masses are assumed to be lumped at the deck level. Note that crane interaction with the wharf is not considered in this study.

At this stage of design, it is assumed that the width of the transverse wharf unit is 6m (i.e. transversal rows of piles are separated 6m). Accordingly, mass contribution from the different components is summarized below:

Table 3.13. Seismic mass of a transverse unit of the wharf of 6m of width.

	Element	Mass (metric tons)
DECK	Slab	330.09
	Dead load	55.02
	10% live load	110.03
	Transversal beam	183.38
	Longitudinal beams	40.77
	Total superstructure	719.30
PILES	Concrete plugs	34.04
	Piles	15.08
	Hydrodynamic mass	19.84
	Total piles	68.96
TOTAL	Total seismic mass	788.26

The hydrodynamic mass in Table 3.13 corresponds to the mass of displaced water by the pile, as well as the enclosed mass of water at the pile interior (POL-B).

The transversal model is used as the base for the complete three-dimensional model, which can be generated by replicating transverse segments.
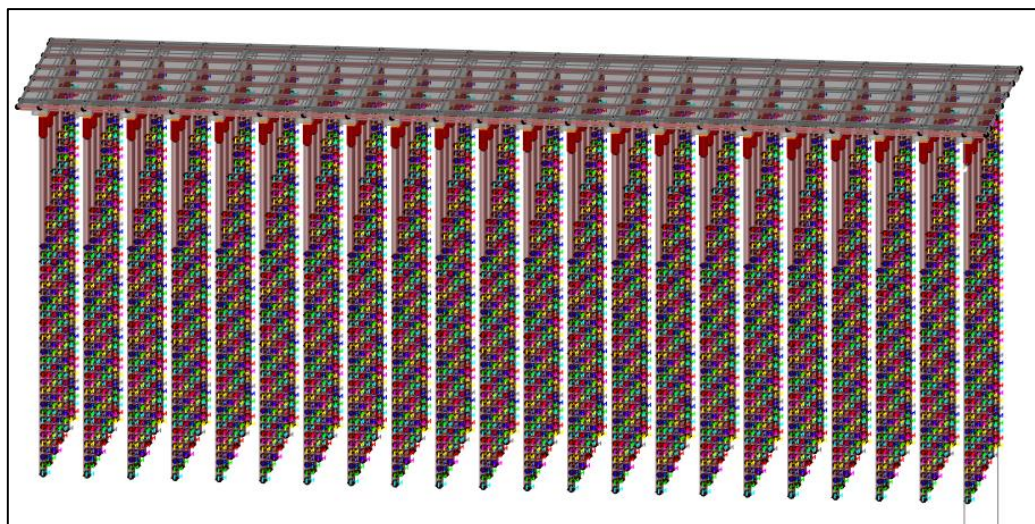
Figure 3.34. Three-dimensional model of the wharf in SAP2000.

4. RESULTS

This section is organized in five main blocks:

- Modal analysis of the wharf.
- Displacement capacity using non-linear static pushover analyses.
- Displacement demand by the substitute structure method.
- Time-history analyses with the "Super-Pile" model.
- Kinematic effects.

4.1.   MODAL ANALYSIS OF THE WHARF

The purpose of this analysis is to identify the main shapes of vibration of the structure, the influence of soil springs, and the monolithism of the deck.

The three-dimensional model of the wharf is used for the modal analysis, which is a linear analysis. Three main vibrational shapes are found, two of which are torsional modes and the other is translational transversally. On these first three modes, the deck behaves as a rigid diaphragm, and therefore it behaves as a rigid solid. Modal participation factors measure the relative influence of modal shapes along each direction with respect to mobilized mass.

Table 4.1. Main modes of vibration shapes of the wharf (sea side to the left).
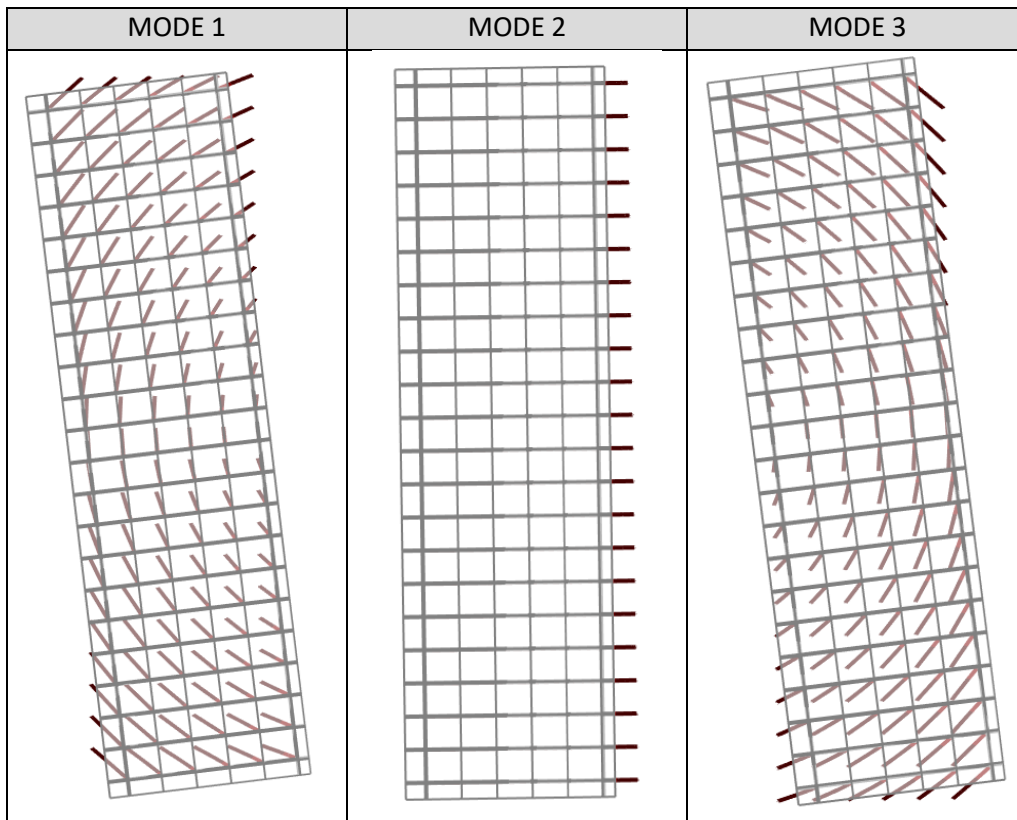
MODE 1	MODE 2	MODE 3

Table 4.2. Main modes of vibration periods and participation factors of the wharf for Lower Bound

MODE 1	MODE 2	MODE 3
T = 1.02 sec	T = 0.89 sec	T = 0.79 sec
PFx = 0 kNm	PFx = -133 kNm	PFx = 0 kNm
PFy = 95 kNm	PFy = 0 kNm	PFy = 94 kNm

Table 4.3. Main modes of vibration periods and participation factors of the wharf for Upper Bound

MODE 1	MODE 2	MODE 3
T = 0.76 sec	T = 0.65 sec	T = 0.56 sec
PFx = 0 kNm	PFx = -132 kNm	PFx = 0 kNm
PFy = 80 kNm	PFy = 0 kNm	PFy = 105 kNm

The only mode that contributes significantly on the transversal translation of the center of mass of wharf is the second one. The other two contribute to the longitudinal response of the wharf center of mass, as well as the torsional response of the deck. This result justifies the use of the use of purely transversal seismic demand methods, such as the substitute structure method, based on single degree of freedom systems.
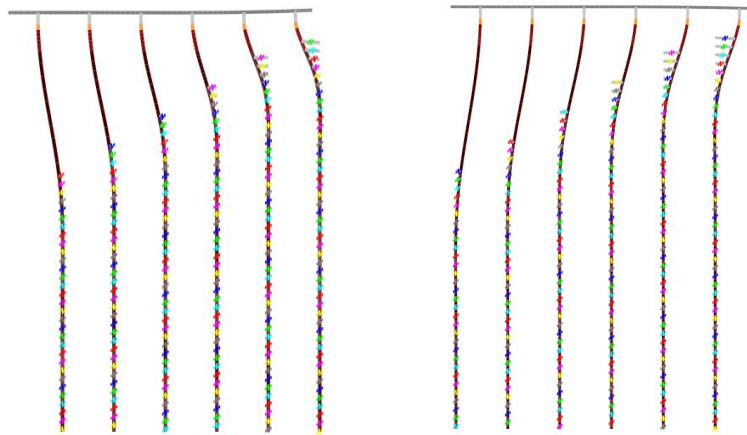
Figure 4.1. Transversal view of mode 2 of the wharf.

Modes of higher order are found to be negligible for the general seismic response of the wharf, as their modal participation factors are orders of magnitude inferior. In fact, these modes mobilize the vibration of the deck, both in plane and out-of-plane, as well as the vibration of individual groups of piles. As an example, the fourth mode has a period of T=0.20 sec and modal participation factors of PFx=-0.3 kNm and PFy=0 kNm, both for Upper Bound and Lower Bound.
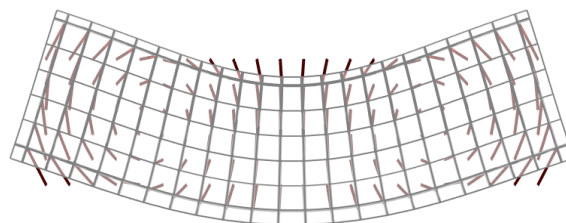
Figure 4.2. Mode 4 of the wharf.

4.2. SEISMIC DISPLACEMENT CAPACITY – PUSHOVER ANALYSES

Non-linear static pushover analyses for the transverse model of the wharf results are presented in this section. The main outputs of these analyses are the capacity curve, and critical displacements corresponding to the three performance levels, OLE, CLE and DE. In all section, displacement is always referred to the horizontal translation of the deck of the wharf, while lateral force or base shear refers to the horizontal load resultant for a given displacement.

The structure of the section is the following. First, pushover analyses are performed for individual piles, which allows to obtain the contribution of each one to the lateral resistance of the wharf. Second, a preliminary seismic design is performed based on the method proposed by (Priestley et al., 2007). Third, non-linear static analyses are performed on the complete transverse model, with all requirements in ASCE 61. The influence of vertical component of seismic load and geometrical non-linearity is studied. Capacity results are used in next section to obtain seismic demand, and verify if the structure verifies design.

4.2.1. Individual pile pushover curves

To obtain the top force-displacement relation for each pile, separate individual models must be used. Two main assumptions are made. First, the top of pile is restrained against rotation, as flexibility of the deck is assumed to be low. Second, the deck load is substituted by a vertical top load, which is obtained by dividing the total load of the superstructure by the number of piles, resulting in 1200kN per pile. Results for both Upper Bound and Lower Bound are shown below.
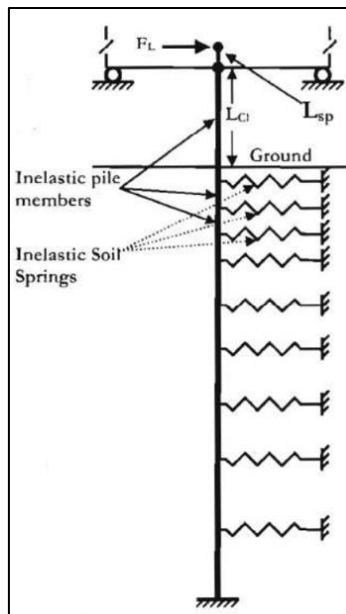
Figure 4.3. Individual pile model for pushover analysis (Priestley et al., 2007).
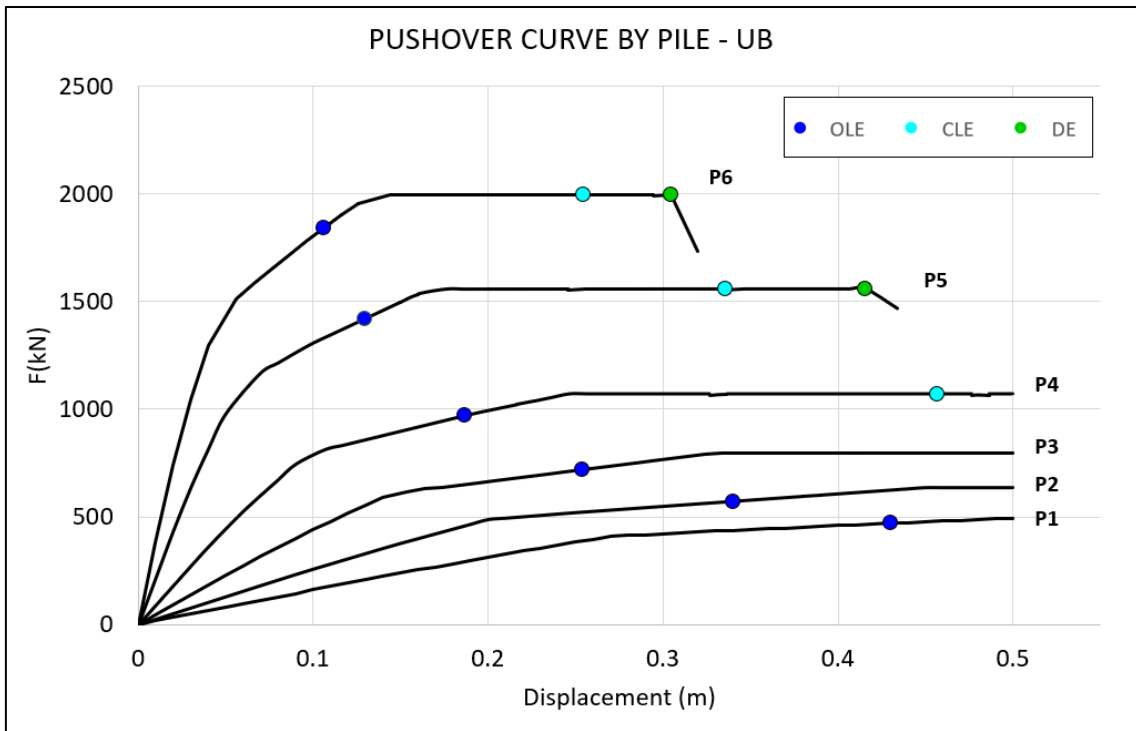
Figure 4.4. Pushover curves and performance levels for each pile with upper bound soil conditions.
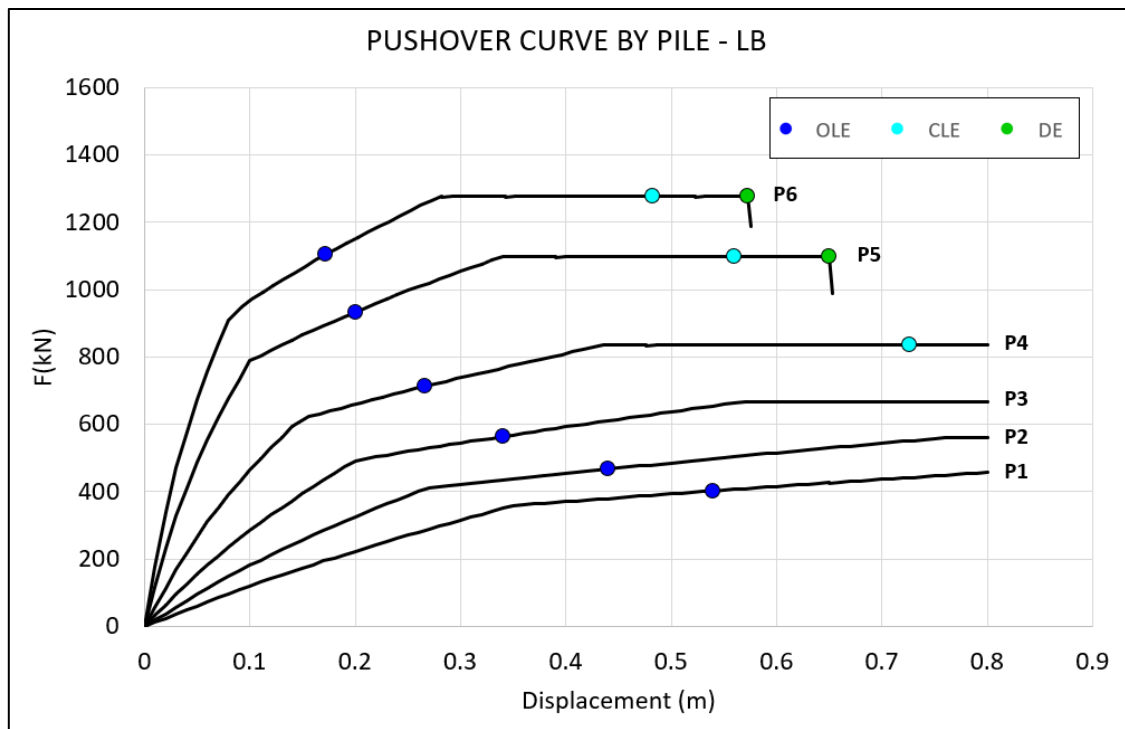
Figure 4.5. Pushover curves and performance levels for each pile with lower bound soil conditions.

It is observed in Figure 4.4 and Figure 4.5 that both initial stiffness and strength (total resisted lateral force) is higher for piles on the land side (P6) than on the sea side (P1). Figure 4.6 shows the relation between free height, defined as the distance between the dike slope and the deck soffit, and lateral strength (maximum resisted lateral force). It is then concluded that most strength is provided by land side piles; therefore, those piles are the ones that mainly contribute

to resist seismic loads. Regarding performance displacements, it is found that for OLE case, piles from P1 to P4 remain in the elastic range, while P5 and P6 suffer some inelastic deformation, both for UB and LB. Plus, it is also found that CLE and DE limits are quite close, and in both cases the inelastic deformation on piles is more generalized. In addition, UB case is characterized by higher stiffnesses and strengths, but lower critical displacements. On the other hand, for LB case, displacement capacity is larger (80% higher for DE), while lateral strength and stiffnesses are lower. Hence, it is difficult to say in advance which case will govern design: having greater strength but lower displacement capacity, or vice versa, which supports the design approach for ASCE 61. Finally, it is also noted that the loss of resistance observed in piles P5 and P6 is arbitrary, and it is due to the modeling of steel hinges, which included a sudden loss of resistance to model local buckling.
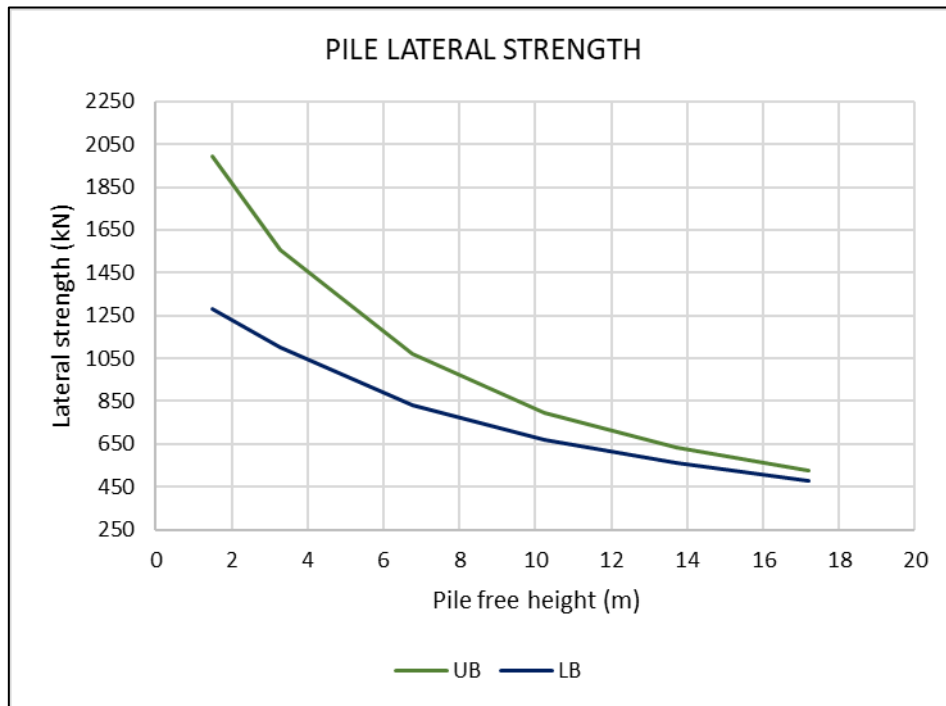
Figure 4.6. Evolution of pile lateral strength with free height.

For displacement-based design, capacity of the structure is defined by the displacement capacity of the most critical element. By regarding individual pushovers, and noting that all piles undergo the same horizontal movement in the complete transverse model, it is clear that P6 governs design.

Table 4.4 and Table 4.5 show the deformation sequence of the critical pile for UB and LB conditions, respectively, indicating the top displacement for each step (lateral force may be obtained from Figure 4.4 and Figure 4.5). The following findings are identified. On the first place, hinging sequence order is equal for upper and lower bound cases, but at different displacements. The concrete plug is found to yield first, and on OLE case no hinging appears in-ground. From a design standpoint, it is very interesting, as high frequency seismic events do not cause in-ground damage, which is considerably more difficult to repair. On CLE capacity, the steel pile hinges in ground. The distance between the surface and the hinge depends on the soil case. CLE capacity is found to be governed by the steel hinge, as well as for DE case.

Table 4.4. Upper Bound P6 hinging sequence.

Sequence:	First plug hinge	OLE capacity (plug)	First soil hinge	CLE capacity (steel)	DE capacity (steel)	Pile failure (steel)
Top displacement	0,06 m	0,11 m	0,14 m	0,25 m	0,30 m	-
Pile Deformed shape						
Legend:		$\varepsilon \leq \varepsilon_{OLE}^{max}$	$\varepsilon \leq \varepsilon_{CLE}^{max}$	$\varepsilon \leq \varepsilon_{DE}^{max}$	$\varepsilon > \varepsilon_{DE}^{max}$	

Table 4.5. Lower Bound P6 hinging sequence.

Sequence:	First hinge (plug)	OLE capacity (plug)	Soil hinge (steel)	CLE capacity (steel)	DE capacity (steel)	Pile failure (steel)
Top displacement	0,09 m	0,17 m	0,29 m	0,48 m	0,57 m	-
Pile Deformed shape						
Legend:		$\varepsilon \leq \varepsilon_{OLE}^{max}$	$\varepsilon \leq \varepsilon_{CLE}^{max}$	$\varepsilon \leq \varepsilon_{DE}^{max}$	$\varepsilon > \varepsilon_{DE}^{max}$	

Table 4.6 summarizes capacity results for each pile, and for both soil conditions. However, note that for design purposes, the only relevant capacity for design is the one from the most critical pile, which defines the displacement capacity of the wharf (Δ_c):

$$\Delta_c = \min\left(\Delta_{c,P_i}\right) \tag{94}$$

Table 4.6. Displacement capacity for each pile with upper (UB) and lower bound (LB) soil conditions. Maximum monitored displacement is 0,5 meters for UB and 0,8 meters for LB.

SOIL CASE	OLE		CLE		DE	
	UB (m)	LB (m)	UB (m)	LB (m)	UB (m)	LB (m)
P1	0.43	0.54	>0.5	>0.8	>0.5	>0.8
P2	0.34	0.44	>0.5	>0.8	>0.5	>0.8
P3	0.25	0.34	>0.5	>0.8	>0.5	>0.8
P4	0.19	0.27	0.46	0.73	>0.5	>0.8
P5	0.13	0.20	0.34	0.56	0.42	0.65
P6	0.11	0.17	0.25	0.48	0.30	0.57

Finally, individual pushover curves can be grouped to provide a first estimation of the global capacity of the wharf in terms of force-displacement relationship. Note, however, that ASCE 61 requires further considerations when analyzing capacity of the wharf, notably vertical seismic influence and potentially P-Delta effects, which is discussed in section 4.2.3.
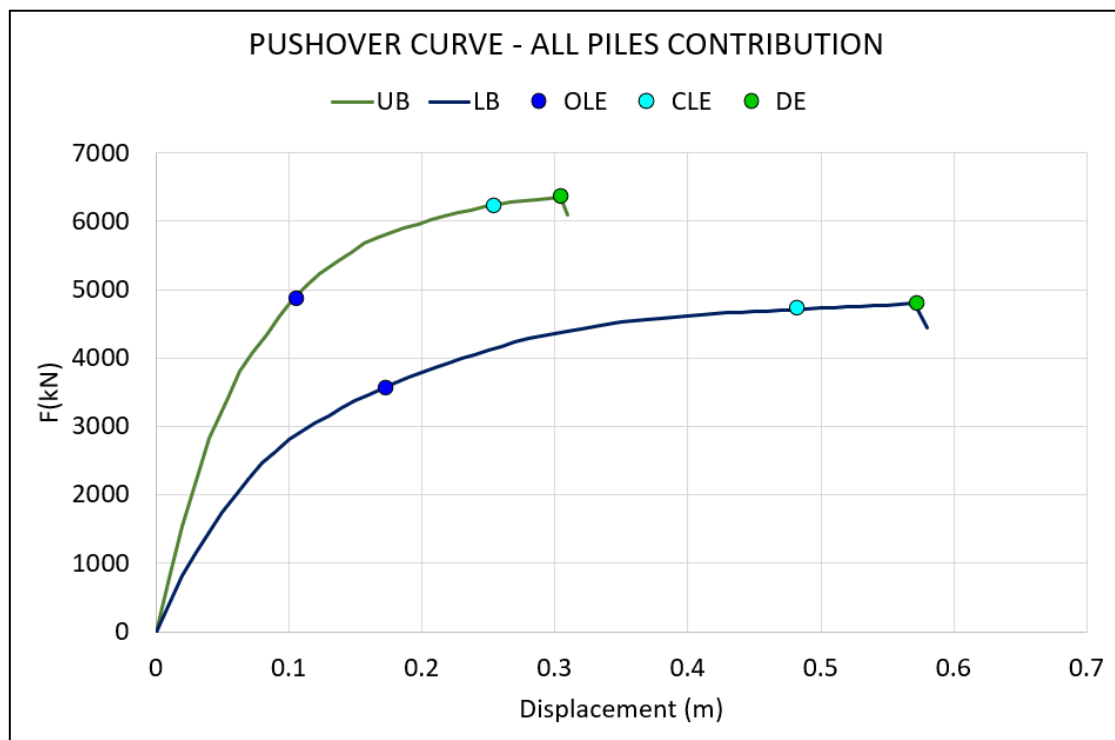
Figure 4.7. Assembly of the six individual capacity curves for UB and LB.

4.2.2. Initial Seismic Design using individual pushover curves

Using pushover curves that have been obtained for the six rows of piles, and assuming that considered axial loads are representative, it is possible to perform a so-called Direct Displacement Based Seismic Design. As it has been previously introduced, the main goal of displacement-based design is to compare the demand to the capacity in terms of displacements, not directly forces.

As a reminder, when performing a substitute structure analysis, the input data is the pushover curve and the seismic mass, and the objective is to obtain the displacement demand. To do so, an iterative approach is required: demand is assumed, effective properties of the system (stiffness and damping) are computed, spectral displacement is obtained, and finally the result is compared to the assumed value. When the iteration converges, the demand is compared to the capacity at the corresponding seismic level. If demand is lower than capacity, then the design is verified. This approach will be developed further in this study.

However, a similar method but following a slightly different approach allows to assess seismic design, also in terms of displacement-based design, without directly referring to the substitute structure method and therefore without the need to iterate. Additionally, this method allows to seize the contribution of each pile to resist seismic loads, and design the number of piles that are needed to perform correctly under seismic situation. The method here described is proposed in (Priestley et al., 2007), which is summarized below. The steps to perform this design, which should be developed for upper bound and lower bound soil conditions, are:

- **Step 1**: Perform individual pushover analyses for each row of piles (P1 to P6).
- **Step 2**: Identify the most critical pile.
- **Step 3**: From pushover curves, obtain the maximum displacement capacity (Δ_c), which is given by the most critical pile, according to performance criteria.
- **Step 4**: Using a Dynamic Magnification Factor (DMF), compute the maximum purely transverse displacement at the center of mass (Δ_t), such that $\Delta_c = DMF \times \Delta_t$.
- **Step 5**: Estimate the ductility demand of the wharf μ_w, based on the ductility of the critical pile $\mu_{P,cr}$. According to (Priestley et al., 2007), this can be approximated as $\mu_w = \mu_{P,cr}/1,2$. Being $\Delta_{y,P}$ the yield displacement of the bilinear approximation of the pushover curve of the critical pile, the pile ductility is defined as $\mu_{P,cr} = \Delta_t/\Delta_{y,P}$.
- **Step 6**: From the expected ductility demand, compute the equivalent viscous damping of the system ξ_{eff}, and obtain the reduced displacement design spectrum.
- **Step 7**: Read from the displacement spectrum the associated effective period T_{eff}. Using the seismic mass (m_s) of a transverse unit of the wharf, the effective stiffness (k_{eff}) is computed.
- **Step 8**: Required total lateral resistance (F_l) is obtained, by definition, multiplying the purely transverse capacity (Δ_t) and the effective stiffness (k_{eff}).
- **Step 9**: If the required lateral resistance is inferior to the total lateral resistance provided by each pile at Δ_t displacement, preliminary design is verified, although the wharf may be over dimensioned. On the contrary, if lateral resistance is not sufficient, it is possible

to obtain straightforwardly a combination of piles that preliminary satisfies design using individual pushover curves (for instance, doubling the number of piles at one row, or reducing the longitudinal distance between pile). Depending on the case, it may also be necessary to reduce free height of piles in order to increase lateral strength, according to Figure 4.6.

- **Step 10**: With the preliminary design, a composite transverse model for a wharf unit is developed, and design is verified.

This method is applied below in detail, for upper and lower bound conditions. Moreover, the method is applied simultaneously for the three seismic levels, OLE, CLE and DE. **Step one**, individual pushover analyses for each pile, has already been performed and presented in previous section. For **step two**, as shown by previous figures, it is clear that the minimum displacement capacity is found at P6, which has the lowest free height. Additionally, due to torsional effects, the most critical pile will be the corner P6 pile, where the distance to the center or rigidity will be the largest. Therefore, critical displacement of the wharf will be based on the displacement capacity of P6 pile.

Next, described steps are applied for UB soil conditions.

4.2.2.1. Preliminary design for Upper Bound soil conditions

Step 3: Critical displacements (displacement capacity)

Referring to Table 4.6 , critical displacements for the three seismic levels are obtained.

Table 4.7. Displacement capacity of the wharf for preliminary design and Upper Bound conditions.

CRITICAL DISPLACEMENTS (Δ_c)		
OLE	0.11	m
CLE	0.25	m
DE	0.30	m

Step 4: Purely transverse displacement of the center of wharf

Previous critical displacements are the ones that applied in any direction at the top of the pile would cause the maximum allowed damage corresponding to the specific seismic intensity. However, as the method is based in a purely transverse single degree of freedom transverse method, the critical displacements need to be reduced. To do so, a Dynamic Magnification Factor (DMF) is used. Although different approaches to the DMF are found in literature (section 2.4), at this stage of the study, ASCE 61-14 expression, based on the eccentricity between the center of rigidity and the center of mass, is used. Note that this expression assumes that 100% of the seismic intensity is applied along the longitudinal direction, while 30% transversally.

$$DMF = \sqrt{1 + \left(0.3\left(1 + \frac{20e}{L}\right)\right)^2} \tag{95}$$

Where L is the length of the wharf unit, which is assumed to be 126m. On the other hand, the eccentricity between the center of mass and the center of stiffness, e, is to be computed. Note that this value may be taken approximately in initial phases of wharf design, as definitive pile layout may be subject to change depending the need of lateral resistance. For instance, it may be initially assumed that longitudinally the same number of piles from P1 to P6 is used, defining a regular grid of piles. However, after initial dimensioning, it may be necessary, for instance, to increase the number of P6 piles, which provide the higher resistance, in order to withstand earthquake loads. In this case, as P6 are the most rigid piles (minimal free height), the center of rigidity would drift towards the land side, and the eccentricity would increase. As a result, torsional effects would be increased and, if necessary, initial design should be repeated in order to verify results. In any case, obtaining the transversal eccentricity of the wharf from an initial regular layout is the most convenient approach. Moreover, it is assumed that the wharf is perfectly symmetric longitudinally, and therefore no eccentricity between center of mass and center of rigidity is found along that direction.

The following assumptions, in line with common practice, are done to obtain the transversal position of the center of rigidity (x_{CR}).

- The deck acts as a rigid diaphragm, therefore only piles influence x_{CR}.
- Due to axisymmetric properties of piles, it is assumed that the rigidity of the pile is independent of the loading direction. Note that this assumption also implies that the dike slope does not have an influence, apart from considering UB and LB springs, on the loading direction of the pile (refined computations may include the increasing resistance of the soil when loading upslope, and loss of resistance downslope, as suggested in POL-B).

With this, the center of rigidity is computed as follows:

$$x_{CR} = \frac{\sum_{i=P1}^{n=P6} k_i x_i}{k_i} \tag{96}$$

Where:

- k_i is the lateral rigidity of the pile.
- x_i is the transversal position of the pile.

The rigidity of the pile is assumed to be governed uniquely by the force-displacement relationship on the top of the pile (therefore, any distributed forces along the free height of the pile are neglected).

$$k_i = \frac{V_i}{u_i} \tag{97}$$

Where V_i is the shear force at the top of the pile, and u_i is the top displacement. Note that rigidity of piles will evolve with displacement demand, as yielding occurs. As a result, eccentricity will tend to reduce as demands increases, as contribution of land piles to stiffness reduces.

Table 4.8. Center of rigidity of the wharf for OLE situation for preliminary design, for UB.

OLE	u_i (m)	V_i (kN)	k_i (kN/m)	x_i (m)	$k_i \cdot x_i$ (kN)
P1	0.1	160.4	1604	3.5	5614
P2	0.1	257.5	2575	9.6	24712
P3	0.1	441.3	4413	15.69	69242
P4	0.1	744.8	8276	21.79	180312
P5	0.1	1305.8	13099	27.88	365238
P6	0.1	1842.6	17383	33.98	590689
TOTAL	-	-	47350	-	1235808
x_{CR} (m)	26.10				

Table 4.9. Center of rigidity of the wharf for CLE situation for preliminary design, for UB.

CLE	u_i (m)	V_i (kN)	k_i (kN/m)	x_i (m)	$k_i \cdot x_i$ (kN)
P1	0.25	382	1528	3.5	5349
P2	0.25	519	2075	9.6	19909
P3	0.25	720	2833	15.69	44460
P4	0.25	1071	4346	21.79	94694
P5	0.25	1557	6337	27.88	176705
P6	0.25	1996	8174	33.98	277738
TOTAL	-	-	25293	-	618854
x_{CR} (m)	24.45				

Table 4.10. Center of rigidity of the wharf for DE situation for preliminary design, for UB.

DE	u_i (m)	V_i (kN)	k_i (kN/m)	x_i (m)	$k_i \cdot x_i$ (kN)
P1	0.30	422	1406	3.50	4919
P2	0.30	548	1825	9.60	17515
P3	0.30	770	2532	15.69	39736
P4	0.30	1071	3613	21.79	78726
P5	0.30	1557	5266	27.88	146847
P6	0.30	1996	6785	33.98	230539
TOTAL	-	-	21427	-	518283
x_{CR} (m)	24.19				

The center of rigidity is found to be, with respect to the extreme of the sea cantilever, at 26,10m for OLE, 24,45m for CLE, and 24,19 for DE. A faster and conservative approach would be to consider for all seismic cases the initial elastic situation for initial design.

The center of mass of the wharf is obtained based on the seismic mass of the wharf, in accordance with ASCE 61 and POL-B, which is found to be at 17,85m. Table 4.11 shows results for the wharf eccentricity and the corresponding DMF values.

Table 4.11. Wharf transversal eccentricity and DMF for initial design according to ASCE 61, for UB.

	x_{CM} (m)	x_{CR} (m)	e (m)	L (m)	DMF
OLE	17.85	26.10	8.25	126	1.22
CLE	17.85	24.47	6.62	126	1.17
DE	17.85	24.19	6.34	126	1.17

As a result, the critical purely transversal center of mass displacement of the wharf, Δ_t is computed as:

$$\Delta_t = \frac{\Delta_c}{DMF} \tag{98}$$

This transverse displacement should be interpreted as the maximum possible demand of the wharf when seismic excitation is purely transversal.

Table 4.12. Total critical wharf displacement and purely transverse maximum displacement for initial design and UB.

	Δ_c (m)	DMF	Δ_t (m)
OLE	0.11	1.22	0.09
CLE	0.25	1.17	0.22
DE	0.30	1.17	0.26

Step 5: Ductility demand

Once torsional behavior and bi-axial seismic excitation is addressed, design follows in a purely transverse manner. Next step is to obtain expected ductility μ_w at seismic demand. To do so, pushover curves are idealized by bi-linear curves, and the yield displacement is identified. Two approaches may be followed. The first, which is proposed in (Priestley et al., 2007), is to obtain expected ductility based on the most critical pile, and then simply assume that the system's ductility is a fraction of that one. The other approach is to assemble the contribution of the six pushover curves, and obtain the global bilinear approximation, thus obtaining the system's ductility directly. It is observed that the first approach offers little advantage over the second one. Additionally, particularly for designing with ASCE 61, the equivalent viscous damping depends not only on the ductility demand, but on the ratio between the slopes of the plastic and initial branches of the pushover curve, referred as the factor r. Thus, even if ductility demand may be addressed as a fraction of the critical pile, the factor r would still be unknown. To illustrate it, both approaches are followed in parallel.

The bilinear approximation is characterized by three parameters:

- k_i: initial elastic stiffness.
- Δ_y: idealized yield displacement.
- r: ratio between plastic slope and initial slope (k_{pl}), such that $k_{pl} = rk_i$.

Knowing Δ_t and k_i from the pushover curve, the idealized yield displacement is determined by equaling areas below both curves. The three bilinear approximations of the composite pushover curve are summarized in Table 4.13 and represented in Figure 4.8.

Table 4.13. Bilinear approximation parameters of the global pushover curve at critical transverse displacement for initial design, and UB conditions.

	Δ_y (m)	k_i (kN/m)	r
OLE	0.04	77532	0.42
CLE	0.05	77532	0.15
DE	0.06	77532	0.11

Figure 4.8 Bilinear approximation of the global pushover curve at critical transverse displacement for initial design, and UB conditions.

Therefore, the ductility of the system is obtained from the previous bilinear curves:

$$\mu_w = \frac{\Delta_t}{\Delta_y} \tag{99}$$

On the other hand, as previously mentioned, (Priestley et al., 2007) proposes to obtain directly the systems ductility as a factor of the critical pile ductility $\mu_{P,cr}$:

$$\mu_w \approx \frac{\mu_{P,cr}}{1.2} = \frac{\Delta_t}{1.2\Delta_{y,P}}$$

The yield displacement of the critical pile ($\Delta_{y,P}$) is obtained from the bilinear approximation of the individual pushover curve of the pile, and therefore ductility may be obtained.

Table 4.14. Bilinear approximation parameters of the critical pile pushover curve at critical transverse displacement for initial design, and UB conditions.

	$\Delta_{y,P}$ (m)	k_i (kN/m)	r
OLE	0.03	37900	0.23
CLE	0.04	37900	0.05
DE	0.05	37900	0.03

Finally, expected ductility demands are obtained. Table 4.15 presents and compares the resultant ductility demand obtained the two described methods.

Table 4.15. Ductility demand of the wharf and of the critical pile using global capacity curve and critical pile capacity, for UB.

	μ_w From composite pushover	$\mu_{P,cr}$ From P6 pushover	$\mu_w \approx \mu_{P,cr}/1.2$ From P6 pushover	$\mu_{P,cr}/\mu_w$
OLE	2.43	2.63	2.19	1.08
CLE	4.00	4.87	4.06	1.22
DE	4.49	5.64	4.70	1.26

Table 4.15 shows that the approach of computing the system ductility as a fraction of the critical pile ductility might be overconservative for high seismic demands (as the ratio between critical pile ductility and system's ductility is found to be larger than 1,2). Indeed, the system ductility from composite response pushover is lower than the one from the critical pile response. Additionally, note that r factor is much lower in the critical pile pushover than in the composite response one. Hence, equivalent viscous damping may be overestimated and therefore seismic demand underestimated. Thus, ductility demand from the composite pushover is used in following steps, and no significant advantage is found for the alternative method.

Step 6: Equivalent viscous damping

At this stage, the equivalent viscous damping expression that is used is the one from ASCE 61-14, which depends both on ductility of the system and the factor r.

$$\xi_{eff,ASCE} = 0{,}05 + \frac{1}{\pi}\left(1 - \frac{1-r}{\sqrt{\mu}} - r\sqrt{\mu}\right) \tag{100}$$

Table 4.16. Equivalent viscous damping according to ASCE 61-14 for each seismic level, for UB.

	$\mu = \mu_w$	r	$\xi_{eff,ASCE}$
OLE	2.43	0.42	5.0%
CLE	4.00	0.15	13.8%
DE	4.49	0.11	16.0%

Table 4.16 shows that for OLE situation, no additional hysteretic viscous damping is obtained. In fact, ASCE 61 damping expression might become smaller than 5% for high values of r, therefore results are restricted to initial elastic equivalent viscous damping.

With these equivalent viscous damping results, the damping scaling reduction factor (DSF) to obtain reduced spectrums needs to be computed. For this particular section, the expression given by EC8-04 (CEN, 2004) is used, as it is usually taken as reference in displacement-based design literature. As a reminder:

$$DSF_{EC8-04} = \sqrt{\frac{10}{5 + \xi_{eff}}} \tag{101}$$

$$S_a^{\xi_{eff}} = DSF \times S_a^{5\%} \tag{102}$$

$$S_d^{\xi_{eff}} = DSF \times \frac{S_a^{5\%}}{\omega^2} = DSF \times S_d^{5\%} \tag{103}$$

Being S_a and S_d spectral acceleration and displacement, respectively. Applying these expressions to this particular case, the following factors are obtained.

Table 4.17. Damping spectrum reduction factor according to EC8-04 for preliminary design and UB conditions.

	ξ_{eff}	DSF_{EC8-04}
OLE	5.0%	1.000
CLE	13.8%	0.729
DE	16.0%	0.691

***Step 7*: Effective properties from displacement design spectrum**

The correlation between maximum admissible displacement (capacity) and seismic demand is done through the reduced design displacement spectrum. As the wharf is fundamentally a one-degree of freedom structure, the transverse displacement maximum demand is directly translated in spectral displacement terms. Then, the reduced displacement spectrum is used to obtain the related period for each spectral displacement (for OLE, CLE and DE), which is shown in Figure 4.9.
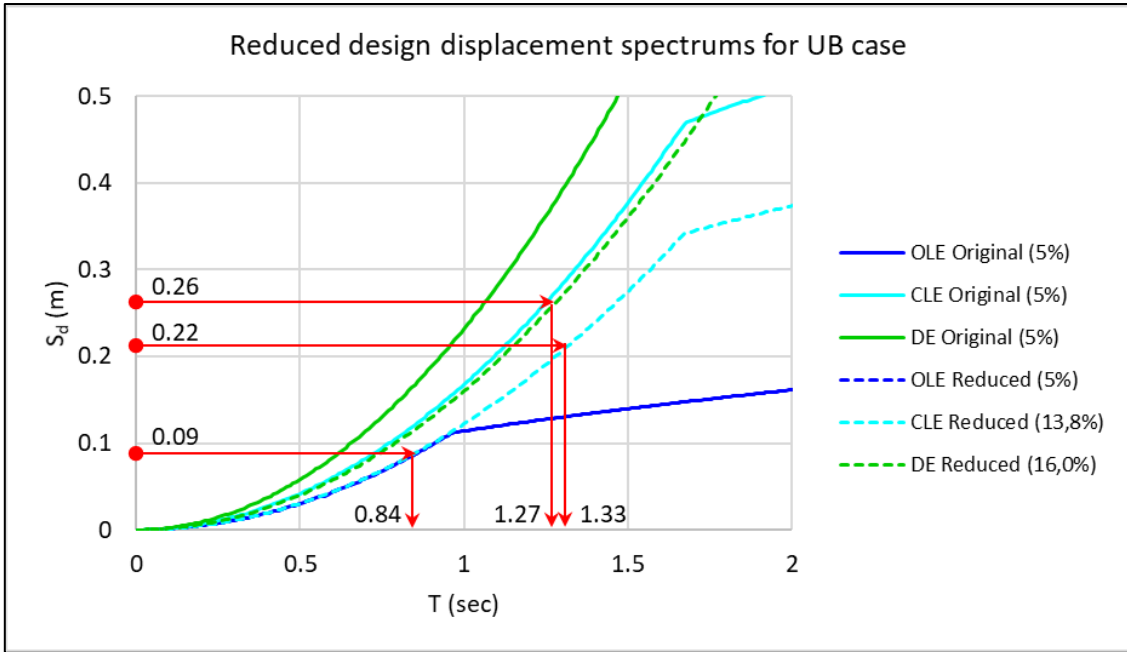
Figure 4.9. Period associated to maximum admissible seismic demand according to design displacement spectrum, for initial design and UB.

Table 4.18. Effective periods associated to maximum admissible seismic demand for initial design, for UB.

	$\Delta_t = S_d^{\xi_{eff}}$ (m)	T_{eff} (sec)
OLE	0.09	0.84
CLE	0.22	1.33
DE	0.26	1.27

Next, effective stiffness of the equivalent structure associated to the effective period is obtained using the following expression:

$$T_{eff} = 2\pi \sqrt{\frac{m_s}{k_{eff}}} \tag{104}$$

$$k_{eff} = 4\pi^2 \frac{m_s}{T_{eff}^2} \tag{105}$$

Where $m_s = 788,26 \; tons$ is the seismic mass, which is defined in section 3.3.5.

Therefore, effective stiffness of the equivalent structure is directly computed for the three seismic cases.

Table 4.19. Effective properties for a 6m transverse unit for initial design, for UB.

	T_{eff} (sec)	k_{eff} (kN/m)
OLE	0.93	44103
CLE	1.36	17592
DE	1.27	19294

***Step 8*: Required lateral resistance**

By definition of the effective stiffness, the force applied to the top of the equivalent oscillator is obtained by multiplying the displacement at the same point by that stiffness. The displacement of interest is the maximum acceptable purely transversal demand for each seismic scenario, Δ_t.

$$F_l = k_{eff} \cdot \Delta_t \tag{106}$$

Then, the required lateral force for each seismic case is:

Table 4.20. Required lateral resistance for each seismic case for initial design, for UB conditions.

	k_{eff} (kN/m)	Δ_t (m)	F_l (kN)
OLE	44103	0.09	3843
CLE	17592	0.22	3809
DE	19294	0.26	5029

Table 4.20 denotes that the lateral resistance for the more intense CLE scenario is inferior to the one for OLE, which may be unexpected. However, this should not be surprising, as performance criteria must be verified for the three seismic cases, and not necessarily the most intense one, the Design Earthquake, is the one that governs design. In fact, in this particular case, more restrictive damage limitations for a smaller earthquake (OLE) are found to be less limiting than less restrictive damage criteria for a more intense seismic scenario (CLE). This is true because the pushover curve before DE has always a positive slope (no loss of resistance), and therefore CLE lateral resistance will necessarily be higher than OLE.

***Step 9*: Available lateral strength**

Lateral required strength must be compared to the resistance provided by considered piles for the corresponding displacement demand. As a reminder, required strength is obtained through the design spectra, while available strength is read from the pushover curves of piles. If available lateral strength is higher than required, preliminary design is completed.

Table 4.21. Available lateral strength of piles at OLE, CLE and DE transverse maximum demands for preliminary design, for UB.

	Piles/unit	OLE F_l (kN)	CLE F_l (kN)	DE F_l (kN)
P1	1	129	327	396
P2	1	207	493	525
P3	1	358	679	720
P4	1	673	1021	1071
P5	1	1214	1557	1557
P6	1	1715	1996	1996
AVAILABLE	-	4295	6073	6264
NECESSARY	-	3843	3809	5029
CHECK	-	Okay	Okay	Okay

For interpretation of results in Table 4.21, it is reminded that using this preliminary design method, the actual seismic demand of the method is not known. On the contrary, it is assumed that demand equals capacity, and from there lateral resistance corresponding to that displacement is obtained. This lateral resistance is shown in the "Necessary" line, while the actual lateral resistance at the same demand according to the capacity is at the "Available" line. If necessary lateral resistance is lower than available, then it is deduced that seismic demand will be lower than the actual displacement capacity, as the capacity curve is found to be increasing up to the DE critical displacement. If the capacity curve of the wharf would coincide with the necessary lateral resistance, then demand would equal capacity.

4.2.2.2.   Preliminary design for Lower Bound soil conditions
As the procedure is analogous, results are given directly, and remarks are placed where relevant.

Step 3: **Critical displacements (displacement capacity)**

Table 4.22. Displacement capacity of the wharf for preliminary design and Lower Bound conditions.

CRITICAL DISPLACEMENTS (Δ_c)		
OLE	0.17	m
CLE	0.48	m
DE	0.57	m

Step 4: **Purely transverse displacement of the center of wharf**

Table 4.23. Center of rigidity of the wharf for OLE situation for preliminary design, for LB.

OLE	u_i (m)	V_i (kN)	k_i (kN/m)	x_i (m)	$k_i \cdot x_i$ (kN)
P1	0.17	194	1143	3.50	4001
P2	0.17	285	1676	9.60	16086
P3	0.17	435	2561	15.69	40186
P4	0.17	631	3797	21.79	82734
P5	0.17	893	5252	27.88	146444
P6	0.17	1106	6420	33.98	218150
TOTAL	-	-	20849	-	507601
x_{CR} (m)	24.35				

Table 4.24. Center of rigidity of the wharf for CLE situation for preliminary design, for LB.

CLE	u_i (m)	V_i (kN)	k_i (kN/m)	x_i (m)	$k_i \cdot x_i$ (kN)
P1	0.48	389	810	3.50	2835
P2	0.48	479	999	9.60	9581
P3	0.48	628	1309	15.69	20539
P4	0.48	834	1752	21.79	38176
P5	0.48	1099	2289	27.88	63837
P6	0.48	1278	2651	33.98	90076
TOTAL	-	-	9810	-	225044
x_{CR} (m)	22.94				

Table 4.25. Center of rigidity of the wharf for DE situation for preliminary design, for LB.

DE	u_i (m)	V_i (kN)	k_i (kN/m)	x_i (m)	$k_i \cdot x_i$ (kN)
P1	0.57	409	718	3.50	2514
P2	0.57	507	889	9.60	8529
P3	0.57	668	1171	15.69	18375
P4	0.57	834	1474	21.79	32108
P5	0.57	1099	1928	27.88	53757
P6	0.57	1278	2234	33.98	75911
TOTAL	-	-	8414	-	191193
x_{CR} (m)	22.72				

Table 4.26. Wharf transversal eccentricity and DMF for initial design according to ASCE 61, for LB.

	x_{CM} (m)	x_{CR} (m)	e (m)	L (m)	DMF
OLE	17.85	24.35	6.5	126	1.17
CLE	17.85	22.94	5.09	126	1.14
DE	17.85	22.72	4.87	126	1.13

Table 4.27. Total critical wharf displacement and purely transverse maximum displacement for initial design and LB.

	Δ_c (m)	DMF	Δ_t (m)
OLE	0.17	1.17	0.15
CLE	0.48	1.14	0.42
DE	0.57	1.13	0.51

As a remark, Lower Bound soil conditions make the land piles less stiff, therefore eccentricity between the center of mass and the center of rigidity is reduced. As a result, the DMF factor is lower than for UB, hence torsional effects are reduced.
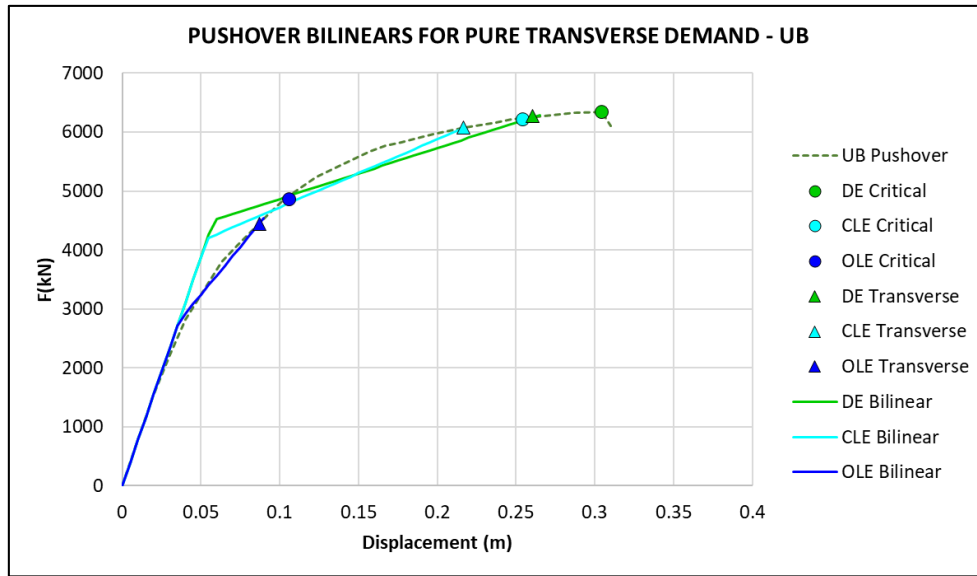
Step 5: Ductility demand
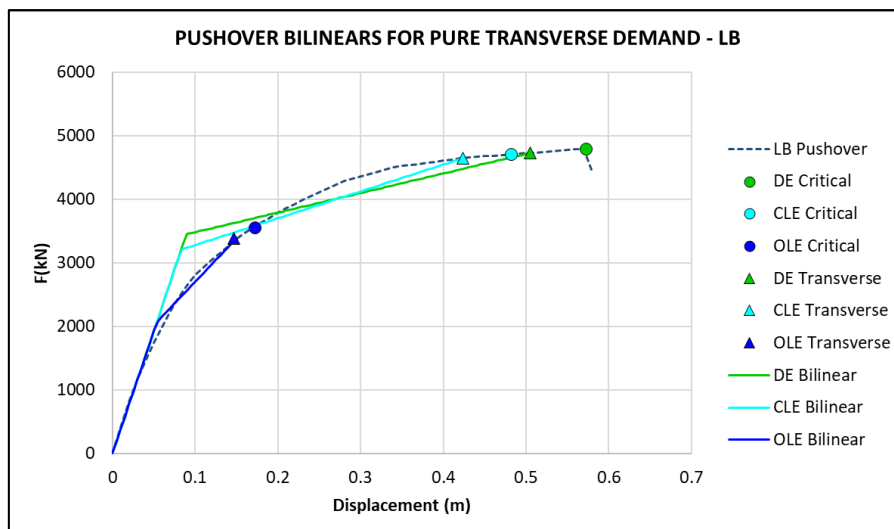
Figure 4.10 Bilinear approximation of the global pushover curve at critical transverse displacement for initial design, and LB conditions.

81

Table 4.28. Bilinear approximation parameters of the global pushover curve at critical transverse displacement for initial design, and LB conditions.

	Δ_y (m)	k_i (kN/m)	r
OLE	0.05	38557	0.36
CLE	0.08	38557	0.11
DE	0.09	38557	0.08

Table 4.29. Bilinear approximation parameters of the critical pile pushover curve at critical transverse displacement for initial design, and LB conditions.

	$\Delta_{y,P}$ (m)	k_i (kN/m)	r
OLE	0.05	15684	0.17
CLE	0.07	15684	0.04
DE	0.07	15684	0.03

Table 4.30. Ductility demand of the wharf and of the critical pile using global capacity curve and critical pile capacity, for LB.

	μ_w From composite pushover	$\mu_{P,cr}$ From P6 pushover	$\mu_w \approx \mu_{P,cr}/1.2$ From P6 pushover	$\mu_{P,cr}/\mu_w$
OLE	2.75	2.88	2.40	1.05
CLE	5.09	6.31	5.26	1.24
DE	5.65	7.22	6.01	1.28

Step 6: Equivalent viscous damping

Table 4.31. Equivalent viscous damping according to ASCE 61-14 for each seismic level, for LB.

	$\mu = \mu_w$	r	$\xi_{eff,ASCE}$
OLE	2.75	0.36	5.7%
CLE	5.09	0.11	16.4%
DE	5.65	0.08	18.5%

Table 4.32. Damping spectrum reduction factor according to EC8-04 for preliminary design and LB conditions.

	ξ_{eff}	DSF_{EN-04}
OLE	5.7%	0.967
CLE	16.4%	0.684
DE	18.5%	0.653

***Step 7*: Effective properties from displacement design spectrum**
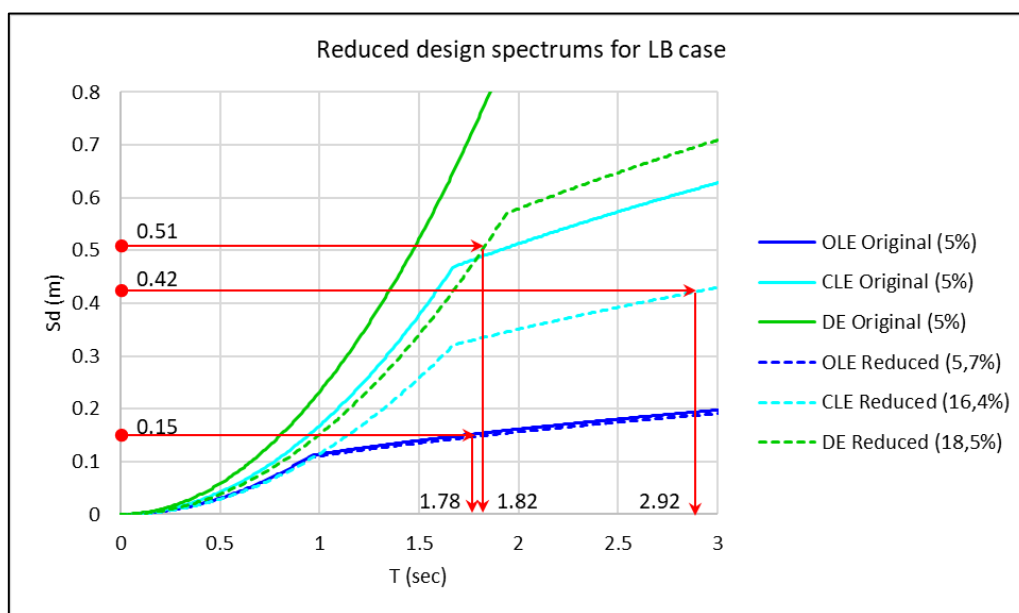
Figure 4.11. Period associated to maximum admissible seismic demand according to design displacement spectrum, for initial design and LB.

Table 4.33. Effective periods associated to maximum admissible seismic demand for initial design, for LB.

	$\Delta_t = S_d^{\xi_{eff}}$ (m)	T_{eff} (sec)
OLE	0.15	1.78
CLE	0.42	2.92
DE	0.51	1.82

Table 4.34. Effective properties for a 6m transverse unit for initial design, for LB.

	T_{eff} (sec)	k_{eff} (kN/m)
OLE	0.93	9822
CLE	1.36	3650
DE	1.27	9395

***Step 8*: Required lateral strength**

Table 4.35. Required lateral resistance for each seismic case for a 6m transverse unit and LB condition.

	k_{eff} (kN/m)	Δ_t (m)	F_l (kN)
OLE	9822	0.15	1445
CLE	3650	0.42	1547
DE	9395	0.51	4746

***Step 9*: Available lateral strength**

Table 4.36. Available lateral strength of piles at OLE, CLE and DE transverse maximum demands for preliminary design, for LB.

	Piles/unit	OLE F_l (kN)	CLE F_l (kN)	DE F_l (kN)
P1	1	163	375	393
P2	1	242	461	485
P3	1	373	602	637
P4	1	593	822	834
P5	1	850	1099	1099
P6	1	1050	1278	1278
TOTAL	-	3271	4637	4727
NECESSARY	-	1445	1547	4747
CHECK	-	Okay	Okay	Fail

Table 4.36 shows that available lateral resistance for DE slightly inferior than required. Therefore, changes in design should be implemented. The following alternatives would be possible:

- Reduce seismic mass:
  o By reducing longitudinal distance between each row of piles (reducing the width of the elementary transverse wharf unit).
- Increase lateral resistance:
  o By increasing the number of piles at each transverse unit (for instance, doubling the number of P6 piles).
  o By reducing the free height of piles (for instance, moving closer P5 to P6).
  o By modifying the pile properties (for instance, changing cross section properties).

It should be noted, however, that increasing lateral resistance will have an impact on ductility of the wharf, therefore on displacement demand.

Note that the easiest modification at this stage is to reduce seismic mass, as it does not modify the calculations regarding seismic capacity (critical displacements, ductility). Passing from the current 6m width transverse unit of the wharf, which implies 21 transverse rows of piles (126 piles total), to a transverse separation of 5,75m (total of 132 piles). This change reduces the seismic mass of one transverse wharf unit of 25,32 tons.

Table 4.37. Seismic mass of a transverse unit of the wharf of 5.75m.

	Element	Mass (metric tons)
DECK	Slab	315,07
	Dead load	52,51
	10% live load	105,02
	Transversal beam	183,38
	Longitudinal beams	37,99
	Total superstructure	693,99
PILES	Concrete plugs	34,04
	Piles	15,08
	Hydrodynamic mass	19,84
	Total piles	68,96
TOTAL	Total seismic mass	762,94

With critical transverse displacement and available lateral strength being unmodified, the reduction in seismic mass implies a reduction of required effective stiffness, and therefore required lateral strength is also reduced.

Table 4.38. Required and available lateral resistance for each seismic case for a 5.75m transverse unit and LB.

	k_{eff} (kN/m)	Δ_t (m)	F_l (kN) required	F_l (kN) available	Check
OLE	9506.3	0.147	1398.73	3270,8	Okay
CLE	3532.5	0.424	1497.61	4637,2	Okay
DE	9093.1	0.505	4594.02	4727,4	Okay

Therefore, the reduction of seismic mass is sufficient to validate preliminary seismic design of the wharf.

4.2.2.3.   Conclusions of preliminary design

The method proposed by (Priestley et al., 2007) allows to systematically following perform a preliminary design following simple steps. It is found that, for the particular study case, Lower Bound soil conditions are governing, and required slight modifications to initial design, by reducing longitudinal spacing of rows of piles. Additionally, as critical displacements for CLE are close to those of DE, while the intensity of the latter is considerably higher, causes that CLE case is comparatively not very demanding for the structure. This method proves to be effective to assess in an initial design phase the influence of design choices such as the number of piles, free height, etc., without the need to develop different models for each design alternative. Additionally, the engineer has complete control over the calculations that are implied, providing better understanding of the method.

4.2.3   Global assembly for pushover analysis

Once preliminary seismic design is completed, then the complete assembled transverse model of a wharf unit may be analyzed. Previous pushover analyses were based on independent response of individual piles. Therefore, two main assumptions where made:

- Piles fixed against rotation at the top.
- Expected equivalent axial load on piles.

Hence, in order to validate the relevance of such simplifications to address initial design, pushover analyzes are obtained modeling the influence of deck stiffness, as well as possible axial load changes in piles with displacement demand. Additionally, the general model also allows to introduce the influence of vertical seismic excitation as per ASCE 61, where permanent gravity loads are increased or decreased according to peak ground acceleration. Finally, the effect of geometric non-linearity of the structure can be implemented in the model. The complete transverse model is analyzed by three separate stages in order to be able to dissociate results:

- No vertical seismic action: validate the assumptions of previous independent pile pushovers.
- Vertical seismic action: influence of vertical loading in wharf capacity.
- Introduction of P-Delta effects: influence of geometric non-linearities.

This will be performed on next sections.

4.2.3.1. Transversal pushover without vertical seismic action

The main purpose of this section is to compare capacity results from individual piles on section 4.2.1 to the global assembly model.

Both for Upper and Lower Bound conditions, two static pushover analyses are performed. One where the structure is pushed towards the sea, and another towards land. Although soil springs are modeled with symmetric response (upslope and downslope), response is found to be not strictly symmetric. Figure 4.12 presents results of the analyses from the complete transverse unit models, applying horizontal loads towards sea and towards land, for upper and for lower cases. Additionally, results from previous initial pushovers (by individual piles) is also shown. Critical displacements for each seismic scenario are also included. Note that displacements are taken as their absolute value, in order to be able to compare graphically the cases sea and land.
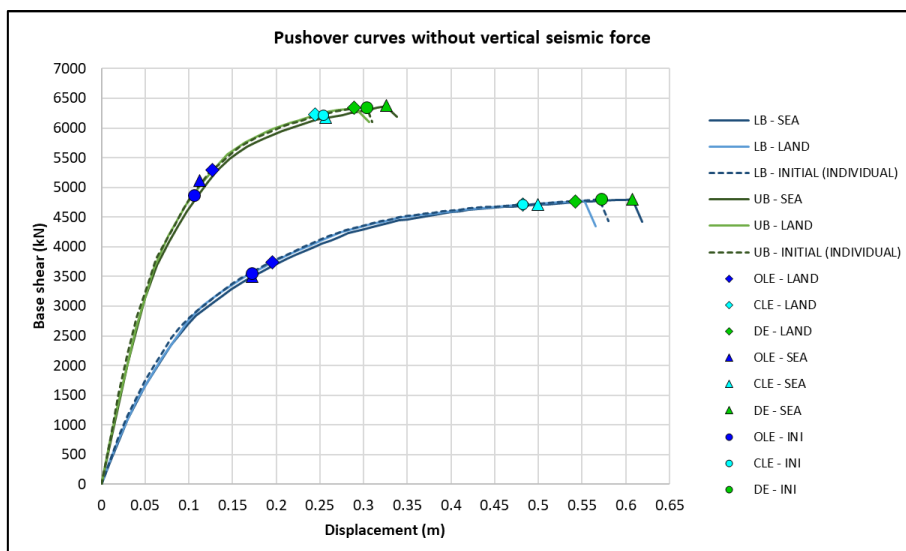
Figure 4.12. Static pushover results for three different cases: towards land (LAND), towards sea (SEA), and initial individual pushovers (INI). Results are shown for upper and lower bound.

The first observation is that lateral strength for both cases (land and sea) are very similar, with differences below 3%, being higher on the land case. Secondly, critical displacements are found to be quite sensible to the direction of loading, reaching differences of 12%. Additionally, it is found that for OLE, the smallest critical displacement is given by sea loading, while for DE is given for land case. Critical displacements are obtained from maximum plastic rotations, which depend on the seismic case and on the applied axial load, as discussed in section 3.2.1. Therefore, by observing actual axial loads for the critical pile, conclusions might be found.

Table 4.39. Critical displacements (Δ_c), associated lateral strength (F_l) and axial load at critical pile P6 (P_{P6}), for each seismic case and loading direction, with Upper Bound conditions. Compression is positive.

SEISMIC CASE	Δ_c (m)	F_l (kN)	P_{P6} (kN)
OLE - LAND	0.13	5294	2592
OLE - SEA	0.11	5114	-85
CLE - LAND	0.25	6224	2606
CLE- SEA	0.26	6181	-123
DE - LAND	0.29	6342	2607
DE - SEA	0.33	6381	-122

Table 4.40. Critical displacements (Δ_c), associated lateral strength (F_l) and axial load at critical pile P6 (P_{P6}), for each seismic case and loading direction, with Lower Bound conditions. Compression is positive.

SEISMIC CASE	Δ_c (m)	F_l (kN)	P_{P6} (kN)
OLE - LAND	0.20	3745	2397
OLE - SEA	0.17	3497	13
CLE - LAND	0.48	4706	2426
CLE- SEA	0.50	4709	-30
DE - LAND	0.54	4764	2428
DE - SEA	0.61	4799	-37

Table 4.39 and Table 4.40 both show that axial load on the critical pile varies significantly if loading occurs towards land or towards sea. Compression is larger for land cases, while for sea cases the critical pile can even be slightly in tension. This fact explains why displacement capacity (determined from performance criteria) varies between land and sea cases, and also why depending on the seismic scenario, the critical case might be one or the other. First, as a reminder, it has been observed that, for the particular case of study:

- OLE scenario is governed by plug hinge on the critical pile (P6).
- CLE and DE scenarios are governed by in-ground hinge on the critical pile (P6).

On concrete hinges, limiting curvatures increased with axial load up to a certain point (much higher than observed axial loads in the models), as well as plastic moments. Therefore, it is logical that for OLE cases higher compression axial loads are beneficial, as displacement capacity, as well as lateral resistance, will be higher. On the other hand, for CLE and DE cases, the situation is reversed. As it was observed in the modeling of steel hinges, compression axial load decreased plastic moment and critical curvatures of the section. Therefore, higher compression axial loads reduce both lateral resistance of the wharf and displacement capacity. Still, lateral strength sensibility on axial load is found to be quite small in comparison with displacement capacity sensibility. This can be explained by the fact that all piles contribute, although in different degrees, to the lateral resistance of the wharf, while only the critical pile determines the displacement capacity of the whole wharf. Additionally, extreme piles (P1 and P6) are the ones with more variability of axial loads, being the rest more uniform in terms of compression for any given displacement demand, which supports the previous conclusion. This observation may be explained by two reasons. First, purely by equilibrium, as the deck moves towards sea, the weight of the deck that is carried by P6 pile decreases, being the exact opposite when loading towards land. Additionally, the deck is not infinitely rigid, as it was initially assumed for preliminary design. Figure 4.13 shows the deformed shapes of the model at DE situation, with loadings towards land and sea. It can be observed in the models that when loading towards sea, the deck tends to produce an uplift movement on the critical pile, which contributes to lowering the axial load. On the contrary, when loading towards land, the deck suffers a downward movement over P6, compressing the pile.
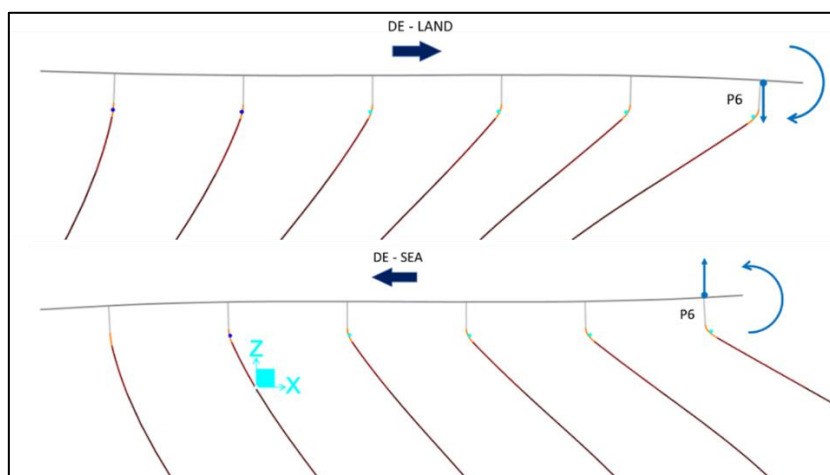
Figure 4.13. Deformed shape of the model (magnification factor of x35). Above, DE-Land; Below, DE-Sea. Both for UB soil conditions.

Naturally, on the real seismic situation, the wharf will oscillate from land to sea, therefore both phenomena will occur repeatedly. The static pushover analysis is a tool for dimensioning seismic capacity, and also for assessing maximum seismic demand, but does not evaluate directly any oscillatory behavior. Therefore, introduced seismic loading directions shall not be understood as the real seismic direction, which has no physical sense, but as a methodology to obtain in design the most critical combination of displacement capacity and lateral resistance.

In conclusion, results from the assembly of lateral resistance of individual pile pushovers and from the complete models are very similar in terms of the relation between displacement and force, and vary more significantly, although still similar, in terms of displacement capacity. Therefore, the initial assumption that a uniform constant axial load could be assumed for all piles and that deck is rigid seems valid for preliminary design, but should always be checked with the complete model and detailed case analysis.

4.2.3.2. Transversal pushover including vertical seismic action

Previous section showed that axial load variations on critical pile affect the seismic capacity of the wharf, while keeping lateral resistance almost constant. ASCE 61 states that combination of loads in seismic case should include the vertical seismic component of the earthquake. The approach is then to multiply permanent actions by a coefficient that considers vertical acceleration, either positive (upwards) or negative (downwards). Therefore, the assessment of the effect of vertical seism is modeled by the modification of axial loads on piles. Note that this methodology is based on the fact that the vertical component of the dynamic movement of the wharf is not expected to play a significant role in the dynamics of the structure. Indeed, from the modal analysis of the complete 3D model of the wharf, it can be observed that vertical movements are orders of magnitude inferior to horizontal ones. However, also note that while vertical excitation does not play a relevant role for the wharf, the vertical component of the dynamic seismic excitation may play a significant role for crane seismic design (Shafieezadeh, 2011), although not considered in this study.

Table 4.41. Critical displacements and lateral strength for each seismic scenario, considering vertical component of earthquake. Values compared (Diff.) to results without vertical component. Lower Bound Case.

CASE	LB - LAND				LB - SEA			
	Δ_c (m)	Diff.	F_l (kN)	Diff.	Δ_c (m)	Diff.	F_l (kN)	Diff.
OLE +	0.20	0.4%	3758	0.3%	0.17	0.5%	3510	0.4%
OLE-	0.20	-0.5%	3733	-0.3%	0.17	-2.7%	3446	-1.5%
CLE+	0.48	-0.3%	4721	0.3%	0.49	-1.2%	4732	0.5%
CLE-	0.48	-0.4%	4673	-0.7%	0.50	-0.9%	4679	-0.6%
DE+	0.54	-0.4%	4794	0.6%	0.60	-1.8%	4828	0.6%
DE-	0.55	2.1%	4742	-0.5%	0.61	0.6%	4765	-0.7%

Table 4.42. Critical displacements and lateral strength for each seismic scenario, considering vertical component of earthquake. Values compared (Diff.) to results without vertical component. Upper Bound Case.

CASE	UB - LAND				UB - SEA			
	Δ_c (m)	Diff.	F_l (kN)	Diff.	Δ_c (m)	Diff.	F_l (kN)	Diff.
OLE +	0.13	0.0%	5296	0.0%	0.11	-0.1%	4986	-2.5%
OLE-	0.13	-0.6%	5265	-0.6%	0.11	-1.0%	4959	-3.0%
CLE+	0.25	0.1%	6236	0.2%	0.26	-0.1%	6198	0.3%
CLE-	0.24	-0.7%	6188	-0.6%	0.26	1.0%	6149	-0.5%
DE+	0.29	-0.3%	6378	0.6%	0.33	-0.2%	6409	0.4%
DE-	0.29	-1.0%	6276	-1.0%	0.33	0.4%	6319	-1.0%

It is observed in tables Table 4.41 and Table 4.42 that sensibility of critical displacements (Δ_c) and lateral strength (F_l) to the vertical component of seismic action is low. The maximum difference between these static pushover analyses and previous ones summarized in Table 4.39 and Table 4.40 is found to be of 3%. Variation of axial load in piles is not very significant, therefore results do not vary considerably. For piles with higher axial load ratio, differences could be multiplied.

These results may indicate, without aim of generalizing to all cases, that seismic design in intermediate phases might be carried without considering this aspect, reducing considerably the number of load cases and analyzes to be developed. However, for final design verification of the solution, as indicated in ASCE 61, the load combination has to include the influence of vertical seismic acceleration.

4.2.3.3. Transversal pushover with P-delta effects

Up to this point, all models have included non-linearity of the force-displacement relationship, through the introduction of plastic hinges on structural elements. However, another type of non-linearity may play a role in design, which is geometric non-linearity. In that case, the model considers the equilibrium equations in the deformed shaped, therefore introducing second order internal forces and, as a consequence, additional deformations. This type of non-linearity is also referred as P-Delta effects.
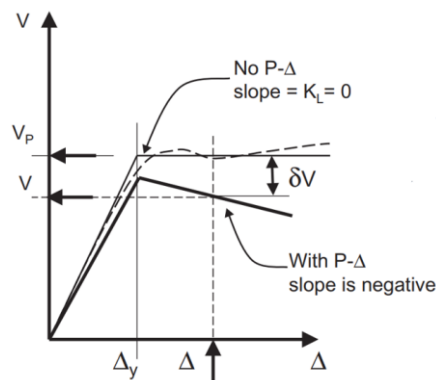
Figure 4.14. P-Delta effects to a capacity curve (ASCE 61).

The main effect of P-Delta effects on a static pushover analysis is that for a given displacement, the corresponding lateral external force is lower than without this non-linearity, as second order internal forces also contribute to the lateral deformation of the structure. As a result, capacity of the wharf may be reduced, as well as demand may increase (Figure 4.14).

ASCE 61 does not require systematically that P-Delta effects due to seismic action are introduced in design models. If the following condition, according to ASCE 61 §6.6.7, is verified, P-Delta effects due to seismic loading shall not be considered in seismic design.

$$\frac{W\Delta}{H} \leq 0{,}25V_p \tag{107}$$

Where:

- W is the total seismic weight.
- Δ is the displacement demand in the studied direction.
- H is the distance between the center of gravity of the deck and the maximum in-ground moment.
- V_p is the lateral force (or base shear) of the structure from the pushover analysis.

Table 4.43 and Table 4.44 check if P-Delta effects should be considered according to ASCE 61, using the capacity curves from section 4.2.3.1 (no vertical seismic influence).

Table 4.43. P-delta effects check according to ASCE 61, considering maximum displacement demand $\Delta = \Delta_c$, for Lower Bound Case.

CASE	$\Delta = \Delta_c$ (m)	H (m)	$V_p = F_l$ (kN)	$W\Delta/H$ (kN)	$0{,}25V_p$ (kN)	Check
OLE LAND	0.20	11.1	3745	132	936	No P-Delta
OLE SEA	0.48	11.1	3497	325	874	No P-Delta
CLE LAND	0.54	11.1	4706	366	1177	No P-Delta
CLE SEA	0.17	11.1	4709	116	1177	No P-Delta
DE LAND	0.50	11.1	4764	337	1191	No P-Delta
DE SEA	0.61	11.1	4799	410	1200	No P-Delta

Table 4.44. P-delta effects check according to ASCE 61, considering maximum displacement demand $\Delta = \Delta_c$, for Upper Bound Case.

Case	$\Delta = \Delta_c$ (m)	H (m)	$V_p = F_l$ (kN)	$W\Delta/H$ (kN)	$0{,}25V_p$ (kN)	Check
OLE LAND	0.13	8.3	5294	115	1324	No P-Delta
OLE SEA	0.11	8.3	5114	102	1278	No P-Delta
CLE LAND	0.25	8.3	6224	221	1556	No P-Delta
CLE SEA	0.26	8.3	6181	231	1545	No P-Delta
DE LAND	0.29	8.3	6342	261	1586	No P-Delta
DE SEA	0.33	8.3	6381	294	1595	No P-Delta

These tables show that, according to ASCE 61, and assuming that seismic demands correspond to maximum capacity, P-Delta effects do not need to be considered in seismic design. Note that

Δ is the actual seismic displacement demand, to be obtained, for example, by the substitute structure iterative method, which has not been done yet.

However, independently of this condition, a static pushover analysis is performed including P-Delta effects in order to observe its actual consequences in this particular design. In line with conclusions in section 4.2.3.2, vertical component of seism is not included in these analyses.
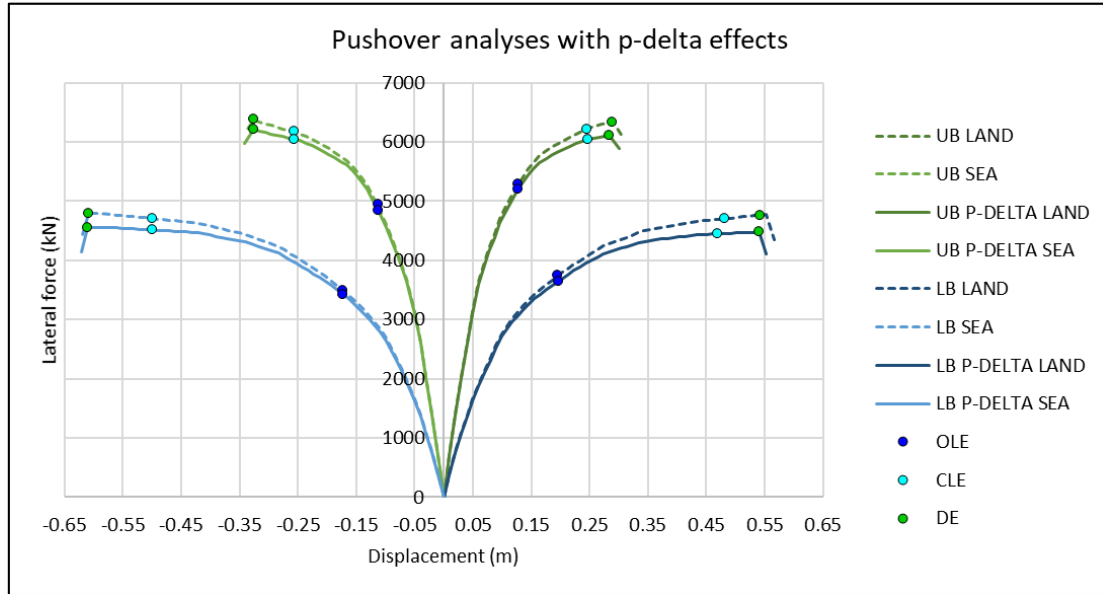
Figure 4.15. Static pushover analysis results including p-delta effects, without vertical component of seismic action.

Critical displacements of the wharf are found to be not dependent on P-Delta effects. However, lateral resistance, as expected, is reduced, especially for larger displacement demands. Table 4.45 and Table 4.46 compare results from models including P-Delta effects from the models without geometric non-linearity (from section 4.2.3.1).

Table 4.45. Critical displacements and lateral forces including p-delta effects, compared to results without p-delta and without vertical component of seismic action, for LB case.

CASE	LB - LAND				LB - SEA			
	Δ_c (m)	Diff.	F_l (kN)	Diff.	Δ_c (m)	Diff.	F_l (kN)	Diff.
OLE	0.20	0%	3652	-2%	0.17	0%	3428	-2%
CLE	0.47	-3%	4451	-5%	0.50	0%	4516	-4%
DE	0.54	0%	4481	-6%	0.61	0%	4560	-5%

Table 4.46. Critical displacements and lateral forces including p-delta effects, compared to results without p-delta and without vertical component of seismic action, for UB case.

CASE	UB - LAND				UB - SEA			
	Δ_c (m)	Diff.	F_l (kN)	Diff.	Δ_c (m)	Diff.	F_l (kN)	Diff.
OLE	0.13	0%	5197	-2%	0.11	-1%	4847	-5%
CLE	0.25	1%	6045	-3%	0.26	0%	6044	-2%
DE	0.28	-2%	6114	-4%	0.33	0%	6209	-3%

It is observed that the larger the demand, the larger the reduction of lateral resistance. This is logical, as second order bending moments in piles are dependent on deflection at the top. Additionally, it is found that P-Delta effects are more significant in Lower Bound case than in Upper Bound. Again, it is coherent with the fact that LB model is laterally less rigid, therefore larger deflections induce larger second order internal forces.

In conclusion, displacement capacity of the wharf (maximum critical displacements) is found to be insensible to P-Delta effects. On the other hand, lateral resistance is more affected by geometric non-linearity, up to 6% for the particular studied models. Therefore, even if P-Delta effects shall not be considered according to ASCE 61, they are found to be more relevant that considering the vertical component of the seismic action. In any case, influence of P-Delta effects on seismic demand are yet to be studied in section 4.3.1.1.

4.3. SEISMIC DISPLACEMENT DEMAND

Displacement based design is based on the comparison of demand and capacity in terms of displacement. Capacity of the wharf is assessed via static non-linear pushover analyses, which require the use of structural modeling software. Previous sections performed these analyses, and critical displacements (i.e., capacity) were obtained for each seismic scenario. Influence of the vertical component of the seismic action was also studied, and its influence was found to be slightly relevant for intermediate phases of design. Note, however, that actual horizontal seismic action has not been used in any calculations (except in preliminary design using individual pile pushovers). Thus, the objective of this section is to obtain the displacement demand for each of the three intensities that are considered in this design. The obtention of seismic demand may be assessed by different methods, as exposed in section 2.2. As a reminder, response spectrum analysis may be appropriate for elastic demands, the substitute structure method for transverse post-yielding demands, while time-history analysis, although complex, may be appropriate for all cases.

Three-dimensional response spectrum analysis is not considered relevant nor useful for this design. Indeed, as observed in capacity curves, inelasticity is present from low demands, therefore the elastic analysis of the structure is not applicable. The same is concluded for the effective elastic stiffness method. Hence, only the substitute structure method and time histories fit this particular design.

4.3.1. Transverse single mode analysis – Substitute structure method

The aim of this section is to obtain seismic demand, and studying the influence of considered aspects in section 4.2.3. Three main inputs are essential to apply the substitute structure method:

- Structural capacity: pushover curve.
- Seismic action: design spectrum.
- Seismic mass.

All three have been obtained in previous sections. Additionally, this method relies on two other aspects that may significantly affects results:

- Effective viscous damping (ξ_{eff}).
- Spectrum reduction factor (DSF).

This section is organized with the following structure. First, seismic demand is computed according to ASCE 61 and the spectrum reduction factor of EC8-04, for the different capacity curves that have been obtained. Note that the particular choice of DSF is taken as a benchmark. Therefore, the first objective is to obtain the influence of vertical component of seismic action and P-Delta effects on seismic demand using the same damping and DSF. Afterwards, for the capacity curves that are judged relevant, seismic demand is assessed using alternative viscous damping expressions and spectrum reduction factors, introduced in section 2.3.3, and compared to the benchmark case.

Note that this section assesses purely transverse seismic demand of the wharf. Simultaneous longitudinal and transversal excitation, as well as torsional effects, are discussed in section 4.3.2using the Dynamic Magnification Factor.

4.3.1.1. Transversal demand according to ASCE 61

As it has been presented in preliminary design, the following damping and spectrum reduction factor are used. Note that ASCE 61 does not specify a specific spectrum reduction factor.

$$\xi_{eff,ASCE} = 0.05 + \frac{1}{\pi}\left(1 - \frac{1-r}{\sqrt{\mu}} - r\sqrt{\mu}\right) \tag{108}$$

$$DSF_{EN-04} = \sqrt{\frac{10}{5 + \xi_{eff}}} \tag{109}$$

For solving the iterative problem of the substitute structure, a tolerance of 1% between consecutive steps is taken, even if ASCE 61 allows a value up to 3%. Additionally, for obtaining the bilinear approach of the pushover curves, a tolerance of 0,2% of the areas under each curve is supposed (which is not specified by the codes). The algorithm is automatized using Excel's VBA code.

In order to visualize results graphically, the Acceleration-Displacement Response Spectra (ADRS) format is used (Applied Technology Council, 1996). In this representation, the capacity curve (force-displacement), obtained by pushover analysis, is transformed to the so-called capacity spectrum (spectral acceleration – spectral displacement), and represented in the same space than the response spectrum. The conversion between force-displacement to ADRS is done in the general case using modal participation factors and modal mass coefficients for the first natural mode. As it has been already mentioned, in the particular case of wharf design, the transversal dynamics of the structure is fundamentally a one degree of freedom system. As a result, both ASCE 61 and POL-B simplify the problem and propose a seismic mass, which is essentially the participating mass of the first mode (only mode transversally relevant). Thus,

transversally, the displacement at the top of the wharf, which is the monitored point in pushover analyses, can be directly understood as the spectral displacement. Therefore, the transformation from Δ (displacement in pushover analyses) and S_d (spectral displacement) is straightforward. On the other hand, lateral force is transformed into spectral acceleration by means of the associated effective period at each point, as indicated in next expression.

$$S_a = \omega^2 S_d = \left(\frac{2\pi}{T_{eff}}\right)^2 S_d = \left(\frac{2\pi}{2\pi\sqrt{m_s/k_{eff}}}\right)^2 S_d = \frac{k_{eff}}{m_s} S_d = \frac{F_l/\Delta}{m_s} \cdot S_d$$
$$= \frac{F_l}{m_s}$$

(110)

Demand without vertical seismic action

The purpose of this section is to obtain seismic demand using the substitute structure method, without considering vertical seismic loading. The effect of loading towards sea or land is studied.

In this section, capacity curves from section 4.2.3.1 are used for determining demand, Therefore, four capacity curves are used, which correspond to the pushover analyses in upper and lower bounds, and applying lateral forces towards land or sea. Plus, demand is obtained for the three seismic scenarios, OLE, CLE and DE. Therefore, a total of twelve cases are distinguished, using the notation indicated in Table 4.47.

Table 4.47. Study cases for the substitute structure method, without considering vertical seismic action.

SEISMIC CASE	UPPER BOUND		LOWER BOUND	
	LAND	SEA	LAND	SEA
OLE	OLE-LAND-UB	OLE-SEA-UB	OLE-LAND-LB	OLE-SEA-LB
CLE	CLE-LAND-UB	CLE-SEA-UB	CLE-LAND-LB	CLE-SEA-LB
DE	DE-LAND-UB	DE-SEA-UB	DE-LAND-LB	DE-SEA-LB

Graphical results from the substitute structure method are provided for upper and lower bound cases with lateral load towards land, using the ADRS representation. The solution to the substitute structure method, in terms of displacement and force of the corresponding seismic demand, is known as the performance point.

OLE
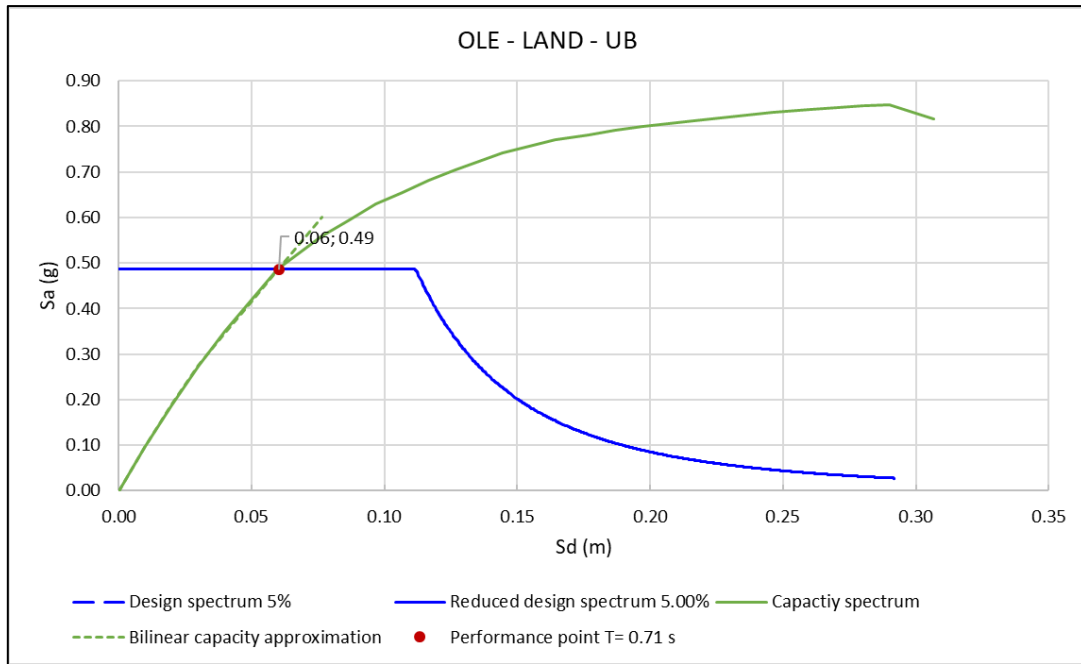
Figure 4.16. Seismic demand for OLE obtained by the substitute structure method, with Upper Bound soil conditions.
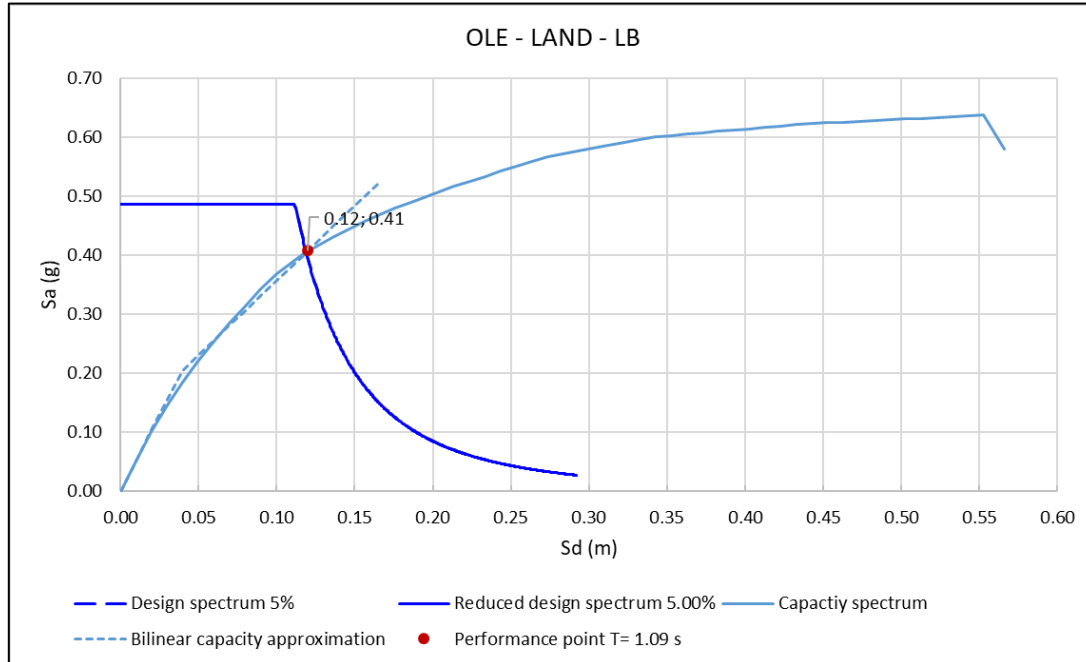
Figure 4.17. Seismic demand for OLE obtained by the substitute structure method, with Lower Bound soil conditions.

CLE
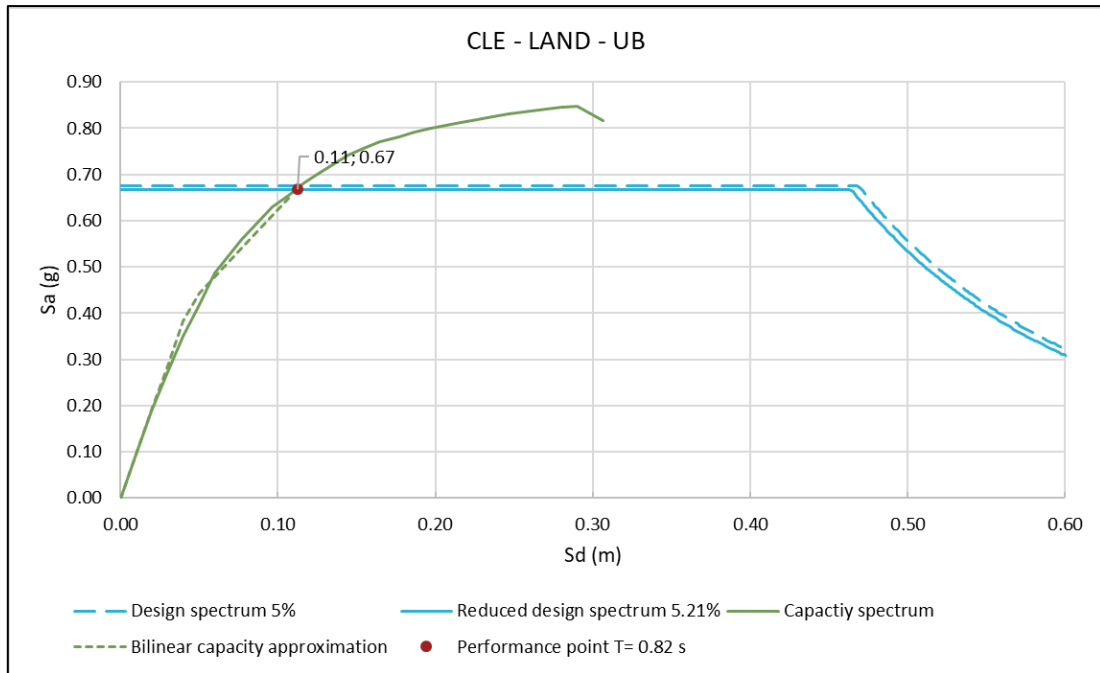
Figure 4.18. Seismic demand for CLE obtained by the substitute structure method, with Upper Bound soil conditions.
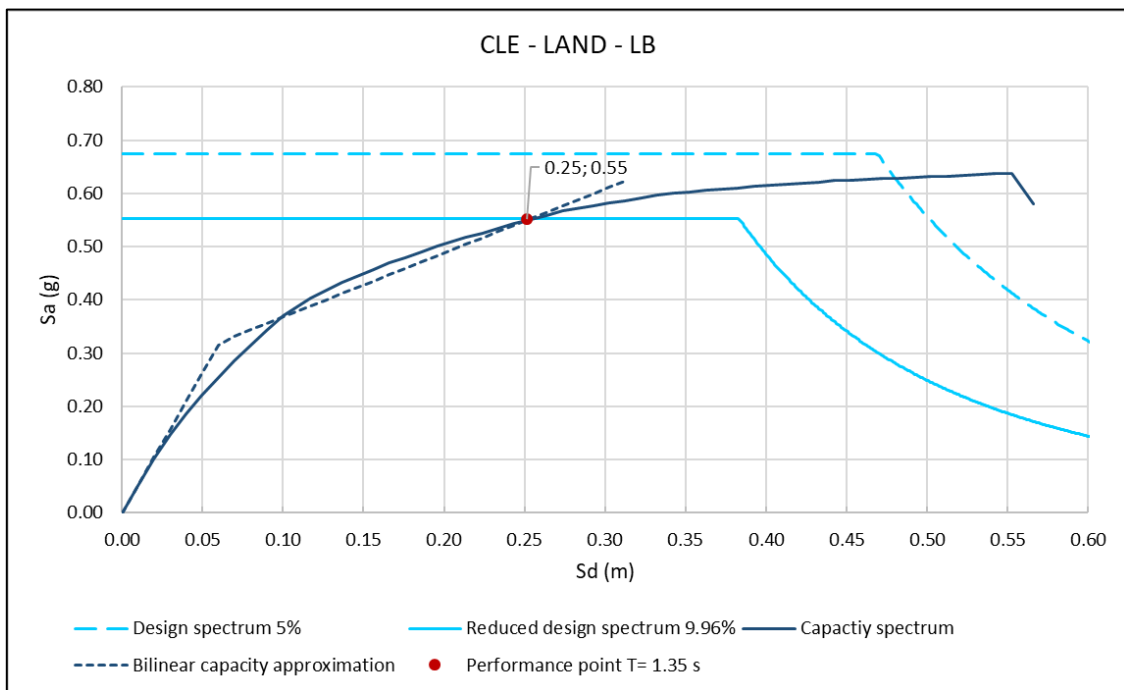
Figure 4.19. Seismic demand for CLE obtained by the substitute structure method, with Lower Bound soil conditions.

DE
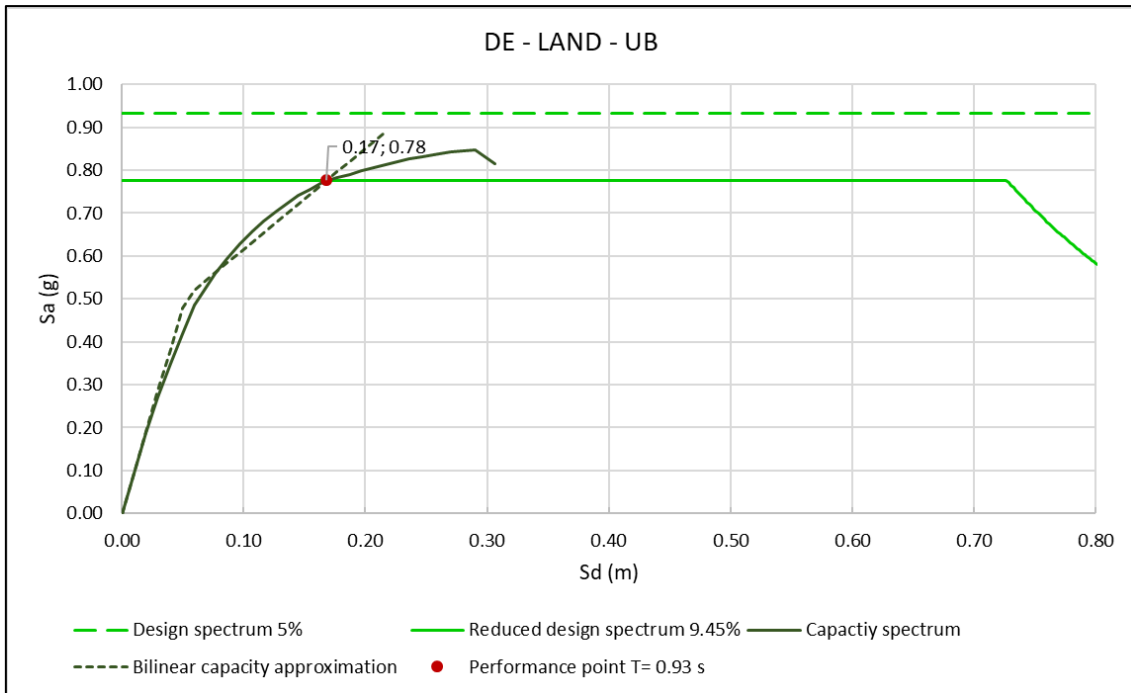
Figure 4.20. Seismic demand for DE obtained by the substitute structure method, with Upper Bound soil conditions.
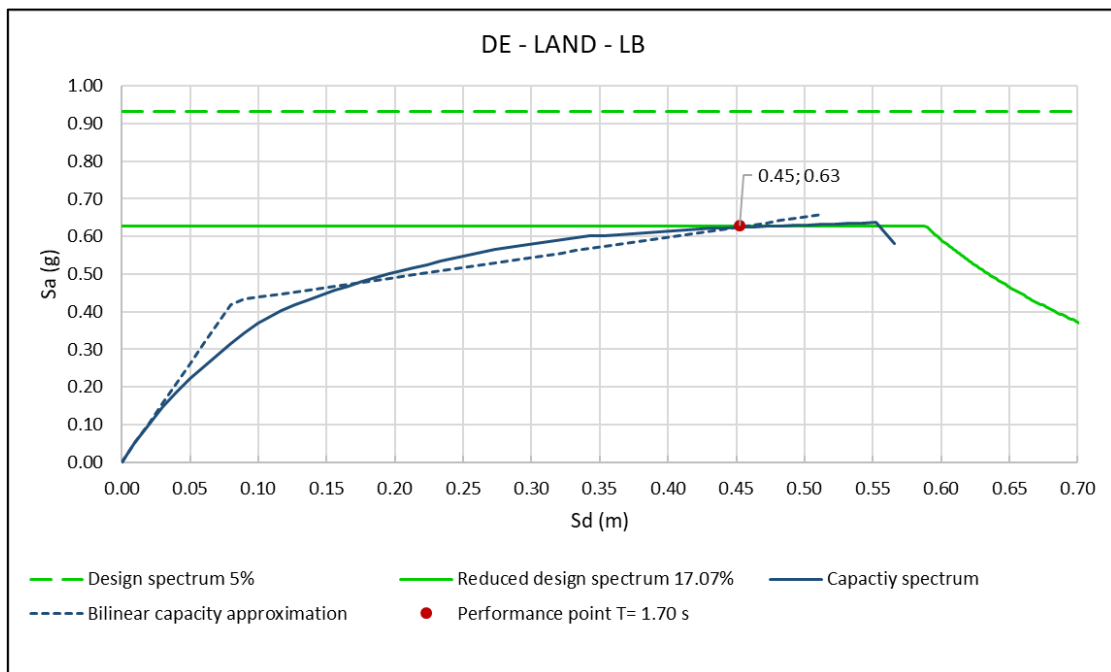
Figure 4.21. Seismic demand for DE obtained by the substitute structure method, with Lower Bound soil conditions.

Table 4.48, Table 4.49 and Table 4.50 summarize demand results obtained by the substitute structure method. All relevant parameters that define the solution (demand, lateral force, viscous damping, effective stiffness, effective period and bilinear approximation parameters) are included.

Table 4.48. Substitute structure results for OLE: displacement demand, lateral force, effective viscous damping, effective stiffness, effective period, idealized yield displacement, initial stiffness, plastic and elastic slopes ratio.

	OLE-LAND-UB	OLE-SEA-UB	OLE-LAND-LB	OLE-SEA-LB
Δ_d (m)	0.06	0.06	0.12	0.12
F_l (kN)	3664	3672	3043	2976
ξ_{eff} (%)	5	5	5	5
k_{eff} (kN/m)	60441	58036	25506	24714
T_{eff} (sec)	0.71	0.72	1.09	1.1
Δ_y (m)	0.03	0.03	0.04	0.04
k_i (kN/m)	71890	69501	39310	37867
r	0.72	0.67	0.48	0.46

Table 4.49. Substitute structure results for CLE: displacement demand, lateral force, effective viscous damping, effective stiffness, effective period, idealized yield displacement, initial stiffness, plastic and elastic slopes ratio.

	CLE-LAND-UB	CLE-SEA-UB	CLE-LAND-LB	CLE-SEA-LB
Δ_d (m)	0.11	0.12	0.25	0.26
F_l (kN)	5040	4993	4097	4067
ξ_{eff} (%)	5.21	5.41	9.96	10.18
k_{eff} (kN/m)	44358	42763	16443	15922
T_{eff} (sec)	0.82	0.84	1.35	1.38
Δ_y (m)	0.04	0.05	0.06	0.06
k_i (kN/m)	71890	69501	39310	37867
r	0.38	0.37	0.23	0.23

Table 4.50. Substitute structure results for DE: displacement demand, lateral force, effective viscous damping, effective stiffness, effective period, idealized yield displacement, initial stiffness, plastic and elastic slopes ratio.

	DE-LAND-UB	DE-SEA-UB	DE-LAND-LB	DE-SEA-LB
Δ_d (m)	0.17	0.17	0.45	0.47
F_l (kN)	5784	5728	4674	4671
ξ_{eff} (%)	9.45	9.75	17.07	16.97
k_{eff} (kN/m)	34662	33254	10394	10127
T_{eff} (sec)	0.93	0.95	1.7	1.72
Δ_y (m)	0.05	0.05	0.08	0.08
k_i (kN/m)	71890	69501	39310	37867
r	0.25	0.24	0.10	0.10
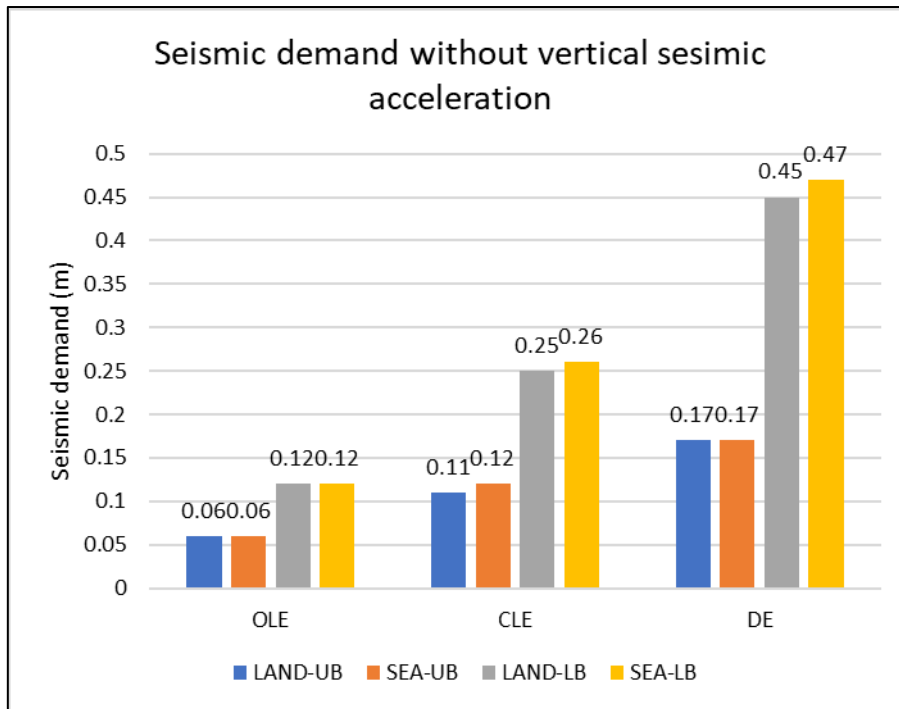
Figure 4.22. Seismic displacement demand without considering vertical component of seismic excitation, for each loading direction and for UB and LB conditions.

Figure 4.22 shows that resultant seismic demand is equal or higher when pushover analysis is performed towards the sea direction. This difference is amplified for higher seismic demands. However, capacity on sea cases was also higher. Therefore, either of both cases may govern design. This corroborates the need to perform detailed analyses to make sure that design considers the worst-case scenario. Additionally, the influence of UB and LB conditions, as discussed, influences greatly results.

Demand with vertical seismic action

The aim of this part is to measure the influence of vertical seismic action on displacement demand, by applying the substitute structure method. Pushover analyses from section 4.2.3.2 (considering the vertical acceleration due to the earthquake load) are used to obtain displacement demand using the substitute structure method. As a reminder, capacity was slightly modified, especially regarding displacement, rather than lateral resistance

Referring to Table 4.51, analyses found that displacement demand obtained from cases where vertical seismic acceleration was considered differ very slightly to the ones without it (less than 2% in terms of displacement for DE demand). Note that for CLE-SEA-UB particular case, the difference of 8% is not significantly relevant in absolute terms (1cm). These differences might be positive or negative. For piles with larger axial load ratios, differences may be amplified.

Table 4.51. Seismic displacement demand considering vertical component of seismic excitation, for each loading direction and for UB and LB conditions. Vertical + refers to upwards acceleration of soil.

	CASE	NO VERTICAL	VERTICAL +	Diff.	VERTICAL -	Diff.
OLE	OLE-LAND-UB	0.06	0.06	0%	0.06	0%
	OLE-SEA-UB	0.06	0.06	0%	0.06	0%
	OLE-LAND-LB	0.12	0.12	0%	0.12	0%
	OLE-SEA-LB	0.12	0.12	0%	0.12	0%
CLE	CLE-LAND-UB	0.11	0.11	0%	0.11	0%
	CLE-SEA-UB	0.12	0.12	0%	0.11	-8%
	CLE-LAND-LB	0.25	0.25	0%	0.25	0%
	CLE-SEA-LB	0.26	0.26	0%	0.26	0%
DE	DE-LAND-UB	0.17	0.17	0%	0.17	0%
	DE-SEA-UB	0.17	0.17	0%	0.17	0%
	DE-LAND-LB	0.45	0.44	-2%	0.46	2%
	DE-SEA-LB	0.47	0.46	-2%	0.48	2%

Demand with P-Delta effects

Last sensibility study of demand corresponds to non-linear geometric effects. As a reminder, for the particular case of analysis, ASCE 61 does not require to consider them in design. Nevertheless, the substitute structure method is applied to the capacity curves from section 4.2.3.3, and purely transversal seismic demand is obtained using the substitute structure method. Results are compared to demand without vertical seismic loading (section 4.2.3.1).

Table 4.52. Seismic displacement demand considering P-Delta effects, for each loading direction and for UB and LB conditions.

	CASE	NO P-DELTA	P-DELTA	Diff.
OLE	OLE-LAND-UB	0.06	0.06	0%
	OLE-SEA-UB	0.06	0.06	0%
	OLE-LAND-LB	0.12	0.12	0%
	OLE-SEA-LB	0.12	0.12	0%
CLE	CLE-LAND-UB	0.11	0.11	0%
	CLE-SEA-UB	0.12	0.12	0%
	CLE-LAND-LB	0.25	0.26	4%
	CLE-SEA-LB	0.26	0.27	4%
DE	DE-LAND-UB	0.17	0.17	0%
	DE-SEA-UB	0.17	0.17	0%
	DE-LAND-LB	0.45	0.50	11%
	DE-SEA-LB	0.47	0.51	9%

Table 4.52 shows that, for higher seismic demand, such as DE scenario, and especially on the Lower Bound condition, seismic demand is considerably modified by P-Delta effects (increasing them approximately by 10%). Nonetheless, it was previously found that displacement capacity of the structure when considering P-Delta effects was unmodified. Therefore, even if P-Delta is not systematically required by ASCE 61, it may be advisable to check them in design.

4.3.1.2. Influence of spectrum reduction factors on transversal seismic demand

Reducing the three original design spectra (OLE, CLE and DE), initially obtained for an equivalent viscous damping of 5%, is also a central parameter influencing the substitute structure method results. The damping spectrum reduction factor (DSF) is used to this purpose. Up to this section, expression from EC8-04 was used systematically, which is recurrent in displacement-based design literature. Other DSF expressions that are identified are summarized in Table 4.53.

Table 4.53. Damping spectrum reduction factor expressions (DSF).

EC8-04	EC8-94	(Newmark & Hall, 1982)	(Calvi et al., 2008)
$\sqrt{\dfrac{10}{5 + \xi}}$	$\sqrt{\dfrac{7}{2 + \xi}}$	$\dfrac{(2{,}31 - 0{,}41 \cdot \ln \xi)}{(2{,}31 - 0{,}41 \cdot \ln 5)}$	$\left(\dfrac{7}{2 + \xi}\right)^{0{,}25}$

Capacity curves from section 4.2.3.1 (no vertical acceleration nor P-Delta effects) are used as input for obtaining demand with the substitute structure method, with lateral loading direction towards land.
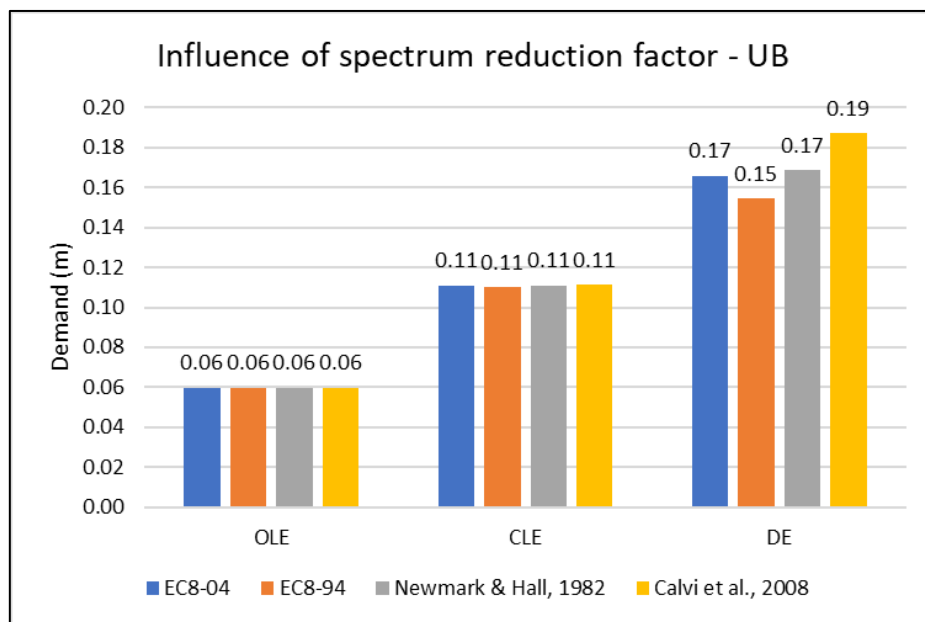
Figure 4.23. Substitute structure demand results for different DSF, using capacity curve without vertical seism towards land, for Upper Bound case.

102
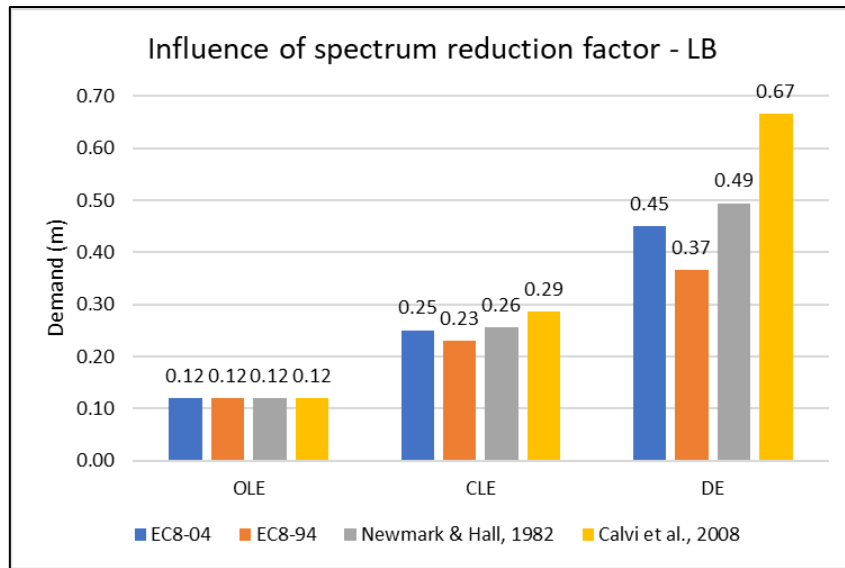
Figure 4.24. Substitute structure demand results for different DSF, using capacity curve without vertical seism towards land, for Upper Bound case.

Figure 4.23 and Figure 4.24 show the influence of different DSF to seismic demand. On the first hand, for OLE situation no effect is observed, since ductility demand is low, thus dissipation is not very relevant. For CLE, Upper Bound shows little influence, while for LB maximum and minimum demand differ by 25%. These effects are amplified when ductility demand is high, reaching differences, for LB, of up to 85%.

DSF from EC8-04 and expression from (Newmark & Hall, 1982) provide similar results. Expression from the older Eurocode seems to be unconservative, with potential danger in design. On the other hand, DSF proposed by (Calvi et al., 2008) provides quite higher results than the rest, and therefore might be overconservative. In any case, the engineer should be aware of the influence of his/her choice of DSF on results. In case of doubt, (Newmark & Hall, 1982) will always provide a slightly more conservative demand (higher) than DSF on EC8-04, which would be on the safe side.

4.3.1.3. Transversal demand using alternative damping expressions

The aim of this section is to measure the influence on seismic demand of another key aspect of the substitute structure method. As mentioned, one of the most important factors is the effective equivalent viscous damping used in the analysis, which, as a minimum, depends on the system's ductility. Reviewed expressions in this section are exposed in section 2.3.2.

Two Design Earthquake cases are analyzed, since the aim is not to assess the complete seismic design again (loading direction, vertical acceleration, P-Delta effects), as it has been previously developed. Upper and Lower bound capacity curves, with loading towards land, are used as input for obtaining demand, following the same methodology of the substitute structure method as before. Vertical component of seismic action and P-Delta effects are not considered in the capacity curve.

POL-B damping

As a reminder, the damping presented in POL-B is similar to a Thin Takeda hysteretic model, with horizontal plastic branch and parameters $\alpha = 0,5$ and $\beta = 0$. Additionally, the elastic part of the equivalent viscous damping is fixed at 10%. From all damping expressions reviewed in this study, it is the most dissipative one.

$$\xi_{eff} = 0,1 + 0,565 \left(\frac{\mu - 1}{\mu} \right) \tag{111}$$

Table 4.54. Substitute structure results using POL-B damping and EC8-04 DSF, for Lower Bound.

	DE-LAND-LB
Δ_d (m)	0.25
F_l (kN)	4100
ξ_{eff} (%)	23.6
k_{eff} (kN/m)	16422
T_{eff} (sec)	1.35
Δ_y (m)	0.06
k_i (kN/m)	39310
r	0.23

It is observed that displacement demand is considerably lower than the one obtained using ASCE 61-14 (0,45m, or 44% less). Indeed, the resultant equivalent damping is higher in this case, compared to 17,1% in the ASCE 61 case.

Assuming a Thin Takeda hysteretic model with $\alpha = 0,5$ and $\beta = 0$, the corresponding hysteretic loop at resulting demand may be obtained by obtaining the unloading and loading slopes. The unloading slope (k_u) is obtained according to the α parameter. Being k_i the initial elastic branch:

$$k_u = k_i \left(\frac{\Delta_m}{\Delta_y} \right)^{\alpha} = 39310 \left(\frac{0,25}{0,06} \right)^{0,5} = 19384 \frac{kN}{m} \tag{112}$$

The reloading slope is defined by the segment between the point where the unloading slope crosses the horizontal axis, and the point on the pushover curve at maximum displacement Δ_m. Figure 4.25 plots the performance point obtained according to POL-B on the pushover curve, as well as its symmetric counterpart, neglecting differences between the opposite loading directions. Additionally, the resulting hysteretic loop corresponding to the Takeda model is plotted.

Figure 4.25. Performance point obtained by the substitute structure method for POL-B damping. Assumed hysteretic behavior is superposed (Thin Takeda). Lower Bound case.

Referring to Figure 4.25, it is possible to compare the assumed equivalent viscous damping from POL-B to the actual equivalent viscous damping particularly for the obtained pushover curve, according to the Thin Takeda model. The definition of the hysteretic part of equivalent viscous damping is:

$$\xi_{hyst} = \frac{2}{\pi} \cdot \frac{A_2}{A_1} = \frac{2}{\pi} \cdot 0{,}0779 = 5{,}0\%$$

(113)

Additionally, POL-B assumes a 10% elastic damping. Therefore, the actual viscous damping that would correspond to the particular obtained capacity curve and the Thin Takeda model, would be of 15%, instead of the resulting 23,6% from applying POL-B damping expression. This result suggests that POL-B damping should not be applied regardless of the structure particular ductile behavior. Indeed, if the bilinear approximation of the pushover curve would have a lower r, closer to 0, the resultant viscous damping would be higher, and demand may correspond to results. However, on the general case, the plastic slope of the capacity curve is not necessarily close to zero, which reduces the dissipation of the structure.

ASCE 61 damping, on the contrary, is based on the particular value of r, and therefore has a wider applicability to less ductile structures. Applying ASCE 61 damping expression for the value of r in

Table 4.54, the same result for the hysteretic component of damping is obtained than from Figure 4.25.

$$\xi_{hyst,ASCE} = \frac{1}{\pi}\left(1 - \frac{1 - 0{,}23}{\sqrt{4{,}17}} - 0{,}23\sqrt{4{,}17}\right) = 5\%$$

(114)

A part from the fact that the hysteretic component of damping of ASCE 61 corresponds well to the particular results of the capacity curve, it is also noted that the elastic component is 5% instead of 10% in POL-B.

The less ductile the structure, the more difference between assumed and actual damping when using POL-B expression. Solving the substitute structure according to POL-B for Upper Bound-Land, it is found that demand is 9cm, while damping is 20,1%. Compared to ASCE 61 results, with a displacement demand of 17cm and damping 9,75%, POL-B results 47% lower for displacement demand and 106% higher for damping. Plotting the assumed hysteretic behavior, the resultant hysteretic part of the equivalent damping is found to be 2,3%. Adding the 10% of elastic part, it gives a total of 12,3% (far from resulting 20,1% from POL-B expression).
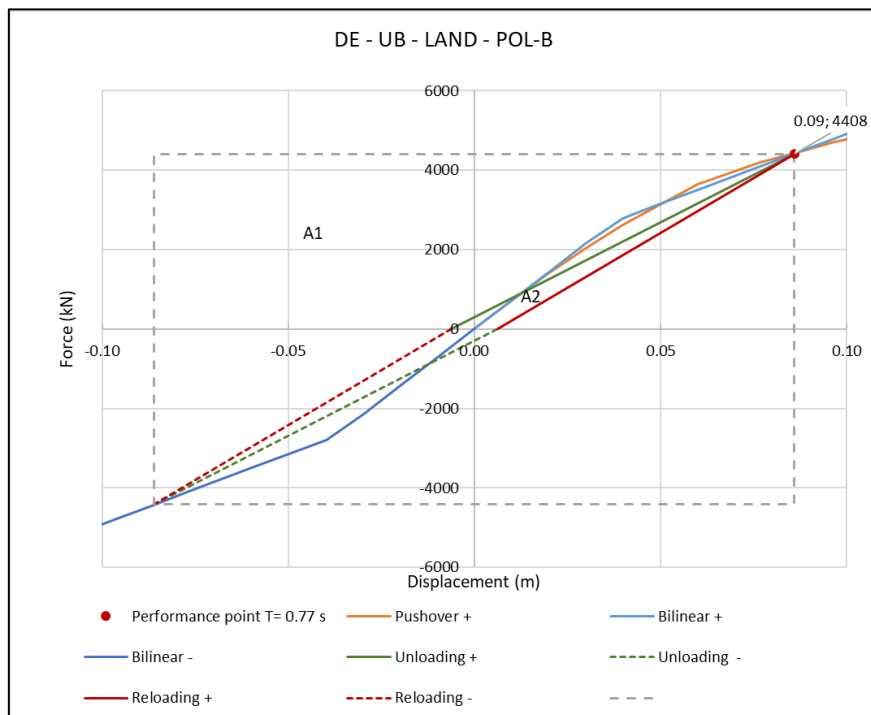
Figure 4.26. Performance point obtained by the substitute structure method for POL-B damping. Assumed hysteretic behavior is superposed (Thin Takeda). Upper Bound case.

Hence, it is concluded that POL-B proposes a non-conservative expression with respect to ASCE 61, and that should only be applied, even if POL-B does not mention it, to structures with a capacity curve with plastic branch close to horizontal. Additionally, the 10% of elastic damping in POL-B adds to the non-conservativism, potentially underestimating seismic demand.

Damping from (Priestley et al., 2007)

(Priestley et al., 2007) directly referring to wharf structures, proposes the following expression of equivalent viscous damping:

$$\xi_{eff} = 0{,}05 + 0{,}444\left(\frac{\mu - 1}{\pi\mu}\right) \tag{115}$$

Table 4.55. Substitute structure results using (Priestley et al., 2007) damping and EC8-04 DSF, for Lower Bound.

	DE-LAND-LB
Δ_d (m)	0.49
F_l (kN)	4705
ξ_{eff} (%)	16.67
k_{eff} (kN/m)	9770
T_{eff} (sec)	1.76
Δ_y (m)	0.08
k_i (kN/m)	39310
r	0.09

Although (Priestley et al., 2007) does not specify the exact assumptions that are made to obtain this expression, it mentions that it is based on the Thin Takeda model. Assuming the parameter $\alpha = 0{,}5$, and $\beta = 0$, the resultant hysteretic loop is represented in next figure.
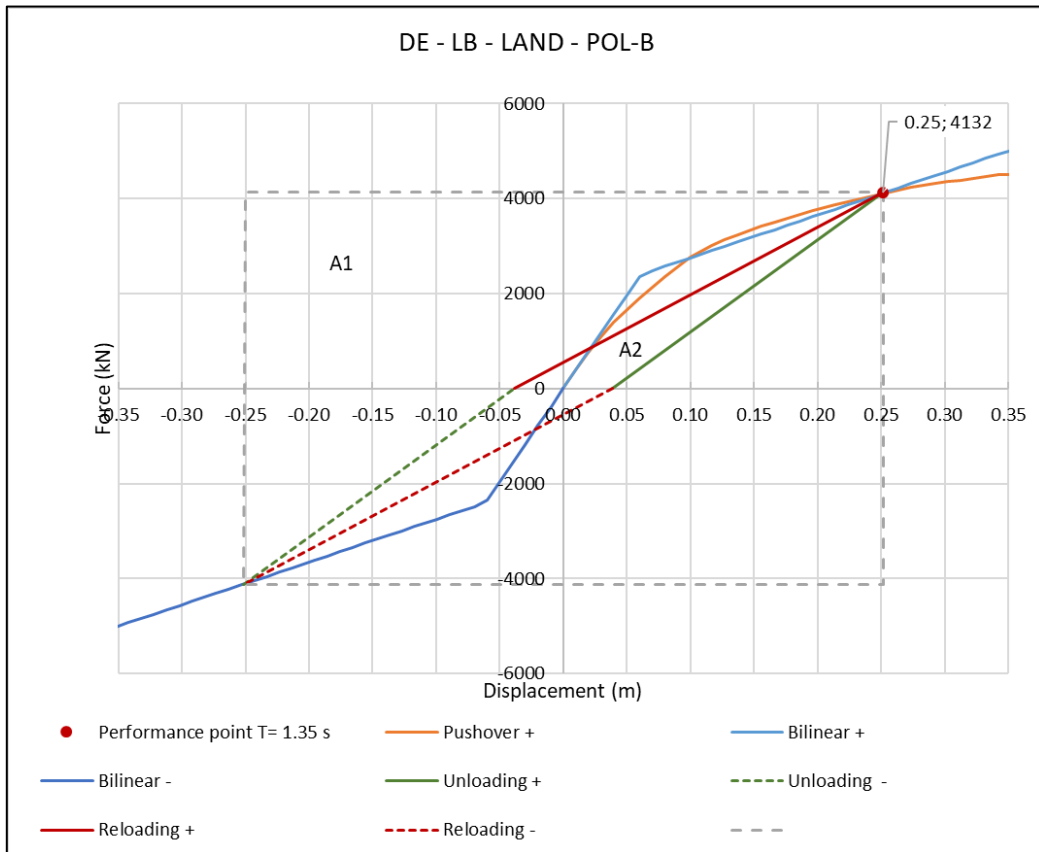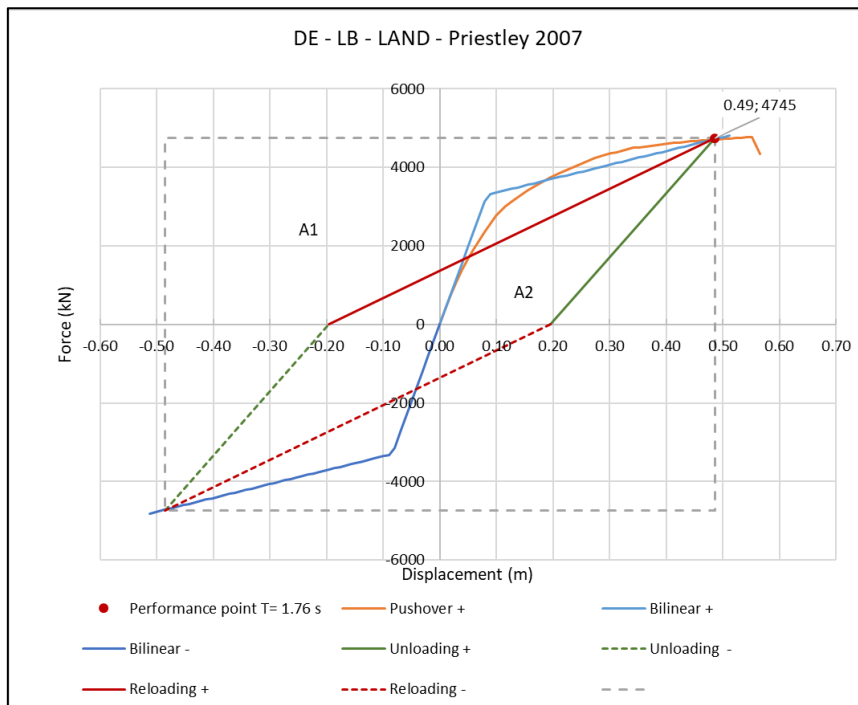

Figure 4.27. Performance point obtained by the substitute structure method for (Priestley et al., 2007) damping. Assumed hysteretic behavior is superposed (Thin Takeda). Lower Bound case.

From Figure 4.27, the actual equivalent viscous damping assuming the Thin Takeda (or Small Takeda) model with $\alpha = 0,5$ and $\beta = 0$ is deduced as follows:

$$\xi_{eff} = 0,05 + \frac{2}{\pi} \cdot \frac{A_2}{A_1} = 0,05 + \frac{2}{\pi} \cdot 0,2 = 5,0\% + 12,7\% = 17,7\%$$

(116)

It is found that the equivalent damping from Figure 4.27 is slightly larger to the one from expression in (Priestley et al., 2007) (6% larger). This should indicate that equation (115) was obtained for a higher value of r (less dissipative), or that a lower α value (less dissipative) was assumed.

For this particular case, this damping provides similar results than following ASCE 61. However, the engineer should be aware that in the general case this could not be the case, as less dissipative systems would be overdamped, or vice versa.

Small Takeda damping from (Dwairi et al., 2007)

Another expression is proposed by (Dwairi et al., 2007) regarding systems following the Thin Takeda model. In this case, the expression is dependent on the effective period of the structure, apart from the system's ductility.

$$\xi_{hyst} = C_{LT} \left(\frac{\mu - 1}{\pi \mu} \right) \%$$
$$C_{LT} = 65 + 50(1 - T_{eff}) \qquad T_{eff} < 1\ s$$
$$C_{LT} = 65 \qquad\qquad\qquad T_{eff} \geq 1\ s$$

(117)

Table 4.56. Substitute structure results using Small Takeda from (Dwairi et al., 2007) damping and EC8-04 DSF, for Lower Bound.

	DE-LAND-LB
Δ_d (m)	0.29
F_l (kN)	4297
ξ_{eff} (%)	20.99
k_{eff} (kN/m)	14971
T_{eff} (sec)	1.42
Δ_y (m)	0.07
k_i (kN/m)	39310
r	0.20
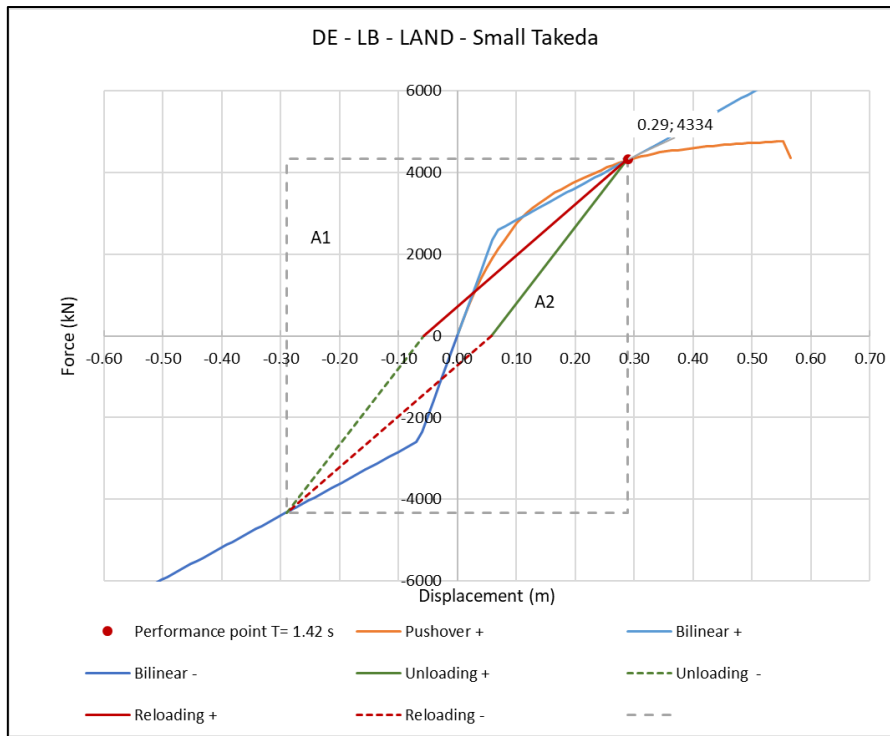
Figure 4.28. Performance point obtained by the substitute structure method for (Dwairi et al., 2007) Thin Takeda damping. Assumed hysteretic behavior is superposed. Lower Bound case.

Again, the difference between damping obtained by the proposed equation and by geometrically analyzing the hysteretic loop under the capacity curve helps to determine the pertinence of the model.

$$\xi_{eff} = 0{,}05 + \frac{2}{\pi} \cdot \frac{A_2}{A_1} = 0{,}05 + \frac{2}{\pi} \cdot 0{,}1 = 5{,}0\% + 6{,}3\% = 11{,}3\% \tag{118}$$

Comparing with Table 4.56 results (damping of 16,67%), it is concluded that the equivalent damping expression is not necessarily adapted to all capacity curves, since it may overestimate it. Even if expression in (Dwairi et al., 2007) was finely tuned according to time-history analyzes, it shows to be of little interest for the general case, where the secondary slope of the bilinear approximation is not known in advance, hence this expression can lead to misinterpretations of the actual hysteretic behavior of the structure.

Elasto-plastic damping

The use of steel piles might suggest applying an elasto-plastic hysteretic behavior, typical of steel members. Next equation models this behavior.

$$\xi_{hyst} = \frac{2}{\pi} \cdot \frac{(\mu - 1) \cdot (1 - r)}{\mu \cdot (1 + r\mu - r)} \tag{119}$$

Again, substitute structure method is performed to obtain seismic demand.

Table 4.57. Substitute structure results using Elasto-Plastic damping and EC8-04 DSF, for Lower Bound.

	DE-LAND-LB
Δ_d (m)	0.23
F_l (kN)	3954
ξ_{eff} (%)	25.91
k_{eff} (kN/m)	17442
T_{eff} (sec)	1.31
Δ_y (m)	0.06
k_i (kN/m)	39310
r	0.25
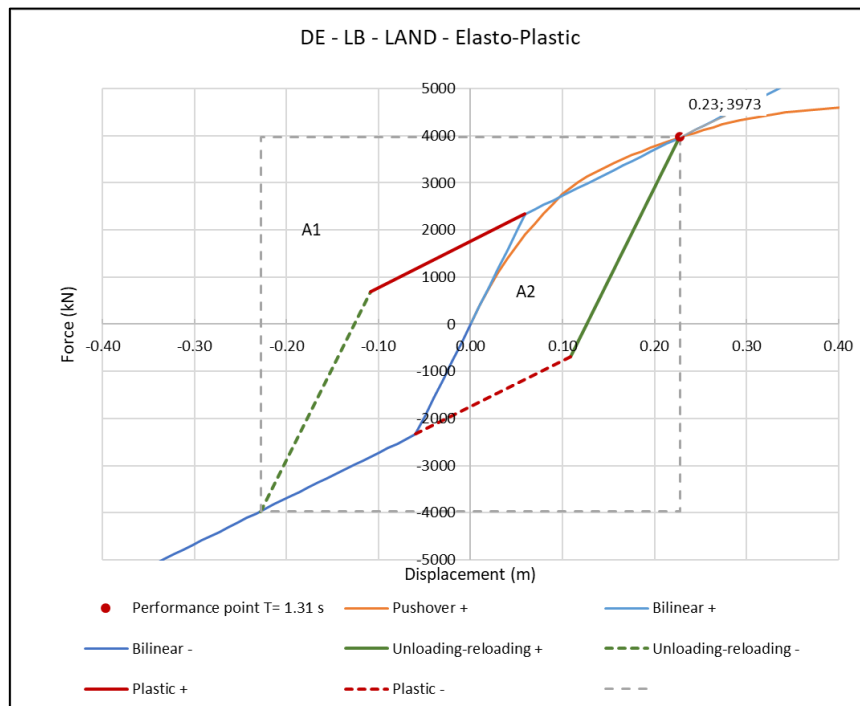
Figure 4.29. Performance point obtained by the substitute structure method for Elasto-Plastic damping. Lower Bound case.

The effective damping is computed as follows:

$$\xi_{eff} = 0,05 + \frac{2}{\pi} \cdot \frac{A_2}{A_1} = 0,05 + \frac{2}{\pi} \cdot 0,2 = 5,0\% + 20,9\% = 25,9\%$$

It is observed that the value obtained from Figure 4.29 is the same than in Table 4.57. This is due to the fact that the equivalent damping expression is purely geometric, and dependent both on ductility μ and the secondary branch relative slope, r.

On the other hand, (Dwairi et al., 2007) modified the elasto-plastic damping expression to match time history analyses, proposing:

$$\xi_{hyst} = C_{EP}\left(\frac{\mu - 1}{\pi\mu}\right)\%$$

$$C_{EP} = 85 + 60\left(1 - T_{eff}\right) \qquad T_{eff} < 1\ s$$

$$C_{EP} = 85 \qquad\qquad\qquad T_{eff} \geq 1\ s$$

(120)

By applying the substitute structure with this expression, the following results are obtained:

Table 4.58. Substitute structure results using a Modified Elasto-Plastic damping (Dwairi et al., 2007) and EC8-04 DSF, for Lower Bound.

	DE-LAND-LB
Δ_d (m)	0.24
F_l (kN)	3999
ξ_{eff} (%)	25.11
k_{eff} (kN/m)	17107
T_{eff} (sec)	1.33
Δ_y (m)	0.06
k_i (kN/m)	39310
r	0.24

Displacement demand is 4% higher than from the purely geometric elasto-plastic damping formulation. Larger differences may be encountered for differently shaped capacity curves.

In conclusion, the elasto-plastic damping expression is significantly dissipative. For r values of the order of 0,25, results are similar than applying POL-B damping. However, even if in this particular case piles are assumed to be made of steel, concrete plugs should be modeled by the Thin Takeda hysteretic model, as largest plastic rotations are located at the top of piles. For pile-supported wharves with welded connections to the deck, where all plasticity occurs on steel (top and in-ground), the elasto-plastic rule may be of better fit. In any case, ASCE 61 does not mention it.

Summary of alternative damping expressions

ASCE 61-14 damping expression adapts to the capacity curve shape of a particular pile supported wharf structure, hence making compatible results from the substitute structure method. In other words, the damping resulting from the iterative process when searching for seismic demand, corresponds to the hysteretic loop, assuming the Thin Takeda model, considered from the performance point. This fact allows the engineer to perform a faster design, as it is not necessary to check systematically if damping is coherent with the assumptions. However, as the expression is based on the Thin Takeda model, it is less dissipative than others, for instance the elasto-plastic model, resulting in higher seismic demands. It is clear that ASCE 61 chooses to stay on the safe side, allowing only the application of the Thin Takeda model to all kinds of pile-supported wharves, independently of constitutive materials.

The elasto-plastic expression obtained by geometrical principles (includes r and μ) is valid from the point of view that, as with ASCE 61, damping results are coherent from the substitute

structure and when plotting the hysteretic loop under the capacity curve. However, it is considerably more dissipative than the Thin Takeda model, therefore seismic demand might be underestimated. In any case, this model could fit structures where all ductility develops on steel members (which is not the case with steel piles with concrete plug connections).

Finally, all expressions that have been calibrated for specific cases, therefore which are only dependent on μ (and not r), might be more exact for those particular cases, but lose its interest when applied to other structures. As an example, POL-B damping applied to the particular case of study has been found incoherent, as original assumptions in POL-B may differ significantly. For this reason, and although POL-B design guidelines are applicable to concrete and steel wharves, it is considered that the damping expression is unconservative for seismic demand. Similarly, other expressions in literature present the same problem.

In brief, the engineer is covered when applying the substitute structure according to ASCE 61, even if in some cases it might be overconservative, since damping results are coherent by definition. However, if alternative expressions are used, it is fundamental that initial assumptions are checked with the corresponding hysteretic loop under the particular capacity curve.

4.3.2. Dynamic Magnification Factor

The substitute structure method allows the engineer to obtain a pure transverse seismic demand. The Dynamic Magnification Factor is defined as a tool to translate pure transverse demand in an equivalent demand that would be obtained by applying seismic load along both horizontal directions, as well as to consider torsional effects of the wharf (see section 2.4).

The main objective of this section is to apply the DMF formulation to the particular case of this study, using the propositions in ASCE 61 and POL-B. As a reminder, the formulation of ASCE 61 is based on an analytical approach, while POL-B introduces expressions which are a result of numerical simulations.

4.3.2.1. DMF in ASCE 61

Although in preliminary design the formulation in ASCE 61 has already been used, here the complete transverse models which are presented in section 4.2.3.1 are employed.

First, it is noted that, according to §3.6.2 of ASCE 61, the ratio between length to width of the wharf must be greater than 3. For the particular studied case, this ratio is $126m/35,98m = 3,5$. Therefore, the application of the DMF approach is permitted.

$$DMF = \sqrt{1 + \left(0,3\left(1 + \frac{20e}{L}\right)\right)^2} \qquad (121)$$

$$e = |x_{CM} - x_{CR}| \qquad (122)$$

$$x_{CR} = \frac{\sum_{i=P1}^{n=P6} k_i x_i}{k_i} \qquad (123)$$

$$k_i = \frac{V_i}{\Delta_i} \qquad (124)$$

Applying previous formulations to capacity curves defined in section 4.2.3.1 (without vertical seismic loading) the DMF is computed for each seismic demands of each performance level, for upper and lower bound cases.

Table 4.59. Dynamic Magnification Factor according to ASCE 61-14 for Lower Bound scenario. Demand for OLE, CLE and DE correspond to section 4.2.3.1.

CASE	x_{CR} (m)	e (m)	Δ (m)	DMF
INITIAL	26.72	8.87	0.02	1.23
OLE	25.32	7.47	0.12	1.20
CLE	23.94	6.09	0.25	1.16
DE	23.20	5.35	0.45	1.14
MAX	22.97	5.12	0.54	1.14

Table 4.60. Dynamic Magnification Factor according to ASCE 61-14 for Upper Bound scenario. Demand for OLE, CLE and DE correspond to section 4.2.3.1.

CASE	x_{CR} (m)	e (m)	Δ (m)	DMF
INITIAL	27.86	10.01	0.02	1.27
OLE	27.03	9.18	0.06	1.24
CLE	26.15	8.30	0.11	1.22
DE	25.29	7.44	0.17	1.20
MAX	24.32	6.47	0.29	1.17
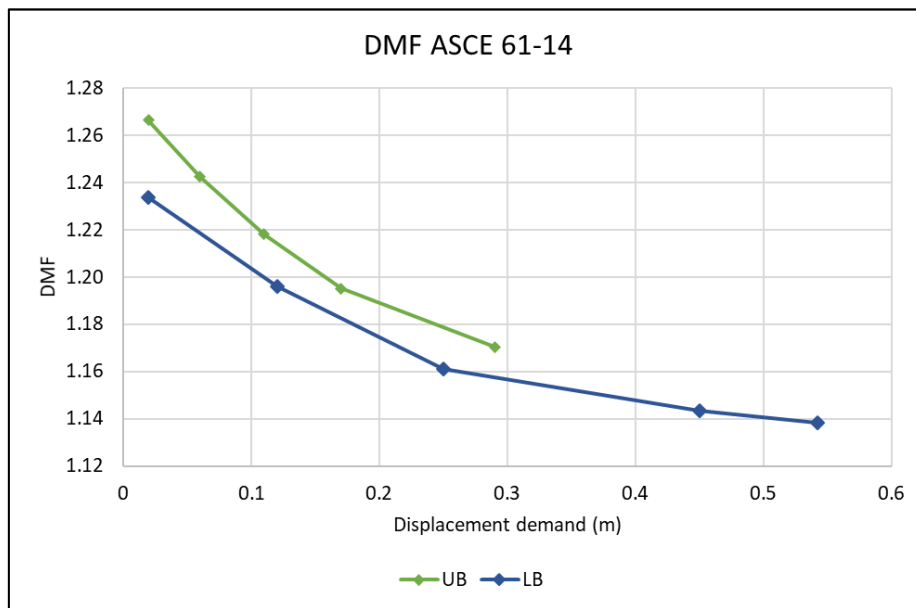
Figure 4.30. Evolution of the Dynamic Magnification Factor in ASCE 61-14 with displacement demand, for upper and lower bound models (without vertical seism nor P-Delta effects).

113

Figure 4.30 represents graphically results from Table 4.59 and Table 4.60 graphically. It is observed that DMF is higher for Upper Bound case than for lower, by approximately 3%. Additionally, it is observed how the DMF decreases with increased displacement demand. The decrement between initial and DMF at critical demand is of the order of 8%. This phenomenon is explained due to the fact that the most rigid piles are the ones to yield first. Thus, as rigidity of critical piles decreases after yielding, the center of rigidity is displaced towards the center of the wharf progressively. These curves are well approximated by cubic polynomials, equations (125) and (126), which may be used to interpolate intermediate seismic demands for the specific studied case.

$$DMF_{LB} = -0.53\Delta^3 + 0.87\Delta^2 - 0.51\Delta + 1.24 \tag{125}$$

$$DMF_{UB} = -0.42\Delta^3 + 0.19\Delta^2 - 0.69\Delta + 1.28 \tag{126}$$

4.3.2.2. DMF in POL-B

When design is based on POL-B guidelines, DMF is obtained according to a classification of the wharf unit (isolated unit or connected to others via shear keys), and according to the aspect ratio of the wharf. For the specific case in this study, the wharf is assumed to be an independent unit (not connected to others). Being L the length of the wharf and B its width, the DMF is directly obtained from the following equations:

OLE

The same expression is used for upper and lower bound situations.

$$DMF = 1,8 - 0,05\frac{L}{B} = 1,62 \tag{127}$$

CLE/DE

For Upper Bound:

$$DMF = 1,65 - 0,05\frac{L}{B} = 1,47 \tag{128}$$

For Lower Bound:

$$DMF = 1,50 - 0,05\frac{L}{B} = 1,32 \tag{129}$$

Note that POL-B does not differentiate between DMF for CLE and for DE, which may be overconservative for design in the most intense seismic scenario.

4.3.2.3. DMF comparison

From the previous two sections, large differences are observed between DMF values from ASCE 61 and those on POL-B, being the second one more conservative. In order to identify those differences, a more in detail analysis of both expressions is performed.

Considering a wharf with the same properties as those on (Blandon, 2007) studies, from which the values of DMF in POL-B are based on, it is possible to properly compare DMF expressions from ASCE 61-14 and POL-B. Those geometrical characteristics were:

- Width (B): 33,5m
- Length (L): from 121m to 243m.
- Center of mass: 16,9m (from landside pile).
- Center of rigidity: 2,1m
- Eccentricity: 14,48m

Figure 4.31 shows the DMF values for a single unit wharf under CLE/DE seismic scenario of width 33m and eccentricity between center of mass and center of rigidity of 14,86m. As it can be observed, ASCE 61-14 DMF is contained between Upper and Lower bound soil cases given by POL-B. Note that, a part from OLE seismic case, the UB soil situation for a single unit wharf is the most severe DMF value given by POL-B. However, as advocated by (Priestley et al., 2007), critical displacements of corner piles could be up to 15% higher than those predicted by ASCE 61-14 expression, under the most unfavorable main seismic loading direction.
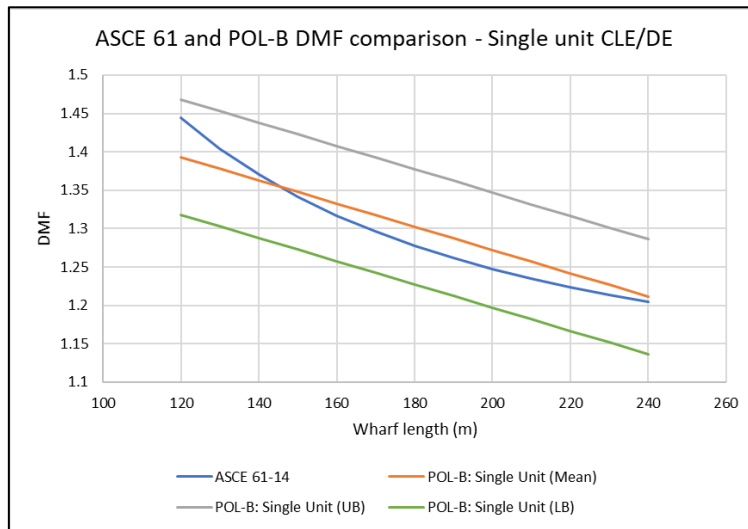
Figure 4.31. DMF values from ASCE 61-14 and POL-B, for a single unit wharf with eccentricity 14,86m and width 33m, for CLE/DE cases.

Figure 4.32 compares, for the same wharf unit as on the previous case, DMF values for OLE given by POL-B, which are the most unfavorable, and modified ASCE 61-14 factors (including additional 15%). It can be observed that these modified factors are similar (less than 5% difference) to OLE DMF values given by POL-B. Thus, for low intensity events, it is possible that ASCE 61-14 underestimates critical displacements. However, although this may have some implications in

terms of excessive damage for serviceability, it should not be an issue for life protection purposes, as DMF values are similar or superior for CLE/DE cases.
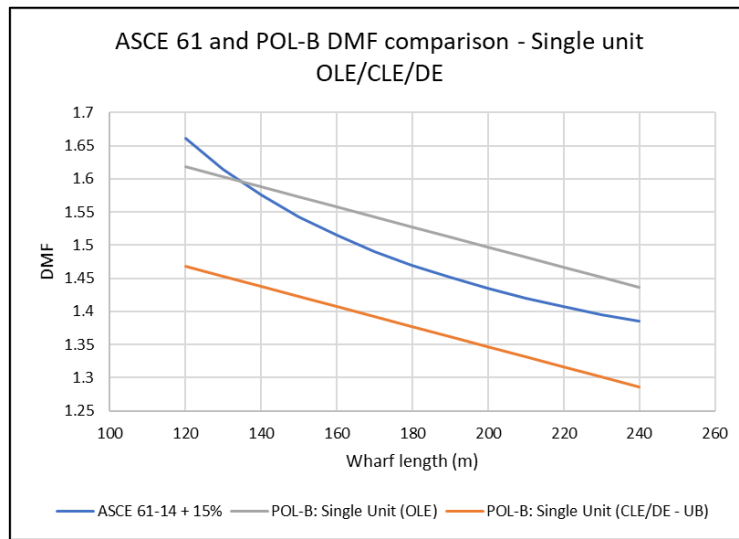
Figure 4.32. DMF values from ASCE 61-14 with additional 15%, and POL-B, for a single unit wharf with eccentricity 14,86m and width 33m.

Next, Figure 4.33 shows DMF values for an external linked wharf unit, with the same dimensions as the previous single unit. ASCE 61-14 seems to be conservative with respect to POL-B expressions, with as much as a 15% difference for a wharf length of 120m with respect to the upper bound soil case.
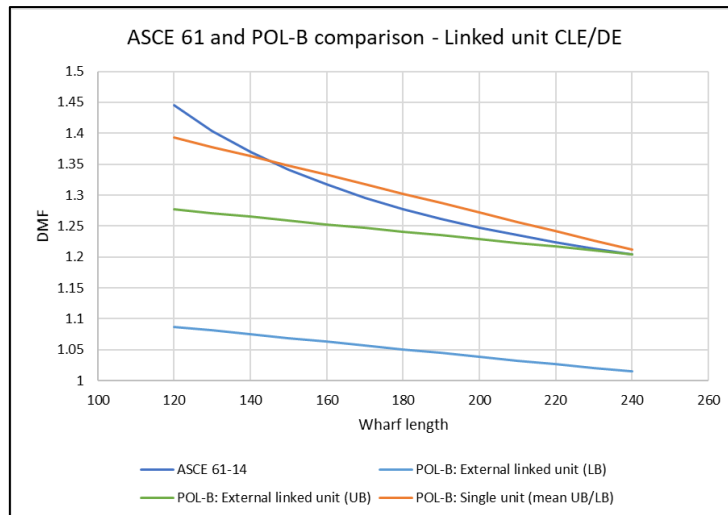
Figure 4.33. DMF values from ASCE 61-14 and POL-B, for an external linked wharf unit with eccentricity 14,86m and width 33m.

To this point, the wharf units that have been analyzed have been consistent with those used in (Blandon, 2007), therefore keeping eccentricity a constant. However, in reality we may encounter wharves on less steep dikes, as in the case of this study, which reduce the eccentricity. Figure 4.34 shows the evolution of DMF using ASCE 61-14 expression for wharves of width 33m and lengths 120m. Eccentricity ranges from zero (center of mass and stiffness are aligned), to 15m (for instance assuming that the center of mass is at the center of the deck, while center of

rigidity is at the landside extreme). Values obtained from POL-B have been plotted in order to provide comparative references. It can be seen that for lower values of eccentricity, POL-B is considerably more conservative.
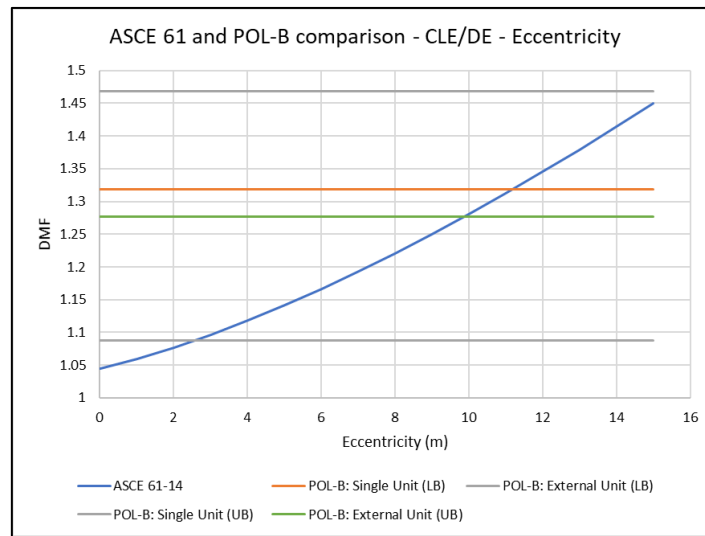
Figure 4.34. DMF values from ASCE 61-14 and POL-B as a function of eccentricity, for a wharf with width 33m and length 120m.

In conclusion, DMF values depend on a significant number of factors, especially center of mass and stiffness eccentricity, wharf length, soil conditions and wharf units considered (single, linked internal or linked external). For wharves within POL-B DMF geometrical conditions and with eccentricity of about 14,8m, these design guidelines may give the best estimate, and with specific expressions for each considered scenario. ASCE 61-14 will be, for the same wharf just mentioned, conservative if the wharf has linked units, and similar to POL-B for a single unit wharf. However, ASCE 61-14 may be unconservative for OLE scenario, but a 15% increase of critical displacement could be used, as suggested by (Priestley et al., 2007). However, for lower values of eccentricity, as in the particular structure considered in this study, POL-B may be overconservative. Also, ASCE 61-14 offers a wider applicability of its expression for the DMF, therefore may be useful for a greater range of designs.

4.3.3. Seismic demand for orthogonal loading

Design has been based on transversal demand and capacity. However, results shall be extrapolated to the real scenario, where seismic loading is simultaneously applied along two orthogonal directions, and to consider torsional effects of the wharf. In this section, results from section 4.3.1.1 to section 4.3.1.3are compared, via the Dynamic Magnification Factor obtained as per ASCE 61, to capacity results from section 4.2.3. According to the fundamental principle of displacement-based design, if demand is smaller than capacity, design is verified.

Without vertical seismic action

Lower Bound conditions result to be more governing than UB; although capacity is higher, demand is also larger. For OLE, loading towards sea governs; capacity was limited by concrete plug damage, where smaller axial load (such as in sea cases) is disadvantageous. On the other

hand, for DE case loading towards land is more limiting, as capacity was governed by damage of the steel pile, where axial load plays a negative role. Note also that for DE case, demand to capacity ratio is close to 100%.

Table 4.61. Demand and capacity - Upper Bound - No Vertical Seism - No Vertical P-Delta

CASE	Δ_d^t (m)	DMF_{ASCE}	Δ_d (m)	Δ_c	Δ_d/Δ_c	Check
OLE - LAND	0.06	1.24	0.07	0.13	59%	Okay
OLE - SEA	0.06	1.24	0.07	0.11	66%	Okay
CLE - LAND	0.11	1.21	0.13	0.25	54%	Okay
CLE- SEA	0.12	1.20	0.14	0.26	56%	Okay
DE - LAND	0.17	1.17	0.20	0.29	68%	Okay
DE - SEA	0.17	1.17	0.20	0.33	61%	Okay

Table 4.62. Demand and capacity - Lower Bound - No Vertical Seism - No Vertical P-Delta

CASE	Δ_d^t (m)	DMF_{ASCE}	Δ_d (m)	Δ_c	Δ_d/Δ_c	Check
OLE - LAND	0.12	1.19	0.14	0.20	73%	Okay
OLE - SEA	0.12	1.19	0.14	0.17	83%	Okay
CLE - LAND	0.25	1.16	0.29	0.48	60%	Okay
CLE- SEA	0.26	1.16	0.30	0.50	60%	Okay
DE - LAND	0.45	1.14	0.51	0.54	95%	Okay
DE - SEA	0.47	1.14	0.53	0.61	88%	Okay

With vertical seismic action

Comparing previous results to capacity curves considering vertical acceleration of the seismic loading, which increases or decreases axial loads on piles, very little differences on demand to capacity ratios are observed.

Table 4.63. Demand and capacity - Upper Bound – With Vertical Seismic – No P-Delta

	CASE	Δ_d^t (m)	DMF_{ASCE}	Δ_d (m)	Δ_c	Δ_d/Δ_c	Check
+ Upwards	OLE - LAND	0.06	1.24	0.07	0.13	59%	Okay
	OLE - SEA	0.06	1.24	0.07	0.11	66%	Okay
	CLE - LAND	0.11	1.21	0.13	0.25	54%	Okay
	CLE- SEA	0.12	1.20	0.14	0.26	56%	Okay
	DE - LAND	0.17	1.17	0.20	0.29	69%	Okay
	DE - SEA	0.17	1.17	0.20	0.33	61%	Okay
- Downwards	OLE - LAND	0.06	1.24	0.07	0.13	59%	Okay
	OLE - SEA	0.06	1.24	0.07	0.11	66%	Okay
	CLE - LAND	0.11	1.21	0.13	0.24	55%	Okay
	CLE- SEA	0.11	1.21	0.13	0.26	51%	Okay
	DE - LAND	0.17	1.17	0.20	0.29	69%	Okay
	DE - SEA	0.17	1.17	0.20	0.33	60%	Okay

Table 4.64. Demand and capacity - Lower Bound – With Vertical Seismic – No P-Delta

	CASE	Δ_d^t (m)	DMF_{ASCE}	Δ_d (m)	Δ_c	Δ_d/Δ_c	Check
+ Upwards	OLE - LAND	0.12	1.19	0.14	0.20	73%	Okay
	OLE - SEA	0.12	1.19	0.14	0.17	83%	Okay
	CLE - LAND	0.25	1.16	0.29	0.48	60%	Okay
	CLE- SEA	0.26	1.16	0.30	0.49	61%	Okay
	DE - LAND	0.44	1.14	0.50	0.54	93%	Okay
	DE - SEA	0.46	1.14	0.52	0.60	88%	Okay
- Downwards	OLE - LAND	0.12	1.19	0.14	0.20	73%	Okay
	OLE - SEA	0.12	1.19	0.14	0.17	85%	Okay
	CLE - LAND	0.25	1.16	0.29	0.48	60%	Okay
	CLE- SEA	0.26	1.16	0.30	0.50	61%	Okay
	DE - LAND	0.46	1.14	0.52	0.55	94%	Okay
	DE - SEA	0.48	1.14	0.55	0.61	89%	Okay

With P-Delta effects and without vertical seismic action

Geometrical non-linearities are found to be irrelevant for UB case. On the other hand, they induce considerable differences in demand to capacity ratios for LB, especially for higher demands (CLE, DE). Indeed, for UB with loading towards land, demand is found to exceed capacity. Although strictly referring to ASCE 61 design would be verified, as P-Delta effects were not required to be included in structural models, this result indicate that when demand is close to capacity the engineer should study their effect, and correct design accordingly.

Table 4.65. Demand and capacity - Upper Bound - No Vertical Seism - With P-Delta

CASE	Δ_d^t (m)	DMF_{ASCE}	Δ_d (m)	Δ_c	Δ_d/Δ_c	Check
OLE - LAND	0.06	1.24	0.07	0.13	59%	Okay
OLE - SEA	0.06	1.24	0.07	0.11	66%	Okay
CLE - LAND	0.11	1.21	0.13	0.25	54%	Okay
CLE- SEA	0.12	1.20	0.14	0.26	56%	Okay
DE - LAND	0.17	1.17	0.20	0.28	70%	Okay
DE - SEA	0.17	1.17	0.20	0.33	61%	Okay

Table 4.66. Demand and capacity - Lower Bound - No Vertical Seism - With P-Delta

CASE	Δ_d^t (m)	DMF_{ASCE}	Δ_d (m)	Δ_c	Δ_d/Δ_c	Check
OLE - LAND	0.12	1.19	0.14	0.20	73%	Okay
OLE - SEA	0.12	1.19	0.14	0.17	83%	Okay
CLE - LAND	0.26	1.16	0.30	0.47	64%	Okay
CLE- SEA	0.27	1.16	0.31	0.50	62%	Okay
DE - LAND	0.5	1.14	0.57	0.54	105%	Fail
DE - SEA	0.51	1.14	0.58	0.61	95%	Okay

Finally, Figure 4.35 and Figure 4.36 summarize all demand and capacity results graphically. Land and Sea sub-cases are not distinguished in these figures. Results are grouped by three categories:

- No vertical seismic acceleration.
- With vertical seismic acceleration.
- P-Delta effects.

Design would be verified if all points fall into the semi-space where demand is lower than capacity (bottom right corner). The closer the points to the line of $\Delta_d = \Delta_c$, the tighter the seismic design. The engineer should however become aware of the main concepts and modeling choices that influence results, many of which covered in this study, to judge up to which point design should be optimized.
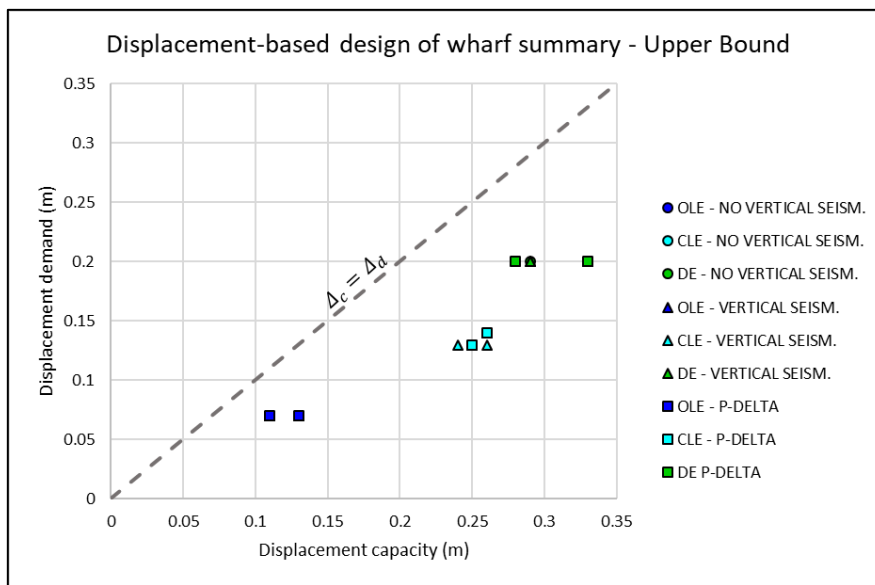

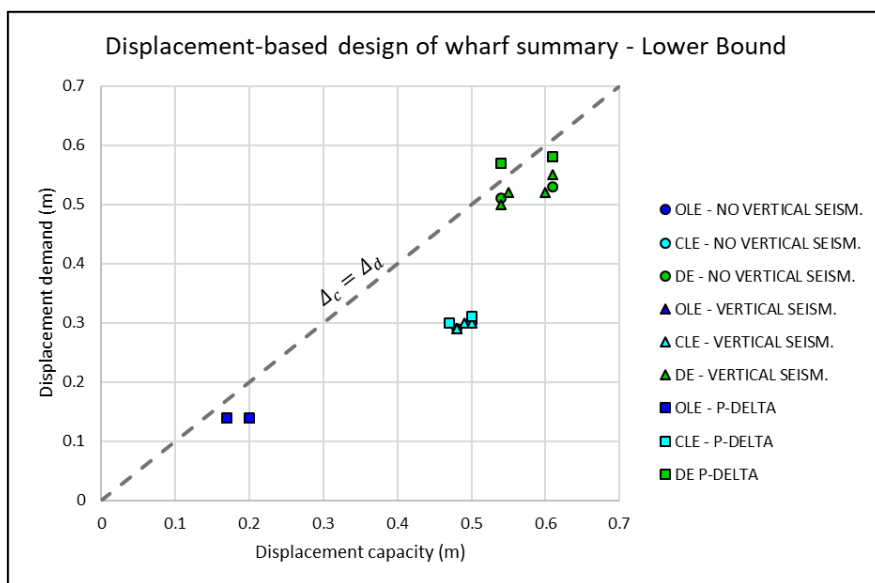*Figure 4.35. Demand and capacity result summary for Upper Bound.*

Figure 4.36. Demand and capacity result summary for Upper Bound.

4.4. TIME-HISTORY ANALYSIS – SUPER PILE MODEL

Seismic design using pure transverse seismic excitation via the substitute structure method, once the methodology is well managed by the engineer, is a convenient approach to obtain seismic demand using a specific design spectrum. However, the approach relies on the DMF formulation, which purely scales transverse demand to simulate simultaneous longitudinal and transversal demand, as well as torsional effects. Furthermore, the DMF approach is restricted to a certain regular type of wharf (for instance an aspect ratio greater than 3 in ASCE 61). On the other hand, design might also aim to analyze the structure for site-specific accelerogram records, apart from using a design acceleration spectrum. Hence, to be able to address these limitations and requirements, or quite simply just as a design verification, a time history analysis might be useful.

However, it has already been discussed that the complete soil-interaction in seismic conditions is extremely complex, and modelling may become overly intricate. A compromise between rich results and modeling simplicity is found in the super-pile model (Blandon, 2007). It shall be noted, however, that the "super-pile" approach is not explicitly mentioned in ASCE 61. In this method, the main hypothesis that are made are:

- The deck acts as a rigid diaphragm.
- The system is independent from vertical excitation.

The first hypothesis is verified in most cases, as the deck in-plane stiffness is much higher than lateral rigidity of piles. This is also checked when analyzing the eigenmodes of the wharf (section 4.1). On the other hand, it has been observed that even if vertical seismic action may induce variations in axial loads in piles, which in turn modifies its capacity, this effect is not very relevant. Therefore, it may be assumed with enough confidence, for verification purposes, that vertical seism does not play a role. As a result, the super-pile model may be applied to the particular case of study.

Although the super-pile model itself is rather simple, it is fully based on the previous analysis of capacity of the wharf. Therefore, this method requires to perform non-static pushover analysis beforehand. To pass from the complete model to the simplified "super-pile" model, the following simplifications are made:

- The 132 piles are substituted by 4 "super-piles", situated at specific locations to constitute a mechanical equivalent system. These super-piles are modeled by non-linear horizontal springs.
- The superstructure is substituted by rigid frames connecting the 4 "super-piles" and defining the contour of the deck.
- Additional nodes are placed at the location of critical piles (corner landside piles) to obtain results.

At the same time, the simplified system has to approximate enough the original mechanical properties of the wharf which are, mainly, its mass, its torsional inertia, its lateral stiffness and resistance, as well as center of mass and rigidity. These global piles must consider the

contribution from all the transversal units of the wharf, which were previously analyzed. For the assumed design, the number of transversal units is $N = 22$.

The wharf is assumed to be longitudinally symmetric, therefore only two "Super-Piles" are distinguished. The notation of S represents the "Super-Pile" (S from Sea) grouping the first three piles (P1, P2 and P3), and L the one representing piles P4, P5 and P6 (L from Land), from all the transverse units in the wharf.

Similarly to the rest of the study, upper and lower bound soil conditions are distinguished. As the mechanical properties are different for both cases (lateral resistance, center of rigidity), two distinct "super-pile" models are developed.

Super-Pile locations

Longitudinally, the position of the "Super-Piles" is chosen such that the mass moment of inertia of the deck is unchanged. By assuming that the mass of the beams and the slab of the deck is uniformly distributed along all its surface, the concept of radius of gyration is employed. Considering the superstructure as a rectangular rigid solid with uniform mass, the radius of gyration is defined as the geometrical locus where if all mass is concentrated at, the moment of inertia with respect to the center of mass is unchanged. According to (Blandon, 2007), the center of gyration of the deck is located longitudinally at a distance from the center equal to y_G:

$$y_G = \frac{L}{2\sqrt{3}} \tag{130}$$

Where L is the length of the wharf, 126m. Therefore, "Super-Piles" will be situated longitudinally at 36,37m from the center of the wharf.

Transversally, the piles are located according to the center of rigidity of each group of piles. According to (Priestley et al., 2007), the evaluation of the center of rigidity of each super-pile should be obtained for initial elastic response, since it will follow the onset of inelasticity. Thus, the transversal position of the sea "Super-Pile", x_S, and the of the land "Super-Pile", x_L, then:

$$x_S = \frac{\sum_{i=P1}^{P3} n_i F_{L_i} x_i}{\sum_{i=P1}^{P3} n_i x_i} \tag{131}$$

$$x_L = \frac{\sum_{i=P4}^{P6} n_i F_{L_i} x_i}{\sum_{i=P4}^{P6} n_i x_i} \tag{132}$$

Where n_i is the number of piles per transverse unit at the row i, and x_i the transversal position of that row. For the particular case of this study, there is one pile per row at each transverse unit. F_{L_i} refers to the lateral strength of each pile, which is obtained from the individual pushover analyses from section 4.2.1.

Table 4.67. Transversal position of the "super-piles", with respect to the sea cantilever.

	x_S (m)	x_L (m)
UB	11.65	30.40
LB	11.47	29.77

Stiffness properties

The springs that model the super-pile lateral resistance have a stiffness that is computed according to the grouped force-displacement relations from individual pile pushover analyses.

$$F_L^{1-3} = \frac{1}{2} \cdot N \cdot \sum_{i=P1}^{P3} n_i \cdot F_{L_i} \tag{133}$$

$$F_L^{4-6} = \frac{1}{2} \cdot N \cdot \sum_{i=P4}^{P6} n_i \cdot F_{L_i} \tag{134}$$
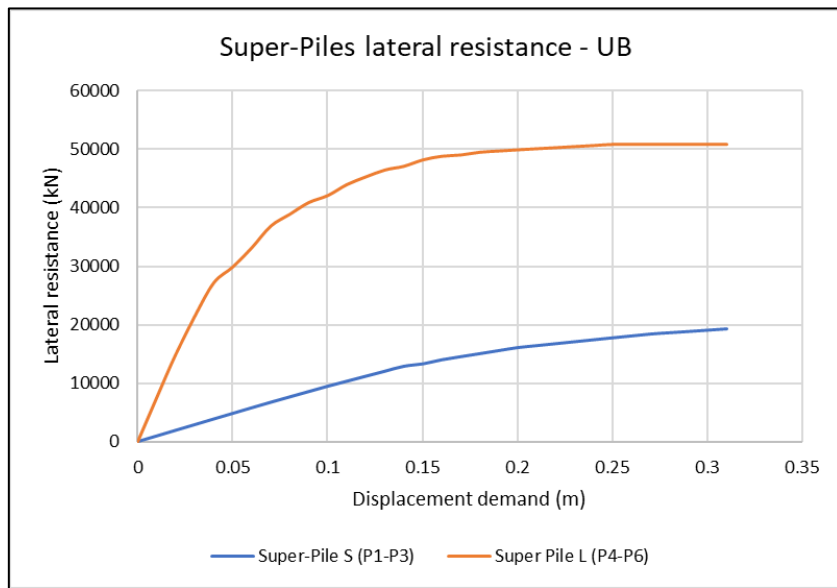
Figure 4.37. Super-Pile lateral resistance for Upper Bound conditions.
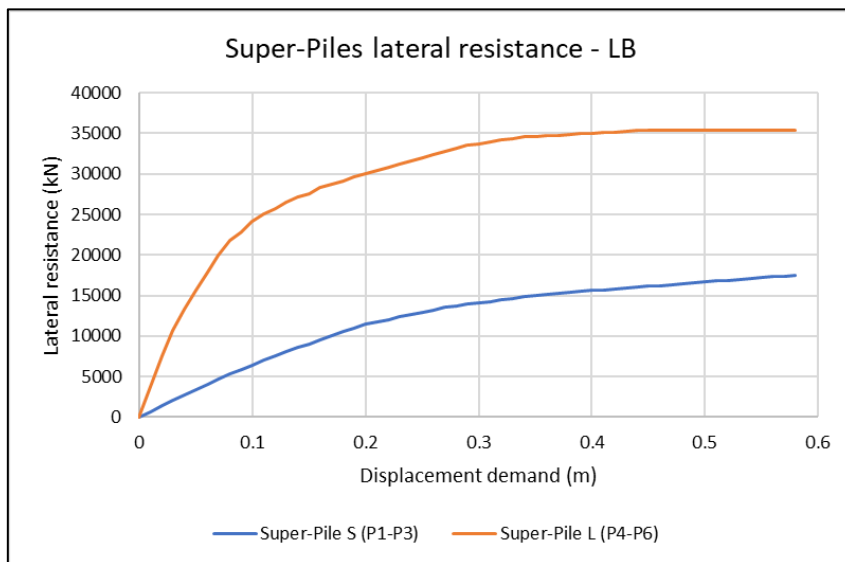
Figure 4.38. Super-Pile lateral resistance for Lower Bound conditions.

Then, the stiffness of each pile is computed as:

$$k_{1-3} = \frac{F_L^{1-3}}{\Delta} \tag{135}$$

$$k_{4-6} = \frac{F_L^{4-6}}{\Delta} \tag{136}$$

Both the lateral resistance of piles and the stiffness is obtained for a specific demand, Δ.

Figure 4.39. Super-Pile stiffness for Upper Bound condition.

Figure 4.40. Super-Pile stiffness for Upper Bound condition.

Springs are modeled as non-linear links for time-history analyses. However, for linear cases such as modal analysis, the initial elastic stiffness is assigned to the spring.

124

Hysteretic properties of Super-Piles

In order to represent the dissipative properties of the grouped piles, an appropriate hysteretic behavior must be given to the non-linear springs used to model "super-piles".

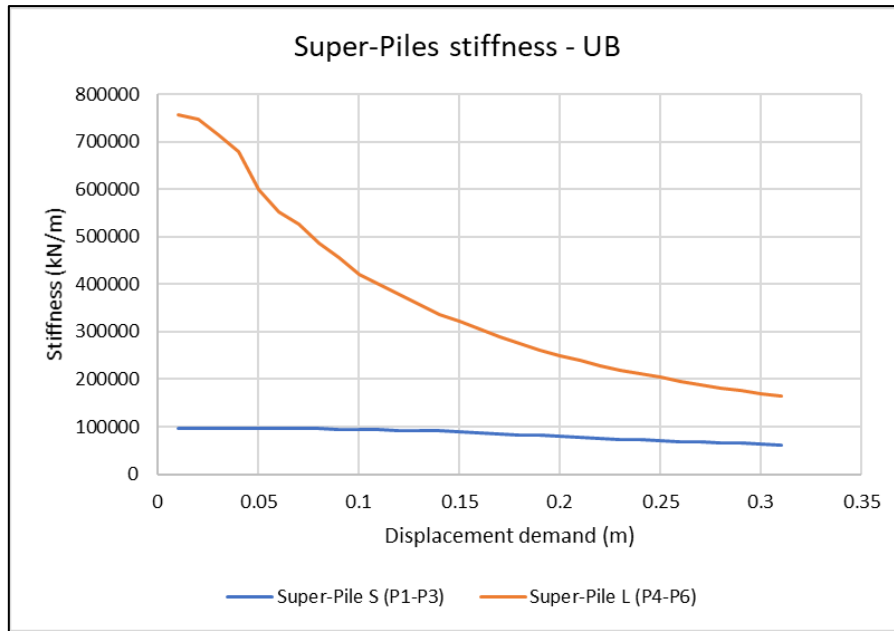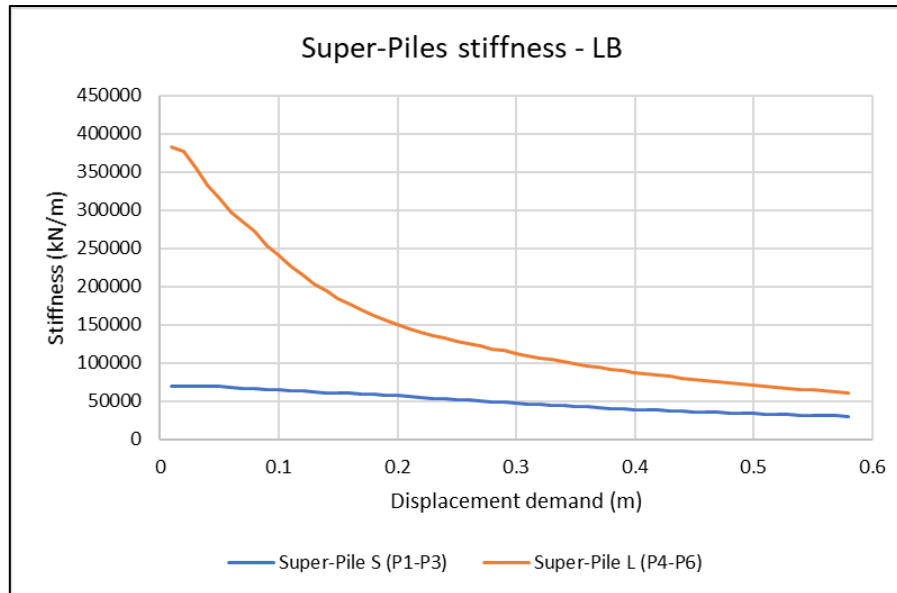However, due to limitations of the analysis software used in this study, SAP2000, the exact hysteretic rule proposed by ASCE 61, which is based on the Thin Takeda model with parameters with $\alpha = 0.5$ and $\beta = 0$, is not available. On the other hand, SAP2000 includes a particular version of the Takeda model, which uses the parameters $\alpha = \beta = 0$, which is the closest to the one proposed in ASCE 61. This hysteretic model is more dissipative than the one in ASCE 61, therefore previous transverse demand results are not comparable to the ones obtained in this section, due to limitations of analysis software.

With the objective of being able to compare purely transverse demand from the substitute structure method to results from the Super-Pile model, an equivalent viscous damping is computed to the Takeda hysteretic rule in SAP2000 (deduced from section 2.3.1). With it, the substitute structure method is used again to obtain purely transverse demand and, through the DMF, total demand is obtained.

$$\xi_{eff,SAP} = 0.05 + \frac{1}{\pi}\left(1 - \frac{1 + r \cdot (\mu - 1)}{\mu}\right) \tag{137}$$

Mass properties

The seismic mass of the whole wharf is distributed in four nodes. Two conditions must be verified:

- The total mass of the system must be equal than the original.
- The center of mass must be equal than the original.
- The mass moment of inertia must be equal than the original.

Being m_s the seismic mass of an individual transverse unit, the mass of each pile must verify:

$$2 \cdot M_S + 2 \cdot M_L = n \cdot m_s \tag{138}$$

Where M_S and M_L are the masses to be assigned to the nodes where the "Super-Piles" are placed. Additionally, the center of mass shall keep constant, therefore:

$$\frac{M_S \cdot x_S + M_L \cdot x_L}{M_S + M_L} = x_{CM} \tag{139}$$

From equations (138) and (139), transversal position of the "super-piles" is determined.

$$M_L = \frac{n \cdot m_s}{2} \cdot \frac{x_{CM} - x_S}{x_L - x_S} \tag{140}$$

Tabla 1. "Super-Pile" masses.

	M_S (ton)	M_L (ton)
UB	5617.3	2775.0
LB	5466.1	2926.3

Assembly of the "Super-Pile" models

With all this in consideration, the models are assembled in SAP2000. Super piles are linked to additional nodes that represent the position of critical piles. This link is performed by rigid frames.
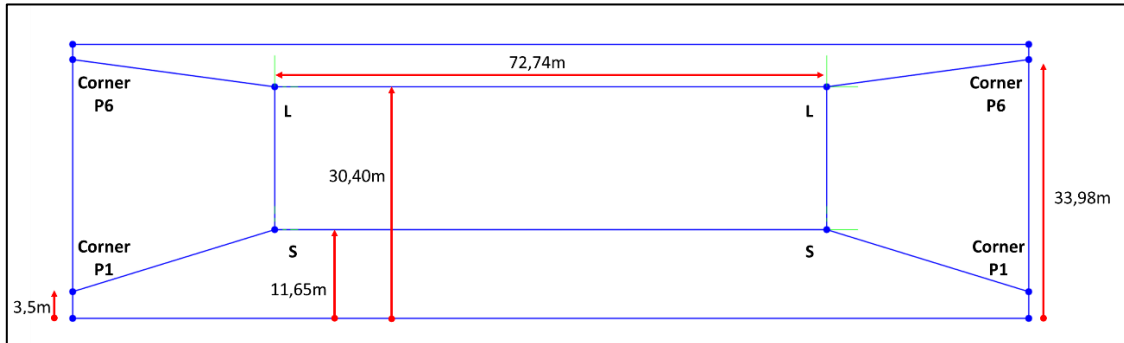
Figure 4.41. Super-Pile Model - UB
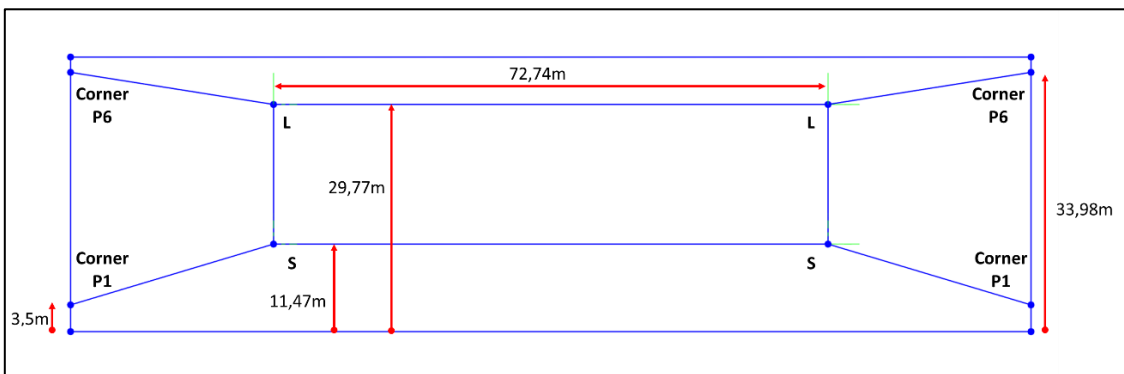
Figure 4.42. Super-Pile Model – LB

4.4.3. Modal analysis

The purpose of this section is to verify the modal behavior of the "Super-Pile" model, and compare it to the complete 3D model. For this linear case, the springs in the model are taken with its linear initial stiffnesses.

Table 4.68 show that the model behaves in a tri-modal fashion, as the original three-dimensional model. The first and third modes are torsional, while the second mode is purely transversal. Table 4.70 compares structural periods from the complete model and from the "Super-Pile" model. Periods from both models are observed to differ by less than 3%. Therefore, the "Super-Pile" model seems to well represent the dynamic behavior of the super-structure.

Table 4.68. Main modes of vibration of the wharf (sea side to the left), for Lower Bound, using the Super-Pile model.
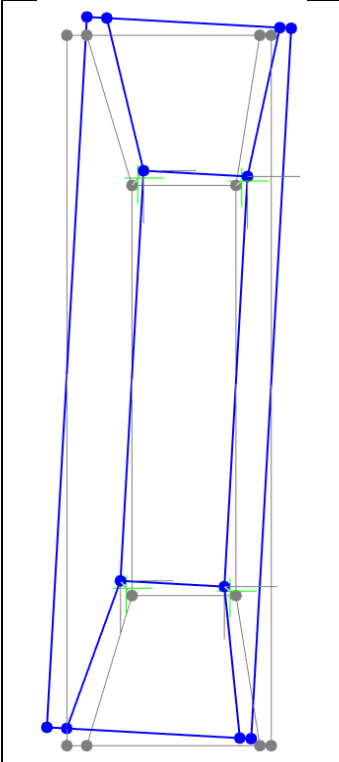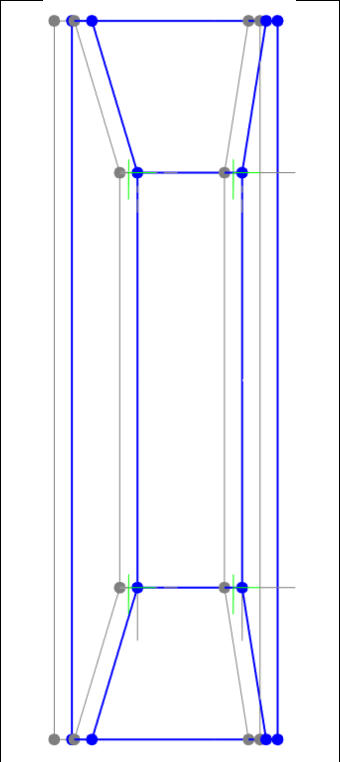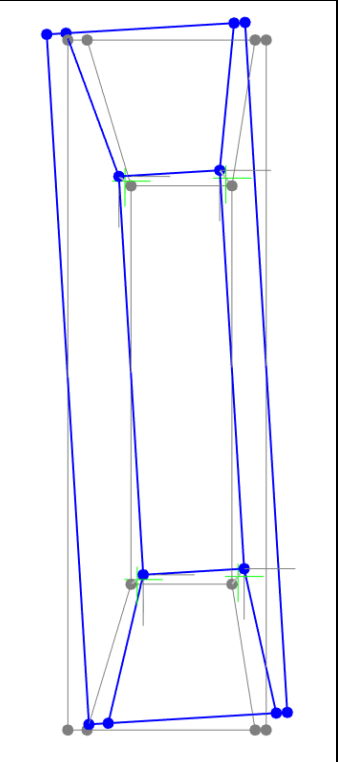
MODE 1	MODE 2	MODE 3
T = 1.01 sec	T = 0.88 sec	T = 0.78 sec
PFx = 0 kNm	PFx = 130 kNm	PFx = 0 kNm
PFy = -95 kNm	PFy = 0 kNm	PFy = -88 kNm

Table 4.69. Main modes of vibration of the wharf (sea side to the left), for Upper Bound, using the Super-Pile model.

MODE 1	MODE 2	MODE 3
T = 0.74 sec	T = 0.64 sec	T = 0.56 sec
PFx = 0 kNm	PFx = 130 kNm	PFx = 0 kNm
PFy = -95 kNm	PFy = 0 kNm	PFy = -88 kNm

Table 4.70. Comparison of the vibration modes of the wharf using the complete 3D model and de Super-Pile

MODES	UPPER BOUND			LOWER BOUND		
	ORIGINAL (sec)	SUPERPILE (sec)	DIFFERENCE	ORIGINAL (sec)	SUPERPILE (sec)	DIFFERENCE
MODE 1	0.76	0.74	-3%	1.02	1.01	-1%
MODE 2	0.65	0.64	-2%	0.89	0.88	-1%
MODE 3	0.56	0.56	0%	0.79	0.78	-1%

127

4.4.4. Non-linear time history analysis

The purpose of this section is to compare displacement demand from the time history model using the simplified Super-Pile approach to results from the substitute structure method. Additionally, the effect of simultaneous longitudinal and transversal seismic excitation is compared to the approach of Dynamic Magnification Factor.

Firstly, transverse demand is obtained by the substitute structure method using the equivalent viscous damping that fits SAP2000 modeling.

Table 4.71. Transverse seismic demand with SAP2000 Takeda equivalent viscous damping, for DE.

	DE-LAND-UB	DE-LAND-LB
Δ_d (m)	0.10	0.25
F_l (kN)	4783	4121
ξ_{eff} (%)	16.59	24.10
k_{eff} (kN/m)	49301	16420
T_{eff} (sec)	0.78	1.35
Δ_y (m)	0.04	0.06
k_i (kN/m)	77532	41064
r	0.39	0.22

Six non-linear time history analyses are considered for UB and for LB, three for purely transversal seismic loading, and three for simultaneous longitudinal and transversal. These records are provided in Annex 7. For the latter cases, the 100% of seismic intensity is applied on the longitudinal direction, while 30% transversally.

Elastic damping of 5% is considered. Rayleigh damping is defined for the first and third modes, using tangent stiffness. However, the fraction of critical damping assigned to the first mode is reduced in order to avoid overestimating elastic damping when inelasticity is engaged (section 2.5). The damping associated to the third mode is taken as 5% of critical damping. Based on equation (35) and results from Table 4.71, the fraction of critical damping assigned to the first mode on both models is:

$$\xi_{UB}^* = 0{,}75 \times 5\% = 3{,}75\% \tag{141}$$

$$\xi_{LB}^* = 0{,}48 \times 5\% = 2{,}4\% \tag{142}$$

4.4.4.1. Purely transverse demand

For these analyses, component H2 of accelerograms is applied on the transversal direction. Next figures show, as an example, displacement demand over time using T1 histogram, applying 100% of intensity. Peak results are shown in Table 4.72.
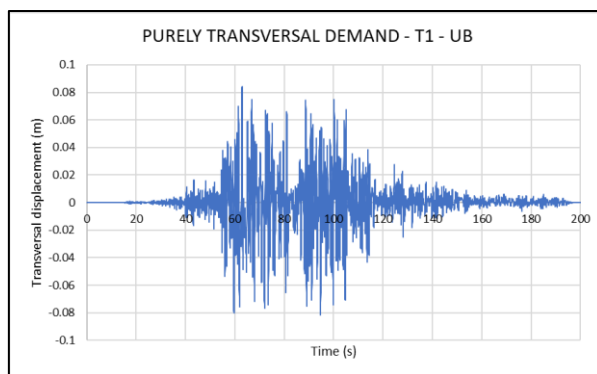
Figure 4.43. Displacement demand results according to time history analysis with the Super-Pile model; T1 histogram, transversal seismic load, component H2. Upper Bound soil case.

Figure 4.44. Displacement demand results according to time history analysis with the Super-Pile model; T1 histogram, transversal seismic load, component H2. Lower Bound soil case.

Since three histograms are considered, according to ASCE 61, envelope of results should be considered. Next table shows peak demand for the three accelerograms.

Table 4.72. Peak displacement demand for purely transverse seismic loading using Super-Pile model and time history analysis.

Histogram	Peak demand – UB (m)	Peak demand – LB (m)
T1	0.08	0.24
T2	0.10	0.22
T3	0.10	0.26
Envelope	0.10	0.26
Mean	0.10	0.24
σ	0.01	0.02

Results from Table 4.72 are consistent with results obtained via the substitute structure method, with differences of less than 5%.

4.4.4.2. Simultaneous longitudinal and transverse demand

Next three analyses consist of simultaneous 100% of component H1 along the longitudinal direction, and 30% of component H2 transversally, for the three accelerograms.
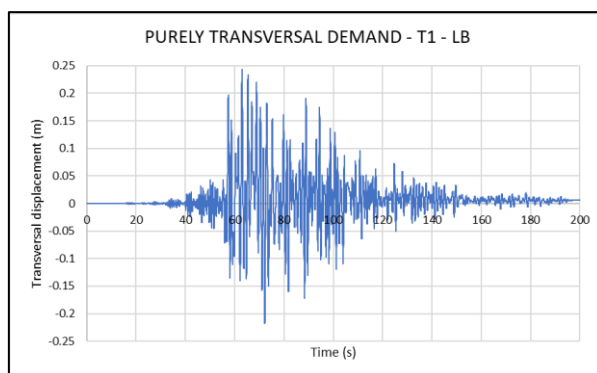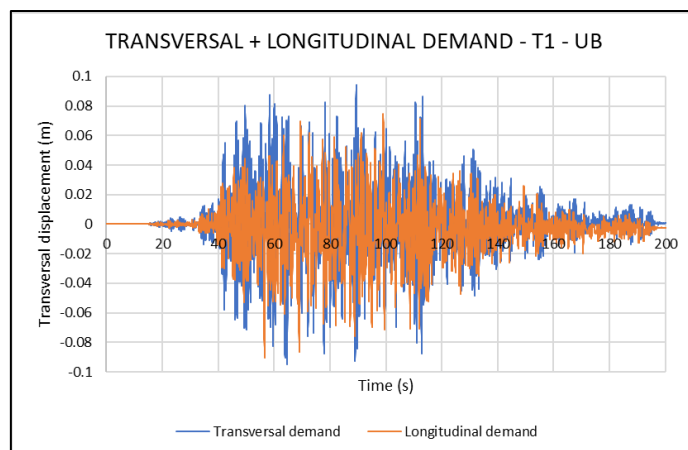
129

Figure 4.45. Displacement demand results according to time history analysis with the Super-Pile model; T1 histogram, 100% longitudinal H1, 30% transversal H2. Upper Bound case.
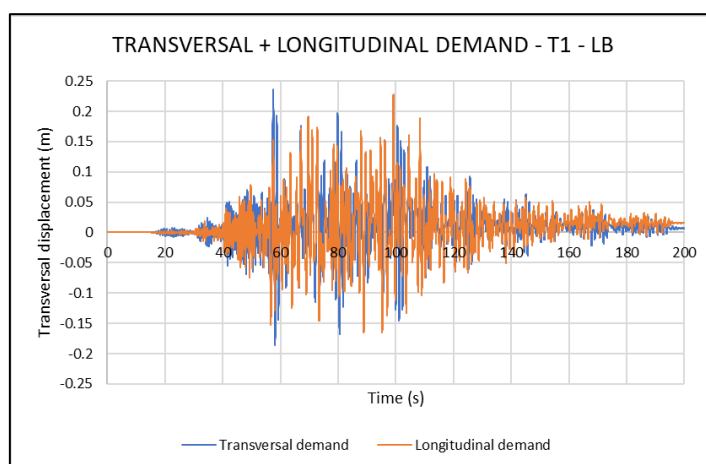

Figure 4.46. Displacement demand results according to time history analysis with the Super-Pile model; T1 histogram, 100% longitudinal H1, 30% transversal H2. Lower Bound case.

Table 4.73 and Table 4.74 summarize demand results from time history analyses. Maximum DMF, computed from time history analyses as the ratio between peak total demand and peak purely transversal demand, is 1,26 for Upper Bound conditions and 1,15 for Lower Bound (referred as DMF_{TH}). However, it is noted that variability is high between different histograms. Maximum ASCE 61 DMF value for UB is found to be inferior to results from time histories, while slightly superior for LB case.

Table 4.73. Peak total displacement demand and DMF using Super-Pile model and time history analysis, for UB.

Histogram	Peak transversal demand (m)	Peak total demand (m)	DMF_{TH}	DMF_{ASCE}
T1	0.08	0.11	1.26	1.23
T2	0.10	0.11	1.11	1.21
T3	0.10	0.11	1.04	1.21
Envelope	0.10	0.11	1.26	1.23
Mean	0.10	0.11	1.14	1.22
σ	0.01	0.00	0.11	0.01

Table 4.74. Peak total displacement demand and DMF using Super-Pile model and time history analysis, for LB.

Histogram	Peak transversal demand (m)	Peak total demand (m)	DMF_{TH}	DMF_{ASCE}
T1	0.24	0.28	1.15	1.16
T2	0.22	0.24	1.11	1.16
T3	0.26	0.26	1.03	1.16
Envelope	0.26	0.28	1.15	1.16
Mean	0.24	0.26	1.10	1.16
σ	0.02	0.02	0.06	0.00

In summary, the "Super-Pile" model is an interesting way of reducing drastically the numerical complexity of a multidirectional model, although its applicability to wharf design for engineering practice may still be limited. Even if the model is small in terms of elements, the complexity behind a non-linear time history analysis still exists. Dependence on input accelerograms, elastic and hysteretic damping definition or the disposition of the equivalent links defining the super-piles is relevant, and therefore results might suffer significant variability. Peer review, as well as performing complementary analyses such as the substitute structure method, are certainly crucial.

4.5. KINEMATIC EFFECTS

This section aims to apply key ideas from literature regarding effects of lateral spreading of soils and its interaction with deep foundations (section 2.6). As a reminder, ASCE 61, although mentioning that these effects shall be considered in design, provides no guidance on this aspect. All analyses in this section use characteristic p-y springs, without any upper or lower bound modification coefficients.

4.5.3. Soil displacement field input

A potential lateral spreading of the soil above the clay layer is considered as a consequence of DE scenario. A simplified displacement field is assumed, considering that failure line passes through the weak clay layer, and all failure wedge moves as block. Below the clay, sand is assumed not to move. The magnitude of the lateral spreading is assumed to be of 7cm towards the sea purely horizontally, from a geotechnical analysis not in scope. Finally, the clay layer is considered to act as a transition zone, in line with POL-B §2.9.
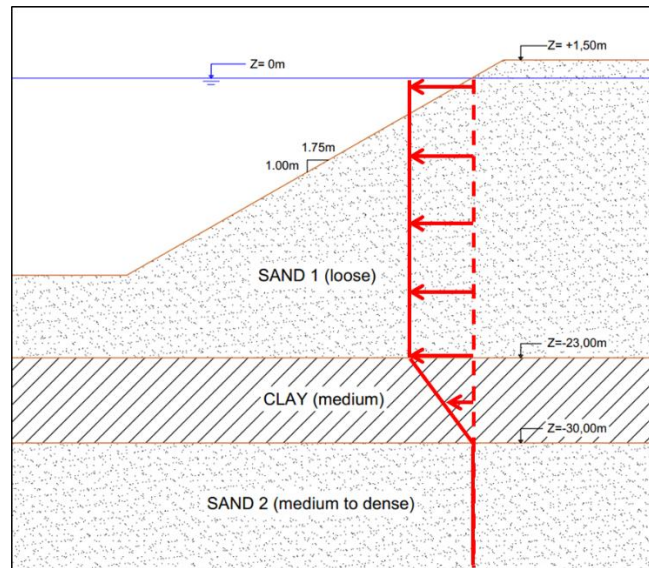
Figure 4.47. Simplified lateral spreading displacement field shape.

4.5.4. Displacement vs pressure methods

As a recap, the two methods found in literature to apply kinematic forces on piles are:

- Displacement method: kinematic forces applied through p-y springs, where a displacement is applied to the node representing the soil, and the resulting force is obtained from the relative movement between the pile node and the soil node.
- Pressure method: forces are directly applied on pile nodes, corresponding to the maximum strength of the associated p-y spring.

Figure 4.48 shows the bending moments law shapes resulting from both methods. Both analyses are based on the 7cm lateral spreading, with a transition zone of 7m. From the models, it is observed that in the displacement method, bending moments are concentrated on the failure zone. On the other hand, with the pressure method, bending moments are distributed from the failure line up to the deck. The fundamental difference between both methods is that with the displacement method, the sliding block of soil is assumed to keep its resistance, while with the pressure method all soil is supposed to yield. No numerical results are provided for the pressure method, as the non-linear analysis is non-convergent. Indeed, structurally speaking, the pressure method is equivalent to considering piles with a very large free height, as cantilevers, with distributed horizontal loads. Being the top rotation of pile restricted by the deck, bending moments appear also in the connection to the superstructure. Therefore, hinges will tend to appear at the failure line and also at the top of piles, interfering with the inertial problem. Additionally, Figure 4.49 represents the shear force laws obtained by both methods. Again, shear concentrates above and below the clay layer for the displacement method, while peaking at the inferior clay-sand interface for the pressure method. Due to relative sliding layers of soil, shear forces are very relevant in kinematic forces, and therefore it is possible that design is governed by them when considering lateral spreading.
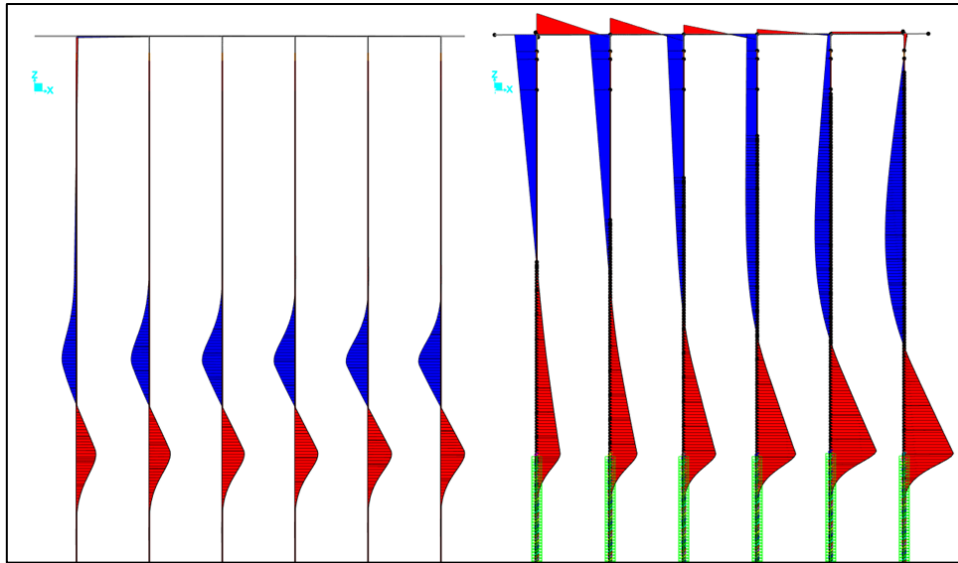
Figure 4.48. Bending moment laws distribution for displacement method on the left, pressure method on the right (linear case). Magnitude of laws is not relevant and not in scale.
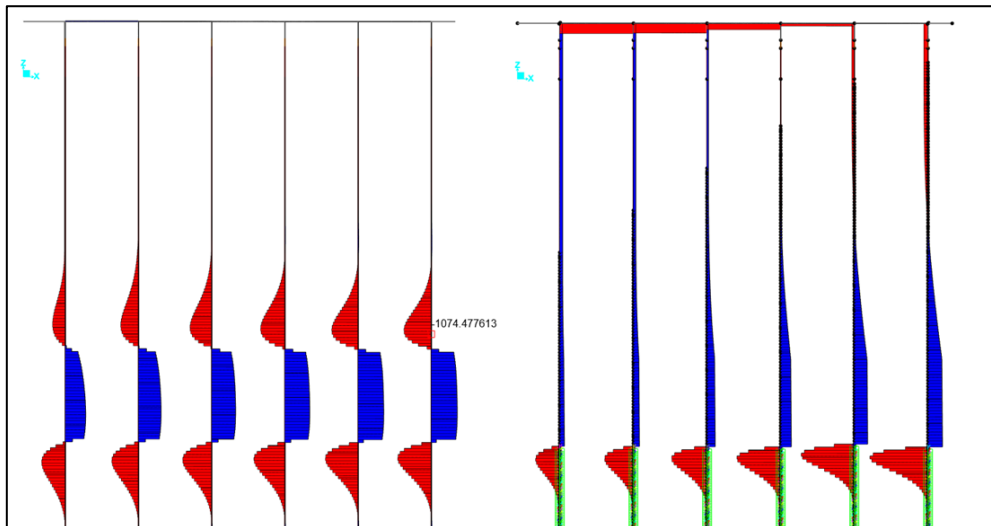

Figure 4.49. Shear force laws distribution for displacement method on the left, pressure method on the right (linear case). Magnitude of laws is not relevant and not in scale.

In summary, both methods are convenient and simple to apply to structural models. However, they are extremely dependent on strong geotechnical assumptions. Therefore, both the geotechnical and the structural engineers should closely collaborate in order to develop a coherent model which well represents the reality of the project. The resisting capacity of lateral spreading block is key to be able to apply the displacement method. A feasible variation would be to reduce resistant properties of spreading soil springs. On the other hand, if the pressure method is considered, it may be impractical to perform seismic design, and other approaches could be followed, as for instance land improvement methods to avoid lateral spreading in the first place.

4.5.5. Variation of p-y density

It is of interest to assess the influence of distribution of p-y springs along piles. Previously in this study, springs where separated 1m, which is sufficient to represent well the bending laws due to inertial effects. However, the appearance of a soil failure line introduces an abrupt discontinuity in the model, and results may be sensible to the discretization. Three cases are considered:

- 1m separation ($\sim 1D$).
- 0,5m separation ($\sim 0,5D$).
- 0,25m separation ($\sim 0,25D$).

Considering the 7m width transition zone (thickness of the clay layer), the displacement method is applied. A non-linear analysis is performed for each separation. Resulting bending moment laws are shown below.
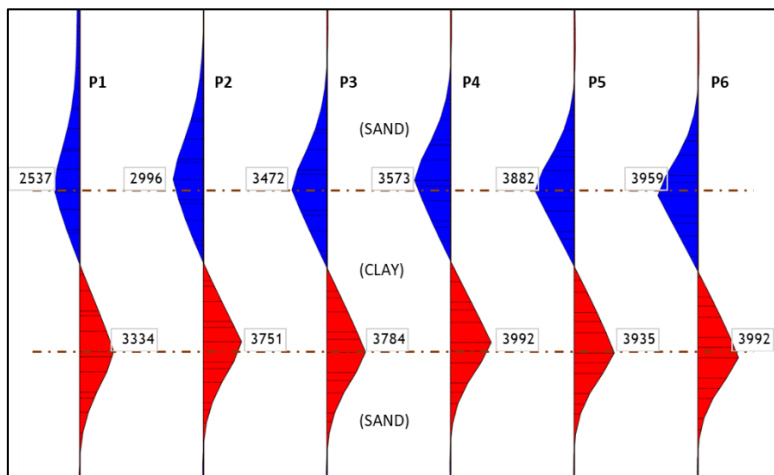

Figure 4.50. Bending moments due to kinematic forces with p-y springs separated 1m.
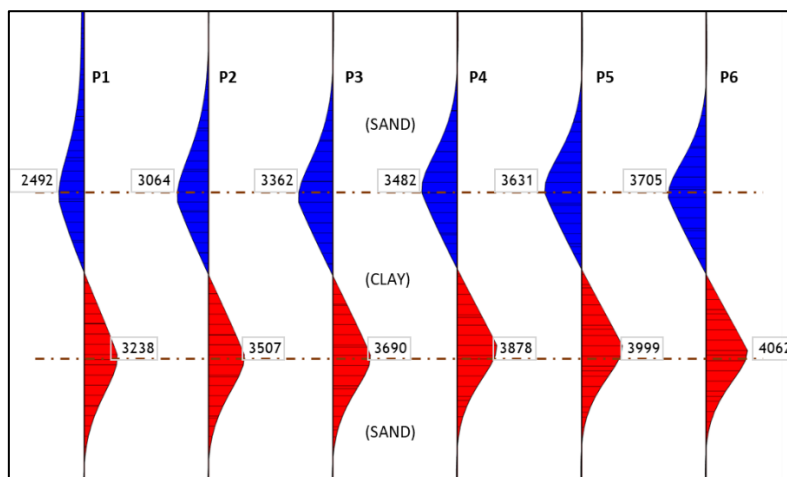

Figure 4.51. Bending moments due to kinematic forces with p-y springs separated 0,5m.
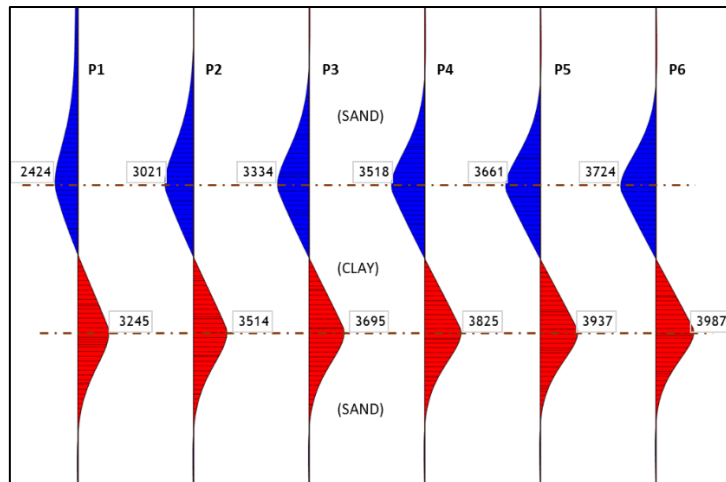
Figure 4.52. Bending moments due to kinematic forces with p-y springs separated 0,25m.

It is observed that with higher density of p-y springs, bending laws are smoothed, and therefore results may be more accurate. Additionally, it is found that even if displacements are applied in every spring above the clay layer, bending moments are concentrated at the interfaces between clay and sand. Plus, the influence of p-y clay springs seems to be small, since bending law is linear along the transition zone. This is due to the fact that strength of p-y clay springs is an order of magnitude inferior to those of sand. A similar situation would be found in a liquefied sand layer, where resistance tends to dissipate.

Figure 4.53. Bending moments at the top sand-clay interface, for each pile, and for three p-y springs densities.

Figure 4.54. Bending moments at the bottom sand-clay interface, for each pile, and for three p-y springs densities.

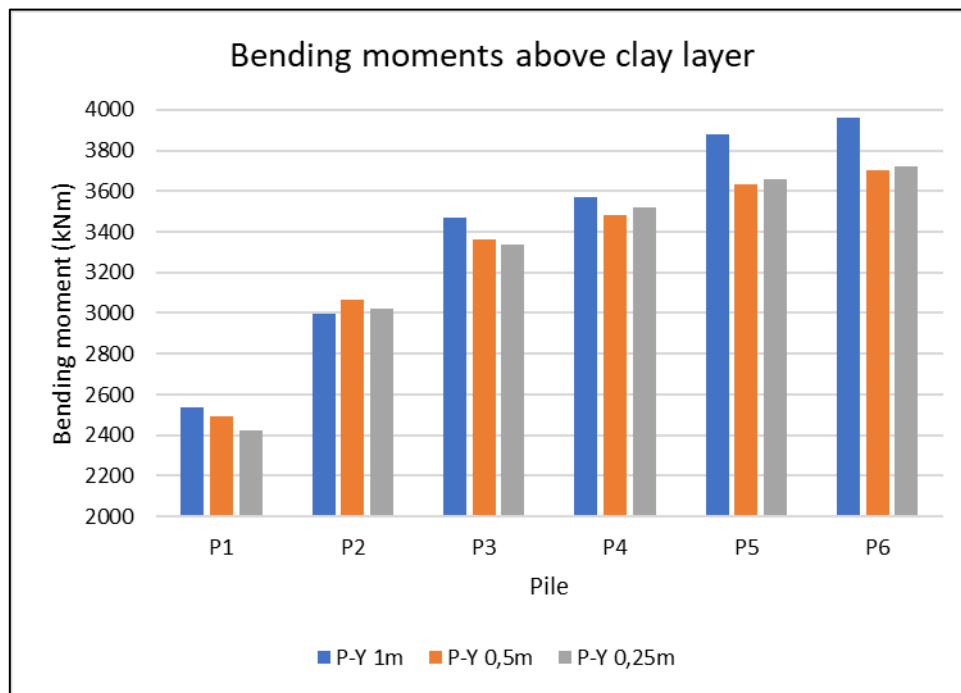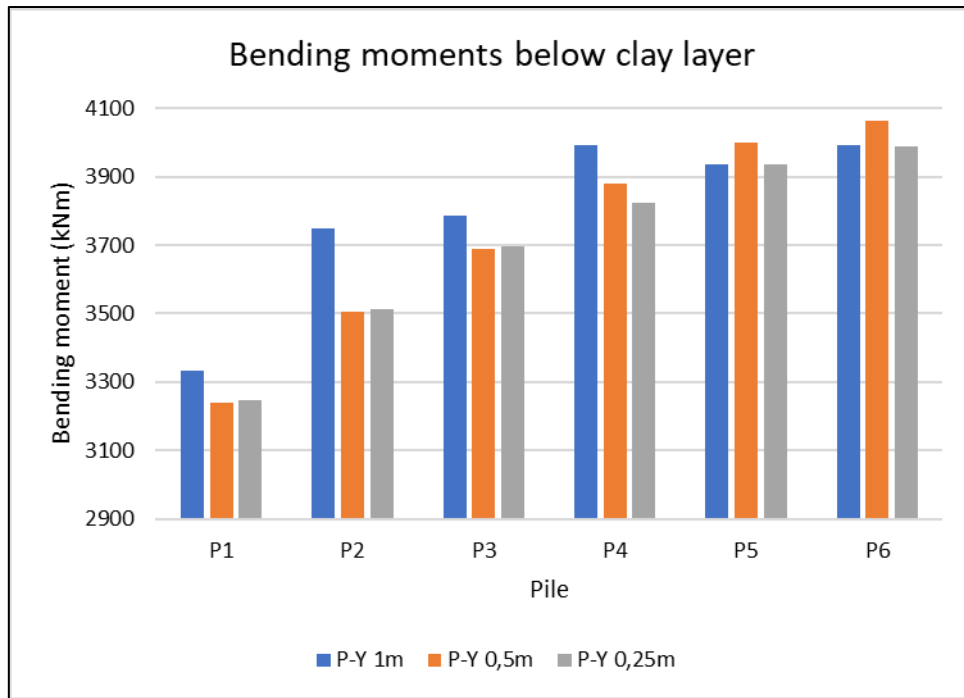Figure 4.53 and Figure 4.54 compare the three densities for each pile. On the one hand, it is observed that when larger separation between p-y springs is applied to the model, larger bending moments are found. By refining the meshing of soil springs, the bending law is smoother and results are found to reduce by up to 6%. Additionally, it is found that bending moments are higher for land-side piles than on sea side. This is due to the fact that, as a consequence of dike slope, the sand-clay interference is deeper at P6 than at P1. Accordingly, P6 springs at that depth are stiffer and with higher strength than those on the sea side.

4.5.6. Variation of transition zone length

Although the failure line might be distributed on the width of the weak layer, it is not guaranteed that the whole layer is mobilized. Therefore, the influence of the length of the transition zone is analyzed by applying the displacement method. Four cases are considered: the full width of clay (7m) of transition between the 7cm of displacement above and 0cm below clay, a 4m transition, a 1m transition and 0,5m transition, as illustrated in Figure 4.55.
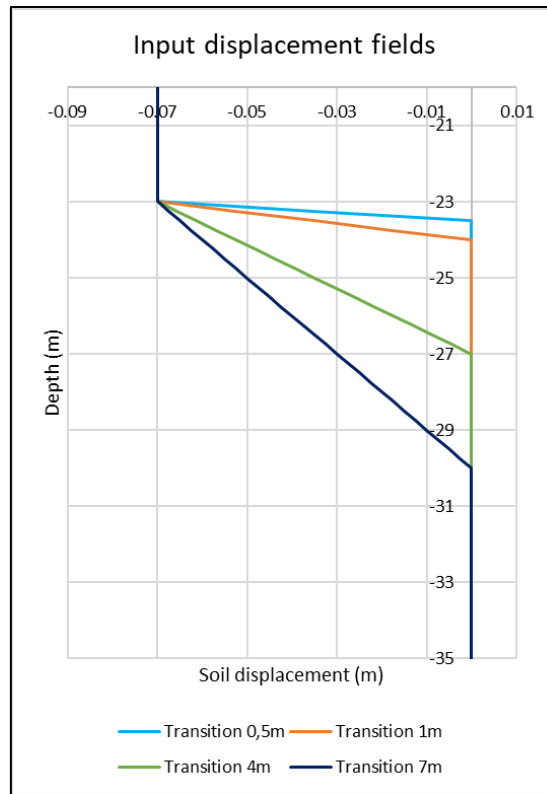
Figure 4.55. Model input displacement fields with different transition lengths.

Figure 4.56 show the bending law shapes, for each pile, for the 7m transition and the 0,5m transition. It is observed that even if clay p-y springs are an order of magnitude less stiff than for sand, varying the transition zone affect results. Concentrating the transition zone in the top interface between soil and clay seems to increase bending moments above the clay, while reducing moments at the bottom interface.
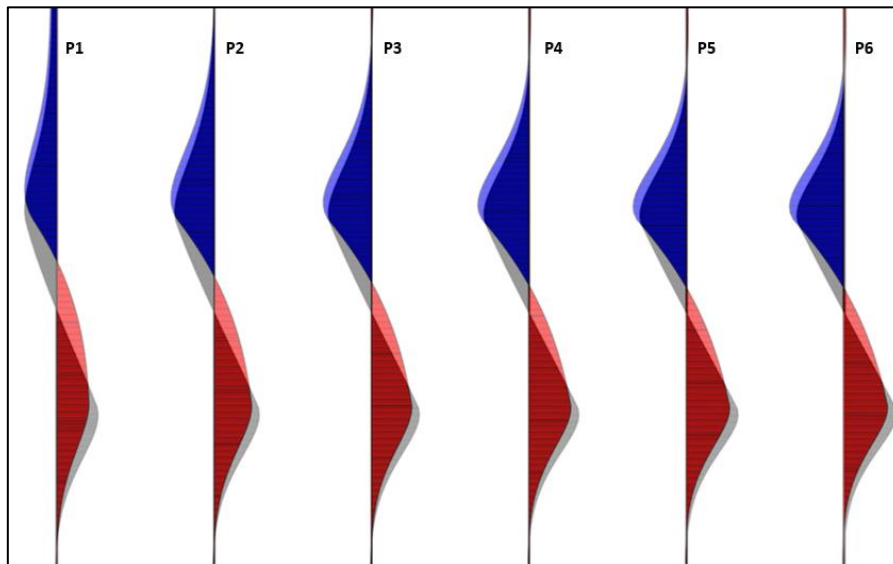
Figure 4.56. Bending moment law shapes due to kinematic effect for two transition lengths: Transition of 7m in black; Transition of 0,5m in color. Maximum values in Figure 4.57 and Figure 4.58.

137
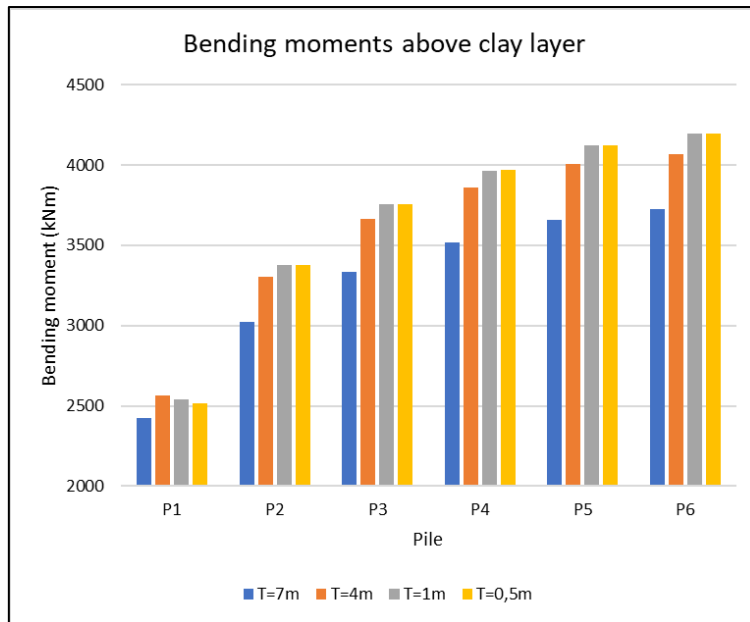
Figure 4.57. Influence of transition zone on bending moments above the clay layer.
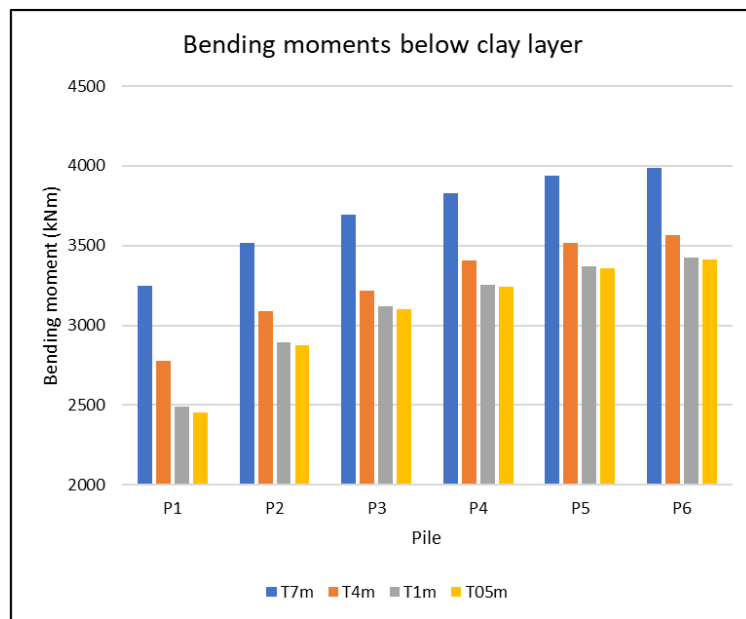
Figure 4.58. Influence of transition zone on bending moments below the clay layer.

Figure 4.57 and Figure 4.58 show that varying transition zone, for this particular case, induces changes of up to 30% for bending moments. These results suggest that different transition zones should be considered in design, if resulting bending moments are close to its resistance. Alternatively, performing additional 2D Finite Element Method geotechnical analysis with time history could provide higher detail profiles. However, simplified methods such as Newmark sliding block method may be enough (N. M. Newmark, 1965).

4.5.7. Combination of kinematic and inertial effects

Two main ideas have been identified for combining inertial and kinematic effects. On the first place, it is recognized that internal efforts due to inertial effects are concentrated at the pile connection, as well as below the dike slope. Kinematic forces, if the failure plane is deep in ground, tends to induce bending and shears that superpose to those caused by acceleration of the structure. On the second place, in reality peak responses of inertial and kinematic effects are usually not temporally in phase (Percher & Iwashita, 2016), which could be beneficial for design. However, for displacement-based design using non-linear static pushover analyses, time is not a relevant variable in analysis. One approach to bypass this problem is to apply full kinematic effects on piles, and then perform a non-linear static pushover analysis starting from the deformed structure.

Figure 4.59 shows bending law shapes for two non-linear cases. On the first case, the pushover analysis is performed form an initial phase where only gravity loads are applied (dead load plus relevant live load). On the second case, additionally, kinematic forces are applied using the displacement method. Results are shown corresponding to the critical DE case with loading towards land, and without vertical seism nor P-Delta effects. It is observed how deep-in-ground moments do not interfere with critical pile moments. On the other hand, on P1 there is some superposition of internal forces, but does not cause yielding of the pile.
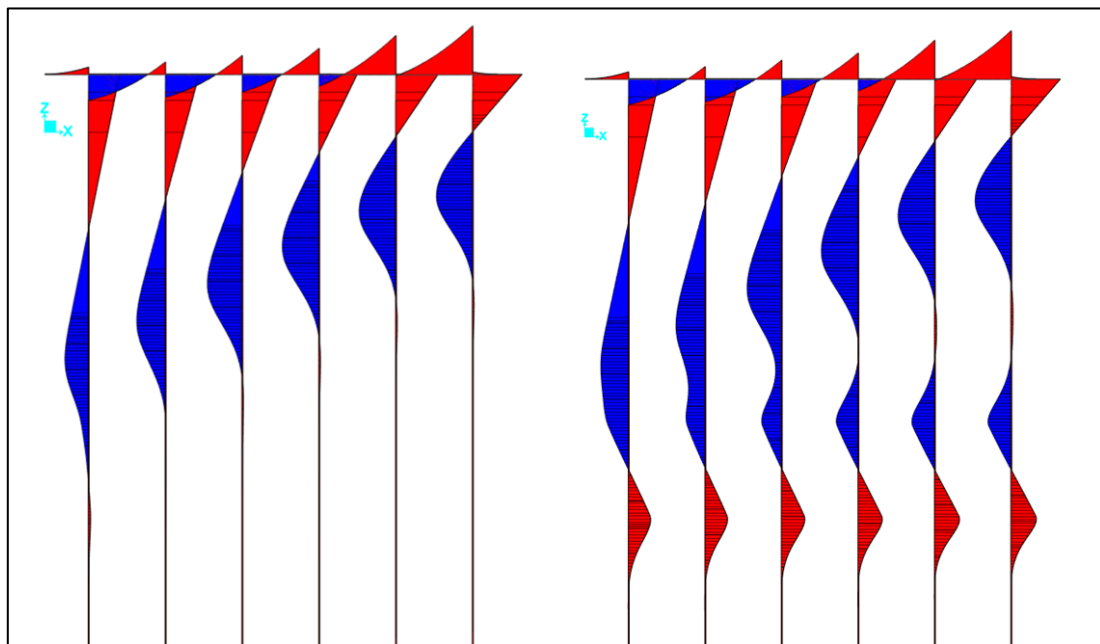
Figure 4.59. Pushover with characteristic soil springs without kinematic forces (left), and with kinematic forces using displacement method (right), at maximum DE displacement.

Figure 4.60 shows results from both pushover analyses in terms of base shear – displacement relationship. It is observed that both curves have the same allure, but they are separated horizontally of about 7cm, which is the displacement caused on the structure from kinematic

effects. As for this particular case there is no relevant interference between kinematic and inertial internal forces, there is no real impact in seismic performance of the structure.
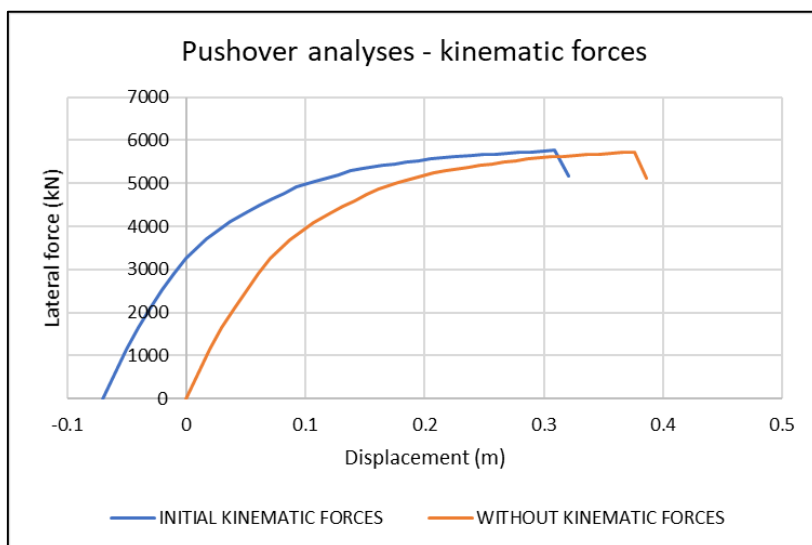
Figure 4.60. Non-linear static pushover analyses with and without initial kinematic forces (from the displacement method).

Table 4.75. Critical displacements of the wharf with and without initial kinematic effects.

CASE	KINEMATIC		NO KINEMATIC	
	ABSOLUTE (m)	RELATIVE (m)	ABSOLUTE (m)	RELATIVE (m)
OLE	0.08	0.15	0.15	0.15
CLE	0.26	0.33	0.33	0.33
DE	0.31	0.38	0.38	0.38

From previous analyses, it is concluded that the combination of kinematic and inertial effects is feasible for design if the failure plane is far from the dike slope (say more than 10 pile diameters). In those cases, applying kinematic forces as the starting point of pushover analyses allows to assess the capacity of the structure for the worst-case scenario with full lateral spreading and seismic loads, if the displacement method is used. However, if lateral spreading happens near the slope, kinematic effects will interact with inertial, potentially reducing seismic capacity. In any case, the structural engineer should be well aware of the assumptions behind this methodology, and work closely with the geotechnical engineer.

5.   CONCLUSIONS

This thesis has reviewed general principles of performance-based design and applied them to a particular case study of a pile-supported wharf. Bibliographic research has raised significant aspects that can have an impact on design, as well as contrasted approaches from different standards and design guidelines.

In the first place, performance limitations for piles provided by ASCE 61-14 and POL-B should be taken as an upper bound of actual maximum strains limited by other critical factors in design. First, regarding steel piles, the need to limit damage strain limitations stated on the standards to avoid local instability due to compression and bending has been identified. Second, concrete plug strength at the pile-to-deck connection is particularly dependent on confinement provided by the steel pipe, which is not considered by typical constitutive models. Modifications to the common (Mander et al., 1988) confined concrete model allow to introduce this effect and to apply it easily to current structural analysis software. Therefore, application of ASCE 61-14 to composite wharf solutions seems to be less straightforward than to fully concrete solutions.

Non-static pushover analyses have shown that most lateral resistance against seismic loading is provided by landward piles, being seaward piles mainly gravitational. Therefore, significant inelasticity, or in performance terms, damage, concentrates on piles on the land side. This justifies the use of displacement-based design rather than force-based design. Due to torsional effects of the wharf, most critical piles are found to be those on the corners of the row closest to land, which determine displacement capacity of the structure.

Axial load on piles is observed to have a significant impact on capacity of the wharf. Composite nature of steel-pile wharves may need a compromise between performance on concrete plug, where axial force is generally beneficial, and on steel piles, where compression is disadvantageous. Geometric non-linearity, or P-Delta effects due to seismic action, are found to have little or no influence on displacement capacity.

Large expected inelastic deformations obtained from capacity curves discards the use of elastic-based demand methods, like the response spectrum analysis or the elastic stiffness method, which some guidelines may propose. On the other hand, modal analyses of the wharf confirm a tri-modal behavior with two torsional modes and one translational along the transverse direction. This justifies the use of purely transverse demand methods, notably the substitute structure method.

The substitute structure method simplifies obtaining seismic demand. However, actual considered hysteretic behavior of the structure, via an equivalent viscous damping, influences greatly results. Thin Takeda formulation in ASCE 61 gives consistent results, although may be conservative compared to other expressions. Additionally, other expressions depending only on ductility, like POL-B, rather than ductility and tangent stiffness, should not be applied systematically. Additionally, reducing design spectra to match equivalent damping using spectrum scaling factors may also significantly impact results. ASCE 61-14 not specifying on this topic, expressions from EC8-04 and (Newmark & Hall, 1982) may be used with similar results, being the latter slightly more conservative.

Regarding transverse demand, no significant changes in axial load caused by vertical seismic loading have been identified. However, this could not be the case for highly axially loaded wharves. On the other hand, P-Delta effects may have a relevant impact on demand, potentially exceeding capacity. ASCE 61-14 requirements regarding geometric non-linearities may be unconservative.

Extrapolating purely transverse demand to the complete problem by the use of the Dynamic Magnification Factor proves to be convenient for design. Formulation in ASCE 61-14 is found to be better suited for design than POL-B, better adapting to the specific design case. POL-B will generally lead to considerably more conservative results, since it is based on studies of particular wharves with fixed geometries. Finally, torsional effects are found to be reduced by increasing demand, which is well captured by the DMF in ASCE 61-14.

Complete non-linear three-dimensional modeling is currently not feasible for design. However, the "Super-Pile" modeling approach reduces vastly numerical complexity of models, allowing simplified non-linear time-history analyses. Although modal behavior of the wharf is well represented by this models, seismic demand is strongly dependent on parameters like elastic damping, equivalent spring distribution, hysteretic modeling and choice of accelerogram records. Moreover, ASCE 61-14 particular hysteretic model may not be currently compatible with structural analysis software, as is the case for SAP2000, limiting its interest for design purposes. In any case, the engineer should be aware of the need of calibration of this model, that may be time-consuming for an engineering project scenario.

Soil-pile interaction through the use of non-linear P-Y springs offers notable convenience for structural analysis modeling. The approach of Upper and Lower bound soil conditions to integrate in structural design geotechnical characterization uncertainties influences greatly results. Capacity is reduced when considering UB with respect to LB, but also seismic demand. Torsional effects show to be slightly higher for UB than LB. In this study softer soils are found to govern design, but it may not be the case for any particular given wharf structure. On the other hand, geotechnical failures of the dike, causing kinematic forces on piles, pose greater concerns regarding structural analysis. The displacement method, if justifiable, preserves resistance of sliding soils and gives less conservative results than the pressure method, which assumes total failure of the soil. If the failure plane is deep and displacement method is used, combination of kinematic and inertial effects is feasible; otherwise, more advanced simulations may be needed. In any case, strong geotechnical hypotheses must be assumed for either method, raising uncertainties of results.

Based on previous results and insight gained during the development of this master's thesis, the following design guidance is proposed to assess a seismic design of a steel pile-supported wharf:

- Keep superstructure mass to necessary, keeping its monolithic nature and allowing its capacity protection, to limit displacement demand (refer to section 3.3.5).
- Perform individual pile pushover analyses with equivalent axial loads, obtain displacement capacities and lateral strength to pile free length relation, and propose pile layout accordingly. Compute wharf required and available strength by assuming critical demand, and modify preliminary design if needed (refer to sections 4.2.1 and 4.2.2).

- Assemble a complete transverse model, and perform pushover analysis. Only considering loading towards sea and land without vertical seismic loading may be sufficient at this stage (refer to section 4.2.3.1). Apply the substitute structure method to resulting capacity curves. ASCE 61-14 damping expression should be used unless specific considerations are assumed. Obtain global demand by multiplying by DMF from ASCE 61 (refer to section 4.3.2.1). Compare capacity to demand. Redesign if needed.

- Introduce P-Delta effects in pushover analyses, even if ASCE 61-14 does not require it, and repeat previous point (refer to section 4.2.3.3). Compare capacity to demand.

- Repeat analyses introducing vertical seismic loading, in accordance with ASCE 61-14 to cover all required cases.

- Although particularly capable structural analysis software allows to model ASCE 61-14 hysteretic model, there is no significant interest in developing "Super-Pile" model for demand purposes (refer to section 4.4). However, for more complex geometries, it may be useful to study its dynamic behavior.

- Finally, close collaboration with the geotechnical engineer is central on this type of design, with special emphasis when dealing with soil failures.

Finally, further research that may offer better understanding of developed modeling and analysis techniques in this study, raising confidence of results for design purposes.

First, a detailed study of the interaction between the concrete plug and the steel pile, by three-dimensional finite element modeling or testing. This would allow to confirm the suitability of developed modeling of pile-to-deck connection.

Second, further investigation on performance damage maximum strains and local buckling of buried piles. This would provide greater confidence for seismic modeling, although future version of ASCE 61 may already suggest revised limitations.

Third, ship-to-shore cranes frequently operate on container wharves, which may have an influence on the dynamic behavior of the structure. ASCE 61-14 and POL-B offer limited guidance on this aspect.

Lastly, more sophisticated soil-structure interaction models could be developed to verify assumptions of kinematic force analysis methods. A model considering a single pile coupled with soil lateral spreading could be a first step.

6. BIBLIOGRAPHY

ACI Commitee 318. (2019). *ACI 318-19 - Building Code Requirements for Structural Concrete*. https://doi.org/10.14359/51716937

AISC 341-16. (2016). *Seismic Provisions for Structural Steel Buildings*.

AISC 360-16. (2016). *Specification for Structural Steel Buildings*.

American Petroleum Institute. (2000). *API SPEC 5L : Specification for Line Pipe*.

American Society of Civil Engineers. (2014). *ASCE 61-14: Seismic Design of Piers and Wharves*. American Society of Civil Engineers. https://doi.org/10.1061/9780784413487

API. (2007). *Recommended Practice 2A-WSD for Planning, Designing and Constructing Fixed Offshore Platforms-Working Stress Design*.

Applied Technology Council. (1996). *ATC-40 Seismic Evaluation and Retrofit of Concrete Buildings*.

Benzoni, G., & Priestley, M. J. N. (2003). Seismic response of linked marginal wharf segments. *Journal of Earthquake Engineering*, *7*(4), 513–539. https://doi.org/10.1080/13632460309350462

Besseling, F., & Lengkeek, A. (2012). *PLAXIS as a Tool for Soil-Structure Interaction Modelling in Performance-Based Seismic Jetty Design*. www.plaxis.nl

Blandon, C. A. (2007). *Seismic Analysis and Design of Pile Supported Wharves*.

Caltrans. (2013). *Seismic Design Criteria*.

Calvi G, Priestley M, & Kowalsky M. (2008). Displacement-Based Seismic Design of Structures. *Earthquake Spectra*, *24*(2), 555–557. https://doi.org/10.1193/1.2932170

CEN. (2004). *EN 1998-1:2004: Design of structures for earthquake resistance-Part 1: General rules, seismic actions and rules for buildings*.

Cubrinovski, M., Haskell, J., & Bradley, B. (2010). *Analysis and Design of Piles in Liquefying Soils*.

Dwairi, H. M., Kowalsky, M. J., & Nau, J. M. (2007). Equivalent Damping in Support of Direct Displacement-Based Design. *Journal of Earthquake Engineering*, *11*(4), 512–530. https://doi.org/10.1080/13632460601033884

Ghobarah, A. (2001). Performance-based Design in Earthquake Engineering: State of Development. *Engineering Structures*, *23*, 878–884. www.elsevier.com/locate/engstruct

Harn, R., Asce, M., Carlos, ;, Ospina, E., & Pachakis, D. (2019). Proposed Pipe Pile Strain Limits for ASCE 61-19. *15th Triennial International Conference*. https://doi.org/10.1061/9780784482612.041

International Navigation Association. (2001). *Seismic Design Guidelines for Port Structures Working Group No. 34*.

Kong, C., & Kowalsky, M. J. (2016). Impact of Damping Scaling Factors on Direct Displacement-Based Design. *Earthquake Spectra*, *32*(2), 843–859. https://doi.org/10.1193/021815EQS031M

Leslie, R., Abhilash, R., & Biju, V. (2009). Effect of Lateral Load Patterns in Pushover Analysis. *10th National Conference on Technological Trends (NCTT09)*. https://www.researchgate.net/publication/319236326

Li, Y. F., Chen, S. H., Chang, K. C., & Liu, K. Y. (2005). A constitutive model of concrete confined by steel reinforcements and steel jackets. *Canadian Journal of Civil Engineering*, *32*(1), 279–288. https://doi.org/10.1139/l04-093

Lu, B., & Silva, P. F. (2006). Estimating Equivalent Viscous Damping Ratio for RC Members Under Seismic and Blast Loadings. *Mechanics Research Communications*, *33*(6), 787–795. https://doi.org/10.1016/j.mechrescom.2006.05.002

Mander, J. B., Priestley, M. J. N., & Park, R. (1988). Theoretical Stress-Strain Model For Confined Concrete. *Journal of Structural Engineering*, *114*(8). https://doi.org/10.1061/(ASCE)0733-9445(1988)114:8(1804)

Martin, G., & Lam, I. (1995). Seismic Design of Pile Foundations: Structural and Geotechnical Issues. *Third International Conference on Recent Advances in Geotechnical Earthquake Engineering & Soil Dynamics*, *III*. https://scholarsmine.mst.edu/icrageesd/03icrageesd/session16/10

Ministerio de Desarrollo Urbano y Vivienda. (2014). *NEC-SE-DS - Peligro Sísmico Diseño Sismo Resistente*.

Newmark, N., & Hall, W. (1982). *Earthquake spectra and design* (3rd ed.). Earthquake Engineering Research Earthquake.

Newmark, N. M. (1965). Effects of Earthquakes on Dams and Embankments. *Géotechnique*, *15*(2). https://doi.org/10.1680/geot.1965.15.2.139

Percher, M. I., & Iwashita, R. (2016). Kinematic Loading from a Structural Perspective. *14th Triennial International Conference*. https://doi.org/10.1061/9780784479902.027

Priestley, M., Calvi, G., Kowalsky, M., & Press, I. (2007). *Displacement-Based Seismic Design of Structures*. IUSS Press.

Priestley, M. J. N. (2000). Performance Based Seismic Design. *Bulletin of the New Zealand Society for Earthquake Engineering*, *33*(3), 325–346. https://doi.org/10.5459/bnzsee.33.3.325-346

Priestley M, Seible F, & Calvi G. (1996). *Seismic Design and Retrofit of Bridges*. John Wiley & Sons, Inc.

Ramirez-Henao, A. F., & Paul Smith-Pardo, J. (2015). Elastic stability of pile-supported wharves and piers. *Engineering Structures*, *97*, 140–151. https://doi.org/10.1016/j.engstruct.2015.04.007

Shafieezadeh, A. (2011). *Seismic Vulnerability Assessment Of Wharf Structures*.

Shibata, A., & Sozen, M. A. (1976). Substitute-Structure Method for Seismic Design in R/C. *Journal of the Structural Division*, *102*(1). https://doi.org/10.1061/JSDEAG.0004250

Su, L., Lu, J., Elgamal, A., & Arulmoli, A. K. (2017). Seismic Performance of a Pile-Supported Wharf: Three-dimensional Finite Element Simulation. *Soil Dynamics and Earthquake Engineering*, *95*, 167–179. https://doi.org/10.1016/j.soildyn.2017.01.009

Takeda, T., Sozen, M., & Nielsen, N. (1970). Reinforced Concrete Response to Simulated Earthquakes. *Journal of the Structural Division*, *96*(12), 2557–2573.

7. ANNEX

ACCELEROGRAM RECORDS FOR TIME-HISTORY ANALYSES